Pushing the Limits of Natural Convection Heat Transfer from the Heatsinks

by

Mehran Ahmadi

M.Sc., Amirkabir University of Technology, 2010
B.Sc., University of Kerman, 2007

Thesis Submitted in Partial Fulfillment of the
Requirements for the Degree of
Doctor of Philosophy

in the
School of Mechatronic Systems Engineering
Faculty of Applied Sciences

SIMON FRASER UNIVERSITY

Fall 2014

Approval

Name:	**Mehran Ahmadi**
Degree:	**Doctor of Philosophy**
Title:	***Pushing the Limits of Natural Convection Heat Transfer from the Heatsinks***
Examining Committee:	**Chair:** Kevin Oldknow Lecturer

Majid Bahrami
Senior Supervisor
Associate Professor _____

John Jones
Supervisor
Associate Professor _____

Jason Wang
Supervisor
Assistant Professor _____

Gary Wang
Internal Examiner
Professor
School of Mechatronic System Engineering _____

Jim Cotton
External Examiner
Professor
Department of Mechanical Engineering
McMaster University _____

Date Defended/Approved: December 19th, 2014

Partial Copyright Licence

Abstract

This research, which has been done in close collaboration with industrial partners, Alpha Technologies and Analytic Systems companies, aims to push the current limits of natural convection heat transfer from vertical heatsinks, with application in passive thermal management of electronics and power electronics. Advantages such as; being noise-free, reliable, with no parasitic power demand, and less maintenance requirements, make passive cooling a preferred thermal management solution for electronics. The focus of this thesis is to design high performance naturally-cooled heatsinks, to increase the cooling capacity of available passive thermal management systems. Heatsinks with interrupted rectangular vertical fins are the target of this study.

Due to the complexities associated with interrupted fins, interrupted rectangular single wall is chosen as the starting point of the project. Asymptotic solution and blending technique is used to present a compact correlation for average Nusselt number of such wall, for the first time. The proposed correlation is verified by the results obtained from numerical simulations, and experimental data obtained from a custom-designed testbed.

In the next step, natural convection heat transfer from parallel plates has been investigated. Integral technique is used to solve the governing equations, and closed-form correlations for velocity, temperature, and local Nusselt number are developed for the first time. The results are successfully verified with the result of an independent numerical simulation and experimental data obtained from the tests conducted on heatsink sample.

In the last step, to model heat transfer from interrupted finned heatsinks, and to obtain compact correlations for velocity and temperature inside the domain, an analytical approach is used. Numerical simulations are performed to provide the information required by our analytical approach. An extensive experimental study is also conducted to verify the results from analytical solution and numerical simulation. Results show that the new-designed heatsinks are capable of dissipating heat five times more than currently available naturally-cooled heatsinks, with a weight up to 30% less. The new heatsinks can increase the capacity of passive-cooled systems significantly.

Keywords: Natural convection; Heatsink; Interrupted fins; Analytical solution; Experimental study; Numerical simulation

To my beloved parents, my dear brothers, and my best friend Maryam

Acknowledgements

I would like to thank my senior supervisor, Dr. Majid Bahrami, for his kind support, guidance, and insightful discussions throughout this research. It was a privilege for me to work with him and learn from his experience.

I am also indebted to Dr. John Jones and Dr. Jason Wang for the useful discussions and comments, which helped me to define the project and to pursue its goals. I would also like to thank Dr. Gary Wang and Dr. Jim Cotton for their time reading this thesis and helping to refine it.

I would like to thank my colleagues and lab mates at Laboratory for Alternative Energy Conversion at Simon Fraser University. Their helps, comments, and assistance played an important role in the development of this thesis. In particular, I want to thank Mohammad Fakoor Pakdaman, Ali Gholami, Marius Haiducu, and Peyman Taheri.

I have received financial support from Natural Sciences and Engineering Research Council (NSERC) of Canada, Mathematics of Information Technology and Complex Systems (MITACS), Alpha Technologies, Analytic Systems, and Simon Fraser University, for which I am grateful. I would also like to appreciate our industrial collaborators, specifically Mr. Kevin Lau, Mr. Steve Pratt, and Mr. Rajiv Witharana for their time, help and kind cooperation.

I have to thank my family that have endlessly encouraged and supported me through all stages of my life. Without their presence and support no achievement was possible in my life. I would also like to thank my dear friends; Hossein Dehghani, Soheil Sadeqi, Arash Tavassoli, Kambiz Haji Hajikolahi, and Fattane Nadimi for their kind support and great memories. Finally special thanks to my best friend, Maryam Yazdanpour for her kind companionship, understanding, and devotion.

Table of Contents

Approval ii
Partial Copyright Licence iii
Abstract iv
Dedication v
Acknowledgements vi
Table of Contents vii
List of Tables ix
List of Figures x
List of Acronyms xii
Symbols xiii
Executive Summary xvi
Motivation xvi
Objectives xvii
Methodology xvii
Contributions xviii
Research Roadmap xix

Chapter 1. Introduction 1
1.1. Research Importance 1
1.2. Research Motivation 3
1.3. Research Scope 4
1.4. Thesis Structure 5
1.5. Literature Review 6
1.6. Research Objectives 11

Chapter 2. Natural Convection from Interrupted Vertical Walls 12
2.1. Numerical Analysis 13
2.1.1. Governing Equations 13
2.1.2. Mesh Independency 15
2.2. Experimental Study 18
2.2.1. Testbed 18
2.2.2. Test Procedure 20
2.2.3. Uncertainty Analysis 21
2.3. Results and Discussion 23
2.4. Conclusion 29

Chapter 3. Natural Convection from Vertical Parallel Plates 30
3.1. Problem Statement 30
3.1.1. Governing Equations and Boundary Conditions 31
3.2. Present Solution 33
3.2.1. Entrance Velocity 33
3.2.2. Integral Technique 34
3.3. Numerical Simulation 37
3.4. Experimental Study 39

3.4.1. Testbed 40
3.4.2. Uncertainty Analysis 42
3.5. Results and Discussion 42
3.6. Conclusion 45

Chapter 4. Natural Convection from Interrupted Fins 46
4.1. Problem Statement 46
4.2. Solution Methodology 47
4.2.1. Channel Flow 48
4.2.2. Gap Flow 49
Governing equations and boundary conditions 50
Integral technique 52
4.3. Numerical Simulation 54
4.4. Experimental Study 57
4.4.1. Testbed 58
4.4.2. Test Procedure 59
4.4.3. Uncertainty Analysis 61
4.4.4. Test Results 61
4.4.5. Validity of Uniform Wall Temperature Assumption 63
4.5. Results and Discussion 64
4.5.1. Total Heat Transfer Calculation 64
4.5.2. Parametric Study 66
Effect of Fin Spacing 66
Effect of Gap Length 66
Effect of Fin Length 67
4.5.3. Heatsink Design Procedure 70
4.6. Conclusion 71

Chapter 5. Summary and Future Work 72
5.1. Summary of Thesis 72
5.2. Future Work 73

References 75

Appendix A. Integral Method for Natural Convection 82
Conservation of mass 83
Conservation of momentum 84
Conservation of energy 85
Appendix B. Calculation of Radiation Heat Transfer from Test Samples 86
Emissivity measurement 87

List of Tables

Table 1.1. Summary of literature on natural convection from parallel plates 10

Table 2.1. Parameters used in the benchmark case for numerical simulations 16

Table 2.2. Dimensions of the interrupted wall samples used in experimental study 19

Table 2.3. Range of important parameters in the experimental study 21

Table 2.4. The uncertainty analysis parameters 23

Table 3.1. Integral form of conservation equations for the integral control volume 33

Table 3.2. Dimensionless parameters 36

Table 3.3. Parameters used for the numerical simulation benchmark 38

Table 3.4. Dimensions of the finned plate samples 40

Table 4.1. Parameters used for numerical simulation benchmark case 55

Table 4.2. Dimensions of the interrupted fin samples used in the experiments 59

Table 4.3. Range of some important parameters in test procedure 60

List of Figures

Figure 1.1. Industrial collaborators products, a) Analytic Systems naturally-cooled power enclosure, b) Alpha technologies outside plant power cabinet. 3

Figure 1.2. a) A sample of commercially available enclosure with interrupted fins, b) effect of adding interruptions on thermal boundary layer and heat transfer 6

Figure 2.1. Effect of interruptions on boundary layer growth in natural heat transfer from a vertical wall 13

Figure 2.2. a) Schematic of the numerical domain and boundary conditions for vertical interrupted wall, b) grid used in the model for interrupted wall 15

Figure 2.3. Grid independency study; walls average heat flux versus number of elements for the benchmark case (see Table 2.1) 16

Figure 2.4. a) velocity domain, and b) temperature domain for the benchmark case; the diffusion of velocity and temperature in the gap causes the air to reach the top wall with higher velocity and lower temperature 17

Figure 2.5. a) schematic and photo of the testbed; b) backside of the samples; positioning of the thermocouples and heater 19

Figure 2.6. Heat transfer versus $\kappa(G/l)$ for different $\zeta(l/t)$ values. The figure also shows the comparison between the numerical data (symbols) and introduced asymptotes (Lines) 26

Figure 2.7. Effective length versus $\kappa(G/l)$ for different $\zeta(l/t)$ values. The figure also shows the comparison between the numerical data (symbols) and the proposed correlation (lines) for the effective length. 27

Figure 2.8. Nusselt number versus $\kappa(G/l)$ for different $\zeta(l/t)$ values. The figure also shows the comparison between the numerical data (hollow symbols), experimental data (solid blue symbols), and the proposed compact relationship (lines) 28

Figure 3.1. a) a naturally-cooled enclosure of a power converter; b) schematic of the heatsink, and c) solution domain, selected as the control volume 31

Figure 3.2. a) schematic of the numerical domain and boundary conditions, b) the grid used in the model, c) velocity domain, and d) temperature domain for the benchmark case 38

Figure 3.3. Grid independency study; walls average heat flux versus number of elements for the benchmark case (see Table 3.3) 39

Figure 3.4. a) schematic of the test-bed; b) samples dimensions, heater and thermocouples positioning; c) testbed casing and insulation; and d) a photo of the testbed 41

Figure 3.5. Comparison between the analytical solution (lines), a) velocity b) temperature distribution and numerical results (symbols) at various cross sections along the channel 43

Figure 3.6. Comparison between the present average Nusselt number, existing semi-empirical relations in the literature [24] and [26], and our experimental data 45

Figure 4.1. A schematic of heatsink with interrupted fins, geometrical parameters used to address fin parameters, and the regions related to channel flow and gap flow 47

Figure 4.2. Schematic of the control volume selected for the channel flow 49

Figure 4.3. Schematic of the control volume selected for the gap flow 50

Figure 4.4. Numerical simulation-benchmark case; a) the domain and boundary condition, b) a sample of mesh, c) velocity distribution, and d) temperature distribution 55

Figure 4.5. Mesh independency study for the benchmark case 56

Figure 4.6. Comparison between the result from integral technique with $\varsigma = 40$ and $\sigma = 95$, and numerical simulations at the benchmark case , a) velocity domain, b) temperature domain 57

Figure 4.7. Experimental setup, a) the position of thermocouples and the heater, b) photos of sample under test, c) schematic of the test bed and insulations 58

Figure 4.8. Comparison between the experimental data and analytical solution, a) fin spacing, b) fin length, c) gap length 62

Figure 4.9. IR image from a) front view, b) side view of the heatsink sample under test 64

Figure 4.10. Effect of fin spacing on heat transfer from the heatsink 66

Figure 4.11. Effect of gap length on heat transfer from the heatsink, a) total heat transfer, b) dimensionless heat transfer with respect to continuous fins 68

Figure 4.12. Effect of fin length on heat transfer from the heatsink, a) total heat transfer, b) dimensionless heat transfer with respect to continuous fins 69

Figure 5.1. Proposed geometries for the future work, a) inclined interrupted fins, b) variable fin parameters along the flow 74

List of Acronyms

DAQ	Data Acquisition System
GA	Genetic Algorithm
IR	Infrared
LED	Light-Emitting Diode
PMMA	Poly Methyl Methacrylate
TCR	Thermal Contact Resistance
TIM	Thermal Interface Material

Symbols

General Symbols

A	Surface area, m^2
c	Constant of blending technique in effective length
c_p	Specific heat, $J/kg.K$
$\dot{E}$	Energy, W
F	Force, N
g	Gravitational acceleration, m/s^2
G	Gap length, m
Gr	Grashof number, $g\beta\Delta Ts^3/v^2$
h	Heat transfer coefficient, W/m^2K
H	Fin height, m
k	Thermal conductivity, $W/m.K$
l	Fin length, m
L	Baseplate length, m
m	Number of fin rows
$\dot{m}$	Mass flow rate, kg/s
$\dot{M}$	Momentum, $kg.m/s$
n	Number of fin columns
Nu	Nusselt number, hs/k
p	Pressure, Pa
P	Heater power, W
Pr	Prandtl number, v/α
$\dot{q}$	Heat flux, W/m^2
$\dot{Q}$	Total heat transfer, W
Ra	Rayleigh Number, $g\beta\Delta Ts^3/v\alpha$
s	Fin spacing, m
t	Thickness, m
T	Temperature, K
u	Velocity in x-direction, m/s
U	Dimensionless velocity in x-direction, us/α

v	Velocity in *y*-direction, *m*/*s*
W	Baseplate width, *m*
x	Direction parallel to fins, *m*
X	Dimensionless *x*, *x*/*l*
y	Direction normal to fins, *m*
Y	Dimensionless *y*, *y*/*s*
z	Direction normal to *x* and *y* in Cartesian coordinate

Greek Symbols

α	Thermal diffusivity, m^2/s
β	Coefficient of volume expansion, K^{-1}
χ	Coefficient appears in channel velocity
δ	Coefficient appears in channel temperature
Δ	Difference
ε	Channel slenderness, *l*/*s*
ϕ	Coefficient appears in gap velocity
φ	Coefficient appears in gap velocity
γ	Parameter appears in channel temperature, 1/*m*
η	Coefficient appears in channel temperature
ι	Coefficient appears in gap temperature
κ	Gap to fin length ratio in interrupted walls, *G*/*l*
λ	Parameter appears in channel velocity, 1/*m*
μ	Dynamic viscosity, *kg*/*m.s*
ν	Kinematic viscosity, m^2/s
θ	Dimensionless temperature, $(T_w\text{-}T)/(T_w\text{-}T_\infty)$
ϑ	Constant appears in gap temperature
ρ	Density, kg/m^3
σ	Parameter appears in gap temperature, 1/*m*
ς	Parameter appears in gap velocity, 1/*m*
τ	Shear stress, N/m^2
ω_R	Uncertainty
ξ	Gap width, *m*
ψ	Constant appears in channel velocity

ζ	Fin length to thickness ratio in interrupted walls, *l*/*t*

Subscripts

∞	Ambient properties
b	Baseplate
$bottom$	Fin's bottom in interrupted walls
C	Channel
$C.V.$	Control volume
$ends$	Fin's top/bottom in interrupted walls
$eff.$	Effective
$F.D.$	Fully developed
G	Gap
in	Inlet of channel/gap
$N.C.$	Natural convection
out	Outlet of channel/gap
$Rad.$	Radiation
$sides$	Fin's sides in interrupted walls
top	Fin's top in interrupted walls
$total$	Total heat transfer
w	Wall properties

Executive Summary

Motivation

Thermal management of electronics/power electronics has wide applications in different industries such as; telecommunication, automotive, and renewable energy systems. About 55% of failures in electronics during operation have thermal root. The rate of failure due to overheating nearly doubles with every 10°C increase above the operating temperature. The importance of efficient thermal management systems is reflected in their worldwide market. Thermal management technology market was valued at $10.1 billion in 2013 and reached $10.6 billion in 2014. Total market value is expected to reach $14.7 billion by 2019. Thermal management hardware, such as fans and heatsinks, accounts for about 84% of the total market.

Passive cooling is a widely preferred cooling method for electronic and power electronic devices. High reliability, no noise and no parasitic power make passive cooling methods such as natural convection, attractive for sustainable and “green” systems. Telecommunication devices are an example of electronic systems that require efficient thermal management. More than 1% of global total energy consumption (3% of US energy consumption) in 2012 was used by telecommunication devices. This is equal to energy consumed by 15 million US homes. About 28% of this energy is required for thermal management of such systems. Studies show that applying passive cooling techniques can reduce the energy required for thermal management from 28% of total energy consumption to 15% in general and 0% in some cases.

In any typical thermal management system, passive or active, there is always a temperature difference between the heat source and cooling medium, called thermal budget, which is the driving force of heat transfer. This thermal budget is spent in the thermal resistances along the heat path. The thermal resistances, in most cases include: i) thermal contact resistance at the solid-solid interface due to surface asperities, ii) spreading resistance, due to changes in geometry and bottle necks, iii) bulk resistance, due to material thermo-physical properties, and iv) film resistance existing at the solid-fluid interface due to boundary layer effects. Except for the film resistance, the rest of the above-mentioned thermal resistances act similarly between active and passive cooling

systems. The effect of film resistance appears in the heatsink, and consequently design of high performance naturally-cooled heatsinks becomes very important in design of next generation passive thermal management system. This thesis aims to address the need, for this design by pushing the limits of natural convection heat transfer from heatsinks.

Objectives

The research objectives are:

- To increase the current heat dissipation limit of naturally-cooled heatsinks, by using interrupted fins instead of conventional fins
- To establish a deep understanding of air flow and heat transfer in naturally-cooled heatsinks
- To develop a design tool for high performance naturally-cooled heatsinks with interrupted fins
- To find the optimum fin arrangement on naturally-cooled heatsinks to maximize the heat transfer

Methodology

This research is focused on film resistance due to thermal boundary layer, which occurs at the solid-fluid interface in the heatsinks. The target of this research is naturally-cooled heatsinks with vertical rectangular interrupted fins, for which no in-depth study was found in the available literature. The research project is divided into three main sub-projects; i) interrupted single wall, ii) natural convection from parallel plates, and iii) natural convection from interrupted fins. Figure 1 shows more details on sub-projects and the roadmap for the main project.

Analytical modeling is used to solve the governing equations for velocity and temperature domain for each sub-project. Integral technique, asymptotic solution, and blending technique are the main mathematical methods used in this research. Numerical simulations are also conducted for each sub-project, to get better understanding of the physics of the flow, and to verify some analytical results. Commercial software packages, COMSOL Multiphysics and ANSYS FLUENT, are used for numerical modeling. At the end, all the obtained correlations are validated by experimental data, obtained from the

custom-designed testbeds, made in the lab. More than 30 heat sinks samples, related to all three sub-projects, are machined out of aluminum and tested.

Results show that our designed heatsinks are capable of dissipating heat up to 12 times more than available naturally-cooled heatsinks, with up to 30% lower weight. The average heat transfer improvement in the designed heatsinks compared to commercially available heatsinks is 500%.

Contributions

The list of contributions resulted from the present study is listed below;

- Developing a closed-form correlation for average Nusselt number for interrupted single walls, published in ASME Journal of Heat Transfer
- Developing closed-form solutions for local Nusselt number, velocity, and temperature distribution in laminar natural convection heat transfer between parallel plates, published in Journal of Thermophysics and Heat Transfer
- Developing compact correlation for velocity and temperature in two dimensional momentum and energy diffusion in a one directional laminar flow
- Design of interrupted fins naturally-cooled heatsinks with average heat dissipation of 5 time higher than similar commercially available heatsinks
- Developing an easy to use tool to design high performance naturally-cooled heatsinks with interrupted fins, published in International Journal of Thermal Sciences
- Design and prototyping of a fully passive thermal management system for outside plant telecom enclosures, presented in IEEE INTELEC 2014 Conference

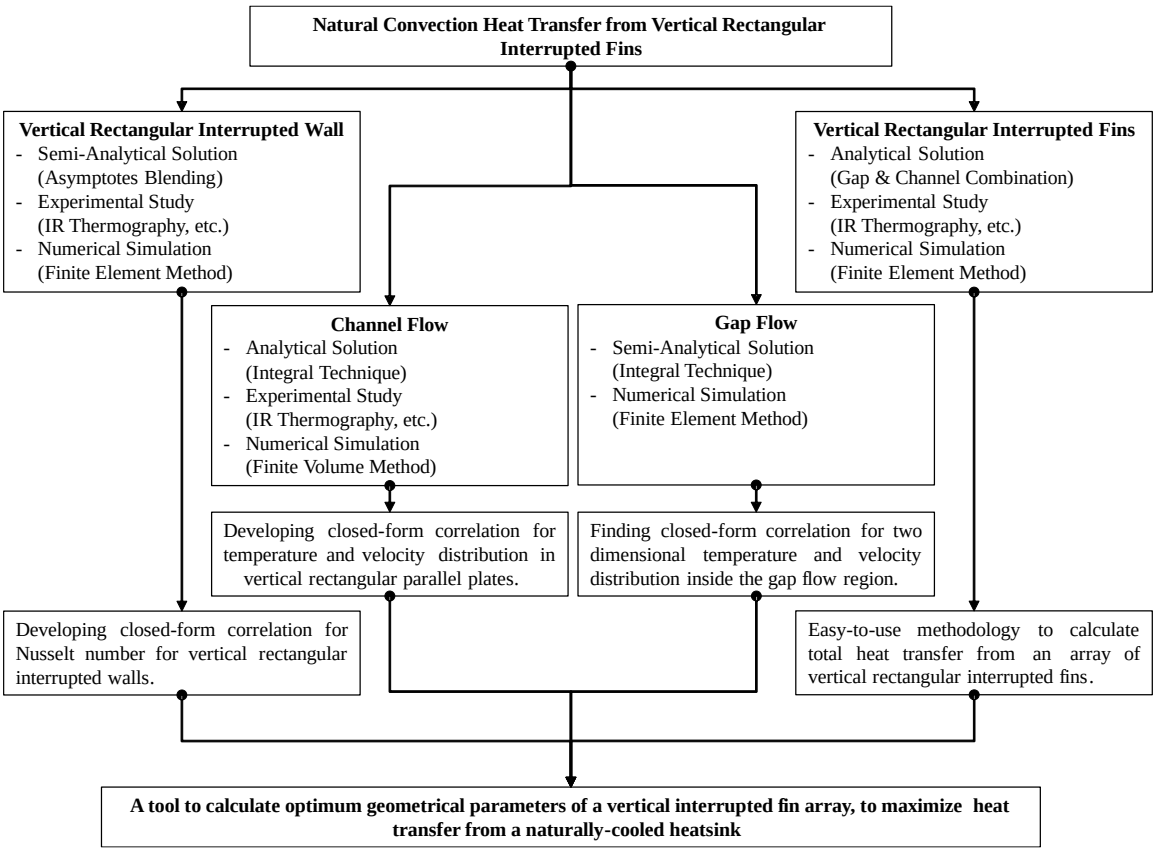

The present research project roadmap and deliverables

Chapter 1.

Introduction

1.1. Research Importance

Thermal management of electronics and power electronics has vast applications in several industries such as; telecom industry (datacenters and outdoor enclosures), automotive industry (conventional vehicles, hybrid vehicles, electric vehicles, and fuel cell vehicles), renewable energy systems (solar panels and wind turbine power electronics), aerospace industry, and light-emitting diode (LED) industry. Efficient thermal management of electronics is essential for optimum performance and durability. About 55% of failures in electronics during operation have a thermal root [1]. The rate of failures due to overheating nearly doubles with every 10°C increase above the operating temperature [2]. Considering the increasing functionality and performance of electronic devices and the ever increasing desire for miniaturization in the industry, thermal management has become the limiting factor in the development of such devices, specifically in case of telecom power-electronics [3], and LEDs [4,5], and reliable low-cost cooling methods are more and more required. The importance of electronics thermal management is also reflected in its worldwide market. Thermal management technology market was valued at $10.1 billion in 2013 and reached $10.6 billion in 2014 [6]. Total market value is expected to reach $14.7 billion by 2019. Thermal management hardware, e.g. fans and heatsinks, account for about 84% of the total market. Other cooling product segments, e.g. software, thermal interface materials (TIM), and substrates, each account for between 4% to 6% of the market [6].

Passive cooling is a widely preferred cooling method for electronic and power electronic devices since it is economical, quiet, and reliable. Moreover, natural convection and other passive cooling solutions require no parasitic power which make them more attractive for sustainable and “green” systems. Telecommunication devices are an

example of power electronic systems that require efficient thermal management. More than 1% of global total energy consumption (3% of U.S. energy consumption) in 2013 is used by telecommunication devices [7], which is equal to annual energy consumed by 15 million US homes, with equivalent CO_2 emission of 29 million cars [8,9]. This value is predicted to increase by 50% by 2017 [10]. About 28% of this energy is required for cooling and thermal management of such systems [11]. Integrating passive cooling techniques with conventional cooling strategies, can reduce this value to 15% [12] in general. Energy demand for cooling can be decreased to 0% [13] if fully-passive thermal management systems are designed and used. As such, passive cooling systems have attracted an immense attention especially in the renewable energy conversion systems and applications in which energy efficiency is of major importance, or applications where using a fan is not essential or possible, e.g. hostile environment, contaminated air, vibration-sensitive systems, noise-limiting regulations, and high levels of humidity.

In any typical thermal management system, passive or active, there is always a temperature difference between the heat source and cooling medium, called thermal budget, which is the driving force of heat transfer. This thermal budget is spent in the thermal resistances along the heat path. The thermal resistances, in most cases include; i) thermal contact resistance at the solid-solid interface due to surface asperities, ii) spreading resistance, due to bottle necks and changes in geometry, iii) bulk resistance, due to material thermo-physical properties, and iv) film resistance at the solid-fluid interface due to boundary layer effects. Except for the film resistance, the above-mentioned thermal resistances are similar between active and passive cooling systems. The effect of film resistance appears in the heatsink, and consequently design of high performance naturally-cooled heatsinks becomes crucial in design of reliable passive thermal management system. Heatsinks are common components of almost all thermal management systems. They are used to dissipate the generated heat in electronic components to the ambient. Heat generating components could be; i) high-power semiconductor devices, such as diodes, Thyristors, IGBTs and MOSFETs, ii) integrated circuits, such as audio amplifiers, microcontrollers and microprocessors, or iii) other electronics such as LEDs or CPUs. To increase the effectiveness and performance of heatsinks, they are usually manufactured with extended surfaces, also known as fins. Fins are used to increase the rate of heat transfer by increasing the surface area. Different fin

geometries are being used in the industry and studied in the literature including; rectangular, circular, conical, pin fins, etc. Orientation of fins, i.e. vertical, horizontal, or inclined, also plays an important role in heatsinks performance.

1.2. Research Motivation

This work has been impelled by a collaborative research project with two local companies; Analytic Systems, a manufacturer of electronic power conversion systems located in Delta, BC, and Alpha Technologies Ltd, a telecom and power solution company located in Burnaby, BC. Both companies were interested in passive cooling solutions for their power electronic systems. Some of the Analytic Systems naturally-cooled enclosures experienced excessive heating causing reliability and performance issues for their clients. Therefore, a research venture was initiated with Analytic Systems with the goal of modifying the naturally-cooled power enclosure to resolve the thermal management problem. Alpha Technologies on the other side, was seeking a fully passive cooling solution for their outside plant power enclosures, used in telecom industry. Their goal was to convert their current fan-assisted heat exchanger-equipped thermal management system of their power enclosures to a fully passive cooling solution. Figure 1.1 shows the sample products from Analytic Systems and Alpha technologies. As such, parallel to the Analytic Systems project, a new research collaboration started with Alpha Technologies, both sharing the concept of passive thermal management systems of power electronics.

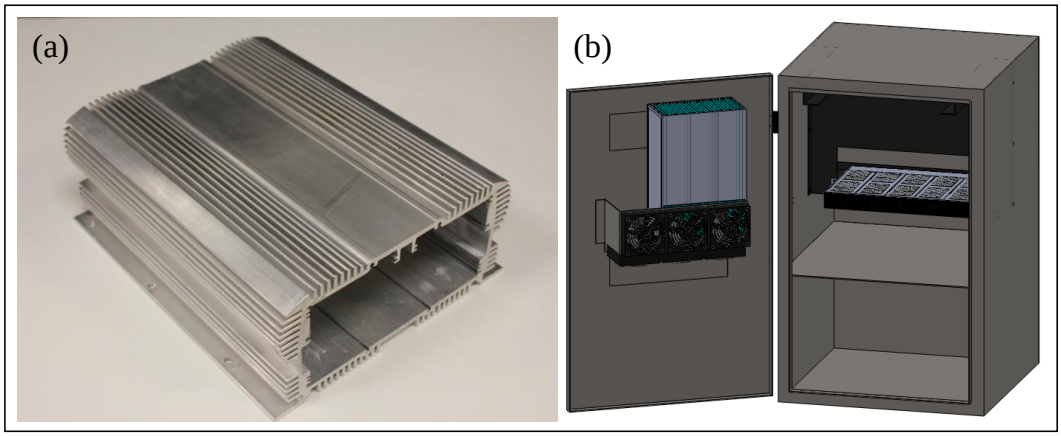

Figure 1.1. Industrial collaborators products, a) Analytic Systems naturally-cooled power enclosure, b) Alpha technologies outside plant power cabinet.

1.3. Research Scope

As mentioned in Section 1.2, the goal of the industrial projects at system level is to design a passive thermal management system for power enclosures. Although the projects are defined for different applications, they share similar architecture for the cooling system. The heat generated at the electrical components should pass through a thermal interface material (TIM) that provides the electrical insulation and minimizes the thermal contact resistance (TCR), spread inside a heat spreader that connects the small area of the heat generating component to a larger part in which heat can transfer more easily, pass through a medium to reach the heatsink, and eventually dissipate to the ambient via convection and radiation. Thermal resistances existing in the heat path, can affect the quality of the heat transfer significantly, by spending the available thermal budget in an ineffective way. Thermal budget is the available temperature difference between the heat source and cooling medium. Thermal resistances, in most cases, include: i) thermal contact resistance at the solid-solid interface due to surface asperities, ii) spreading resistance, occurring in the geometrical bottle necks, iii) bulk resistance, due to material thermo-physical properties, and iv) film resistance existing at the solid-fluid interface due to boundary layer effects. In an efficient thermal management system, all the above-mentioned resistances should be minimized. Therefore the main projects are divided to sub-projects, each focusing on one thermal resistance. The target is to get better understanding of each resistance by doing fundamental research including; mathematical modeling, experimental study, and numerical simulation. Each part is assigned to a graduate student, and at the end the results gathered from sub-projects at the component level, are integrated at system level to design a fully passive thermal management system for power electronic enclosures. The sub-project related to thermal spreading resistance is successfully finished by another researcher at Laboratory for Alternative Energy Conversion (LAEC), and more details can be found in [14]. The other sub-project with goal of minimizing the thermal contact resistance (TCR), is targeting the thermal interface materials (TIMs), and is currently an ongoing research at LAEC, conducted by another researcher. The focus of the research in this thesis, is on the film resistance at the solid-fluid interface, which is related to the design of high performance naturally-cooled heatsinks. At the system level, a heatpipe-integrated fully-passive thermal management

system is designed, built, and successfully tested, by the author. The results of the system level design, are presented in INTELEC 2014 conference [15].

1.4. Thesis Structure

The main challenge in heatsink design is to find the best geometry, orientation, and arrangement for the fins, to maximize the heat transfer from a given surface area. In the quest to find the best fin arrangement, some of the pioneer industries in the field are noticed to be using a specific fin arrangement, namely “interrupted fins” or “discrete fins” (Figure 1.2.a). However, as shown in Section 1.5, our literature review shows that no in-depth study has been performed to investigate the external laminar natural convection heat transfer from interrupted fins, and the parameters for currently used interrupted fins are solely selected by a trial and error process. It is expected that proper selection of geometrical parameters leads to a higher thermal performance, which is based on the fact that interrupted fins disrupt the thermal boundary layer growth, and maintain a thermally developing flow regime along the fins which leads to higher heat flux dissipated from the heatsink (Figure 1.2.b). Fin interruption also results in a considerable weight reduction, however on the other hand, adding interruption to fins leads to losing surface area, which decreases the total heat transfer. These two competing trends clearly indicate that an “optimum” fin arrangement exists that will provide the maximum heat transfer rate from naturally-cooled heatsinks. The main goal of this thesis is to find the optimum fin arrangement for naturally-cooled heatsinks with vertical rectangular interrupted fins.

The governing equations of natural convection heat transfer are rather complex partial differential equations to be solved analytically. The reason for this complexity is that the driving force of fluid flow in natural convection is buoyancy force, while this body force itself is result of fluid density change due to temperature variation. Consequently, momentum and energy equations are coupled in the conservation equations, and temperature term appears in the momentum equation. When natural convection occurs in open ended channels, buoyancy force effect causes a fluid flow between the channel walls that makes the evaluation of inlet boundary conditions rather difficult. At the first step, in order to get rid of this complication, the neighboring fins are eliminated from the geometry to create an interrupted vertical wall. After simplifying the problem, asymptotic solution

and blending technique are used to obtain a closed-form correlation for average Nusselt number in laminar natural convection heat transfer from vertical interrupted walls. The details on this part are given in chapter 2. In the next step, laminar natural convection from parallel plate is targeted. For laminar natural convection from the parallel plates, compact correlations are presented for velocity, temperature and local Nusselt number, for the first time. Chapter 3 contains the details on laminar natural convection from parallel plates. Eventually at the final step, the effect of top and bottom fins are also considered in the problem, and laminar natural convection from vertical rectangular interrupted fins is targeted. Results obtained from the parallel plates are combined with the developed closed-form correlations and an easy-to-use method is presented to design naturally-cooled heatsinks with interrupted fins. Details about this work are given in Chapter 4.

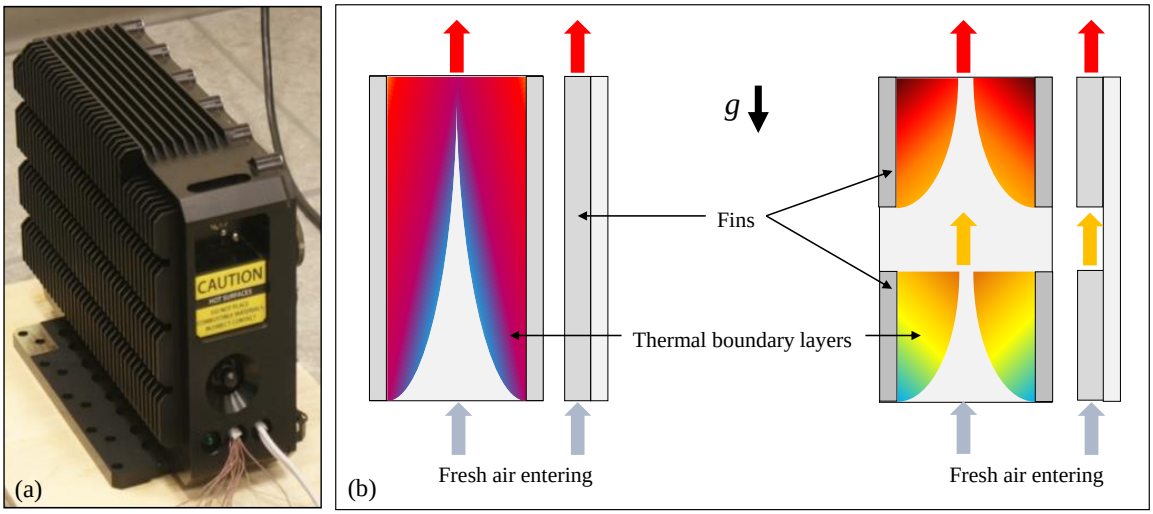

Figure 1.2. **a) A sample of commercially available enclosure with interrupted fins, b) effect of adding interruptions on thermal boundary layer and heat transfer**

1.5. Literature Review

A general overview on pertinent literature in the area of natural convection heat transfer from fins is provided in this section. The focus of this study is on natural convection heat transfer from vertical rectangular interrupted fins. As mentioned in Section 1.3, vertical single wall is selected as a starting point, before analyzing fin array or more complex geometries. As such, our literature review begins by looking into researches done

on single wall, then extended to parallel plates or continuous fins, and ended with the fins array.

Interrupted walls: A variety of theoretical expressions, graphical correlations and empirical equations have been developed to calculate the coefficient of natural convection heat transfer from vertical plates. Ostrach [16] made an important contribution on analysing the natural convection heat transfer from a vertical wall. He analytically solved laminar boundary layer equations using similarity methods for uniform fin temperature condition and developed a relationship for the Nusselt number for different values of Prandtl number. As well, Sparrow and Gregg [17] used similarity solutions for boundary layer equations for the cases of uniform surface heat flux. Merkin [18], also used similarity solution to solve natural convection heat transfer from a vertical plate with non-uniform wall temperature and wall heat flux. Churchill and Chu [19] developed an expression for Nusselt number for all ranges of the Rayleigh, and Pr numbers. Yovanovich and Jafarpur [20] studied the effect of orientation on natural convection heat transfer from finite plates. Cai and Zhang [21] found an explicit analytical solution for laminar natural convection in both heating and cooling boundary conditions. The focus of the available literature on natural convection from vertical plates has been on continuous rectangular walls and, to the author's best knowledge, no comprehensive study is available for natural convection from interrupted walls.

Parallel plates: Finned surfaces are widely used for enhancement of heat transfer [22,23]. Natural convection heat transfer from vertical rectangular fins is a well-established subject in the literature. Pioneering analytical work in this area was carried out by Elenbaas [24]. He investigated isothermal finned heatsink semi-analytically and experimentally. His study resulted in general relation for average Nusselt number for vertical rectangular fins; which was not accurate for small values of fin spacing. Churchill [25] and Churchill and Chu [19] developed a general correlation for the average Nusselt number for vertical channels using the theoretical and experimental results reported by a number of authors. Bar-Cohen and Rohsenow [26] also performed a semi-analytical study to investigate the natural convection heat transfer from two vertical parallel plates. They developed a relationship for the average Nusselt number as a function of the Rayleigh number for isothermal and isoflux plates. Bodoia and Osterle [27] followed Elenbaas [24] and used a

numerical approach to investigate the developing flow in a vertical and the natural convection heat transfer between symmetrically heated, isothermal plates in an effort to predict the channel length required to achieve fully developed flow as a function of the channel width and wall temperature. Ofi and Hetherington [28] used a finite element method to study natural convection heat transfer from open vertical channels. Culham *et al*. [29] also developed a numerical code to simulate free convective heat transfer from a vertical fin array. Several experimental studies were carried out on this topic. Sparrow and Acharya [30], Starner and McManus [31], Welling and Wooldridge [32], Edward [33], Chaddock [34], Aihara [35–38], Leung *et al*. [39–45], and Van de Pol and Tierney [46] are some examples. These studies were mostly focused on the effects of varying fin geometric parameters, the array, and baseplate orientation. Table 1.1 provides a brief overview on the pertinent literature; more detailed reviews can be found in [1]. All the above-mentioned studies reported average Nusselt number for natural convection heat transfer from vertical rectangular fins, however; to the best knowledge of author, velocity profile, temperature profile, and local Nusselt number for the buoyancy-driven channel flow are not available in the literature. Complexities such as coupled governing equations make the finding of full analytical solutions for temperature and velocity domains rather difficult. In-depth understanding of velocity/temperature behavior is required before taking the problem to the next step which is natural convection from interrupted fins.

Interrupted fins: Effect of interruptions on forced convection natural convection is a mature subject in the literature. DeJong and Jacobi [47] did an extensive experimental study on different geometries of fin arrangement, including offset strip (staggered) fins and louvered fins. Brutz *et al*. [48] investigated the effect of unsteady forcing on forced convection heat transfer from interrupted fins. Jensen *et al*. [49] also performed a multi-objective thermal design optimization on different forced-air-cooled heatsinks, including continuous fin, pin fin, and interrupted fin with in-line and staggered arrangement. In case of natural convection heat transfer, Bejan *et al*. [50] used constructal method to optimize the distribution of discrete heat sources cooled by laminar natural convection. Sobel *et al.* [51] experimentally compared a staggered array of interrupted fins to continuous fins. They concluded that there is a significant increase in Nusselt number even beyond the meeting point of the boundary layers in the channel. However their results show that as the fin length increases, the relative advantage of the staggered arrangement decreases and the

performance falls eventually below that of continuous fins. Sparrow and Prakash [52], numerically solved natural convection heat transfer from a staggered array of interrupted fins and compared the total heat transfer to continuous fins with the same surface area. They showed 100% enhancement for cases similar to pin fins, for a specific range of hydraulic diameter and Rayleigh number. Daloglu and Ayhan [53] investigated the effects of periodically installed fin arrays inside an open ended enclosure experimentally. They tested various arrangements and relatively large range of Rayleigh number, and showed the diverse effect of interrupted fins on internal natural convection heat transfer compared to continuous fins. Gorobets [54] performed and analytical study on natural convection heat transfer from staggered arrangement of fins and showed 50-70% enhancement compared to continuous fins. The few available studies on interrupted fins are mainly focused on staggered fin arrangement. Recently in an experimental and numerical study, we showed higher performance of interrupted fins compared to continuous fins [55,56]. However no detailed information, including velocity and temperature behavior, heat transfer calculation, fin design criteria, etc. is available for such fin type. To the best knowledge of author, no systematic study on interrupted vertical naturally-cooled fin arrays is currently available in the literature for the case of laminar natural convection heat transfer.

As a summary to this section, the lack of information on the naturally-cooled fin arrays, in the available literature can be listed as below;

- Interrupted walls
  - No in-depth study on vertical interrupted single walls
- Parallel plates
  - No available closed-form correlation for velocity and temperature distribution in natural convection from parallel plates
  - No available correlation for the local Nusselt number or local heat transfer coefficient in natural convection from parallel plates

Interrupted fins

  - No comprehensive study on natural convection from vertical rectangular interrupted fins

As such, the goal of this thesis is to address this shortcoming in the literature and to study; i) natural convection heat transfer from vertical interrupted walls, to obtain an closed-form solution for heat transfer calculations, ii) fluid flow and heat transfer in buoyancy driven flow between parallel plates, to obtain correlations for velocity and temperature distribution, and iii) natural convection heat transfer from vertical rectangular interrupted fins, and develop a design tool to enable finding the optimum fin arrangement in such heatsinks. The results obtained from the first two studies will be used as a platform to provide better understanding of interrupted fins problem.

Table 1.1. Summary of literature on natural convection from parallel plates

Ref	Method	Ra	Nu	Highlights
[57]	Empirical	all	$Nu_s = \frac{1}{24} Ra_s \left(\frac{s}{l}\right)\left\{1-e^{-12.5/\left[Ra_s\left(\frac{s}{l}\right)\right]^{3/4}}\right\}$	Isothermal
[24]	Analytical/ Empirical	$10^{-1}-10^{5}$	$Nu_s = \frac{1}{24} Ra_s \left[1-\exp\left(-\frac{35}{Ra_s}\right)\right]^{\frac{3}{4}}$	Symmetric Isothermal
[26]	Analytical/ Empirical	all	$Nu_s = \left[\left(\frac{24}{Ra_s}\right)^2 + \left(\frac{1}{0.59\,Ra_s^{0.25}}\right)^2\right]^{-0.5}$	Symmetric Isothermal
			$Nu_s = \left[\left(\frac{6}{Ra_s}\right)^2 + \left(\frac{1}{0.59\,Ra_s^{0.25}}\right)^2\right]^{-0.5}$	Asymmetric Isothermal
[34]	Empirical/ Numerical	all	$Nu_s = \left[\left(\frac{12}{\frac{s}{L}Ra_s}\right)^2 + \left(\frac{1}{0.619\left(\frac{s}{L}Ra_s\right)^{0.25}}\right)^2\right]^{-0.5}$	Isothermal
[19]	Analytical/ Empirical	all	$Nu_L = \left\{0.825 + \frac{0.387\,Ra_l^{\frac{1}{6}}}{\left[1+(0.492/Pr)^{\frac{9}{16}}\right]^{\frac{8}{27}}}\right\}^2$	Isothermal Isoflux
[30]	Empirical	$s < 50\,mm$	$Nu_s = 6.7\times10^{-4} Ra_s \left[1-\exp\left(\frac{7460}{Ra_s}\right)^{0.44}\right]^{1.7}$	Isothermal Horizontal
		$s > 50\,mm$	$Nu_s = 0.54 Ra_s^{0.25}$	

1.6. Research Objectives

In Section 1.5 it has been indicated that the focus of the pertinent research in the area of the natural convection heat transfer from finned plates has been mostly on continuous/pin fins, and no in-depth study has been performed to investigate external natural convection heat transfer from interrupted fins. Interrupted fins have been mostly studied for internal natural convection or staggered fin arrangement. This type of fin is a more general form, and it can include both continuous fin as the gap length approaches zero, or pin fin as the fin length approaches the fin thickness. At a closer look, continuous fins and pin fins are two extreme cases of the interrupted fins which are the target of this study. The present thesis aims to address the literature's shortcoming by investigating the effect of adding interruptions to a single wall or to a fin array, on natural convection heat transfer. The goals of this study can be summarized as below;

- To develop in depth understanding of external laminar natural convection from interrupted single walls, and formulate heat transfer from the geometry
- To provide deeper information compared to what is currently available, for laminar natural convection from parallel plates and formulate the flow behavior in such problems
- To establish a deep understanding of air flow and heat transfer in external laminar natural convection from heatsinks with interrupted fins
- To develop a design tool for high performance heatsinks
- To find the optimum fin arrangement for heatsinks to maximize the total heat transfer

Chapter 2.

Natural Convection from Interrupted Vertical Walls

Steady-state external natural convection heat transfer from interrupted rectangular vertical walls is investigated in this chapter. A systematic numerical, experimental, and analytical study is conducted on the effect of adding interruptions to a vertical plate. COMSOL Multiphysics is used to develop a two dimensional numerical model for investigation of fin interruption effects on natural convection. A custom-designed testbed is built and six interrupted wall samples are machined from aluminum, and tested to verify the numerical results. An effective length is introduced for calculating the natural convection heat transfer from interrupted vertical walls. Performing an asymptotic analysis and using a blending technique, a new compact relationship is proposed for the Nusselt number. Our results show that adding interruptions to a vertical wall can enhance heat transfer rate up to 16% and reduce the weight of the fins, which in turn, lead to lower manufacturing and material costs.

Interruptions are discontinuities added in vertical walls to postpone the thermal boundary layer emergence in the channel flow between two adjacent walls; thus increase the total heat transfer rate [57]. A schematic for interrupted wall is shown in Figure 2.1. It should be noted that this arrangement is a more general form of geometry and includes both continuous and pin fins at the limit, where the interruption length approaches zero, or very large values, respectively. Fin interruption is common in industry and has been studied for internal natural convection [58] and forced convection [59]. However, as mentioned in Section 1.5, to the author's best knowledge, no comprehensive study is available for natural convection from interrupted walls.

The focus of this chapter is on the effects of fin length and interruption length. To study the natural convection heat transfer from interrupted walls, a new concept, "effective length", is introduced and a new compact relationship for the Nusselt number is developed based on non-dimensional geometrical parameters.

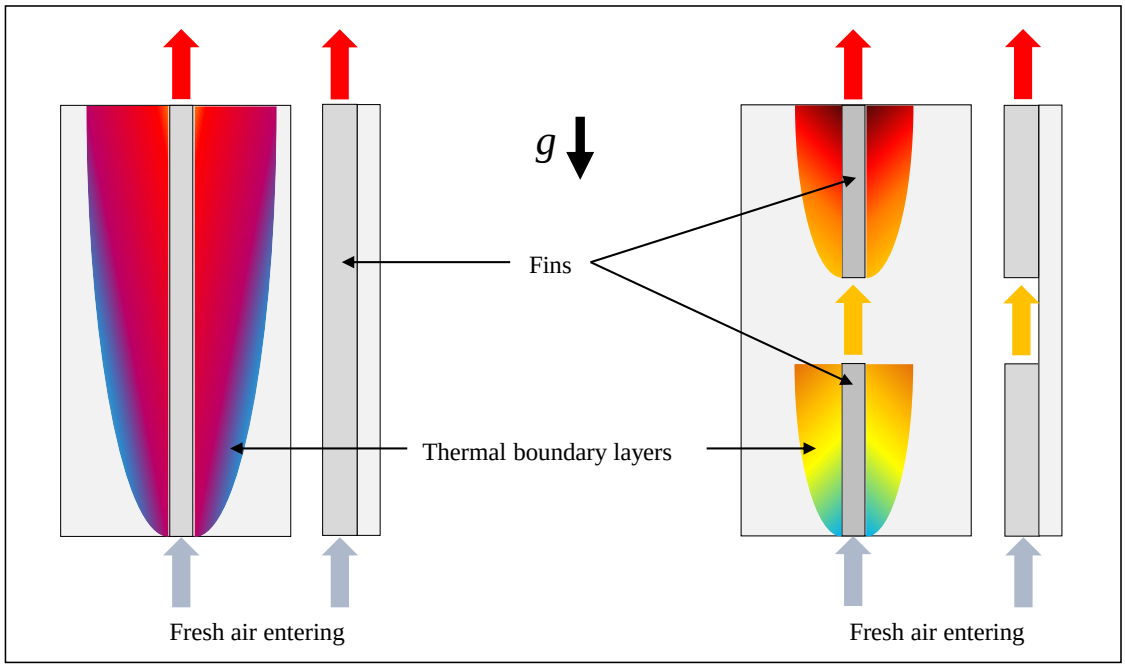

Figure 2.1. Effect of interruptions on boundary layer growth in natural heat transfer from a vertical wall

2.1. Numerical Analysis

2.1.1. Governing Equations

We seek a solution for steady-state, laminar natural convection heat transfer from an isothermal vertically-mounted interrupted wall, as shown schematically in Figure 2.1. The conservation of mass, momentum and energy in the domain are based on assuming a fluid with constant properties and the Boussinesq approximation [60] for density;

$$\frac{\partial u}{\partial x}+\frac{\partial \upsilon}{\partial y}=0 \qquad 2.1$$

$$\rho\left(u\frac{\partial u}{\partial x}+\upsilon\frac{\partial u}{\partial y}\right)=-\frac{\partial P}{\partial x}+\mu\nabla^2 u-\rho g \qquad 2.2$$

$$\rho\left(u\frac{\partial \upsilon}{\partial x}+\upsilon\frac{\partial \upsilon}{\partial y}\right)=-\frac{\partial P}{\partial y}+\mu\nabla^2 \upsilon \qquad 2.3$$

$$u\frac{\partial T}{\partial x}+\upsilon\frac{\partial T}{\partial y}=\alpha\nabla^2 T \qquad 2.4$$

where y is the direction normal to the gravitational acceleration and x is the direction parallel to the gravitational acceleration, u and v are the velocity in *x*-direction and *y*-direction, respectively. Here $\rho, \mu,$ and α are the fluid's density, dynamic viscosity and thermal diffusivity, respectively.

Considering $\frac{\partial P}{\partial x} = \frac{\partial P_\infty}{\partial x}$, where P_∞ is the ambient hydrostatic pressure, and assuming Boussinesq approximation, Eq.2.2 yields to:

$$u\frac{\partial u}{\partial x} + \upsilon\frac{\partial u}{\partial y} = \nu\frac{\partial^2 u}{\partial x^2} + g\beta(T - T_\infty) \qquad 2.5$$

In our numerical simulations, the buoyancy term, $-\rho_\infty g\beta(T - T_\infty)$, is added to the momentum equations as a body force term. Kinematic viscosity, ν in Eq.2.5, is following Boussinesq approximation and can be defined as μ / ρ_∞. Pressure inlet, with gauge pressure set to zero, is applied to the bottom of the domain. For the top and right side of the domain outlet boundary condition is applied, which imposes a constant pressure, gauge pressure of zero in case of our problem. Symmetry boundary condition was chosen for the gap region. This type of boundary condition is equivalent to a no-heat flux in the direction normal to the boundary plane. No-slip isothermal solid surface is considered as the boundary condition for the walls. Figure 2.2.a shows a schematic of the domain considered for the numerical simulation, along with the chosen boundary conditions for the fins. COMSOL Multiphysics 4.3 has been employed for mesh generation and to solve the above-mentioned system of partial differential equations.

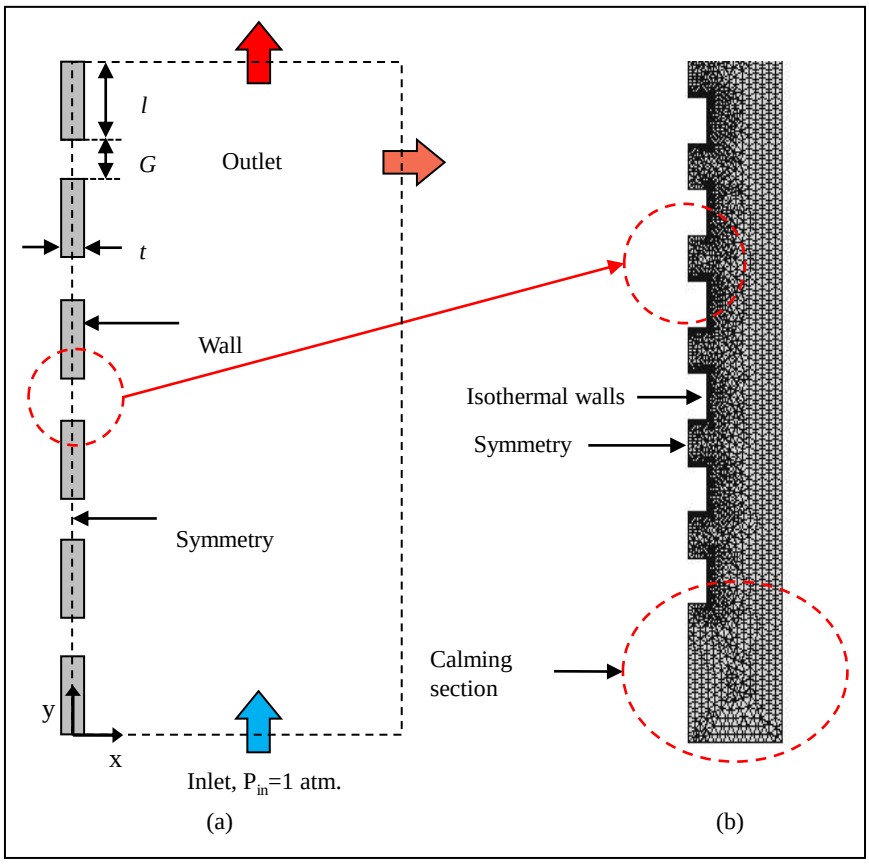

Figure 2.2. **a) Schematic of the numerical domain and boundary conditions for vertical interrupted wall, b) grid used in the model for interrupted wall**

2.1.2. Mesh Independency

For simulating the heat transfer in the fins, a 2D model is created in COMSOL Multiphysics 4.3, by coupling the fluid flow and heat transfer modules. As mentioned in Section 2.1.1, the coupling has been done by adding the Boussinesq buoyancy term to the momentum equation. Boussinesq assumption relates the fluid density to its temperature with a linear approximation in buoyancy term, and uses the fluid density at ambient temperature in convective term of momentum equation. Finer grid size has been used near the fin surface to resolve the boundary layer with enhanced accuracy. Increasingly, coarser mesh was chosen in the regions far from the walls in order to reduce the computational time (see Figure 2.2.b). Five different numbers of mesh elements are used for the benchmark cases and compared in terms of average heat flux from the walls to ensure a mesh-independent solution. The parameters chosen for the benchmark case

are shown in Table 2.1. Accordingly, for the mesh number of approximately 45,000, we found that the simulation gives approximately 0.01% deviation in average heat transfer rate from walls as compared to the simulation of fins with mesh number of 65,000, while for the number of elements less than 6,500, the model does not converge to a reasonable solution. Figure 2.3 shows the mesh independency analysis for the benchmark case. As the figure shows, the results are not too sensitive to the grid size, and the wall heat flux ranges from 332.5 W/m^2 for 6,500 elements to approximately 333.3 W/m^2 for 68,000 elements.

Table 2.1. Parameters used in the benchmark case for numerical simulations

Parameter	Description	Value	Unit
l	Fin length	5	[cm]
G	Gap length	2	[cm]
t	Fin thickness	1	[cm]
T_∞	Ambient	20	[°C]
T_w	Wall temperature	60	[°C]
m	Number of fins	5	-

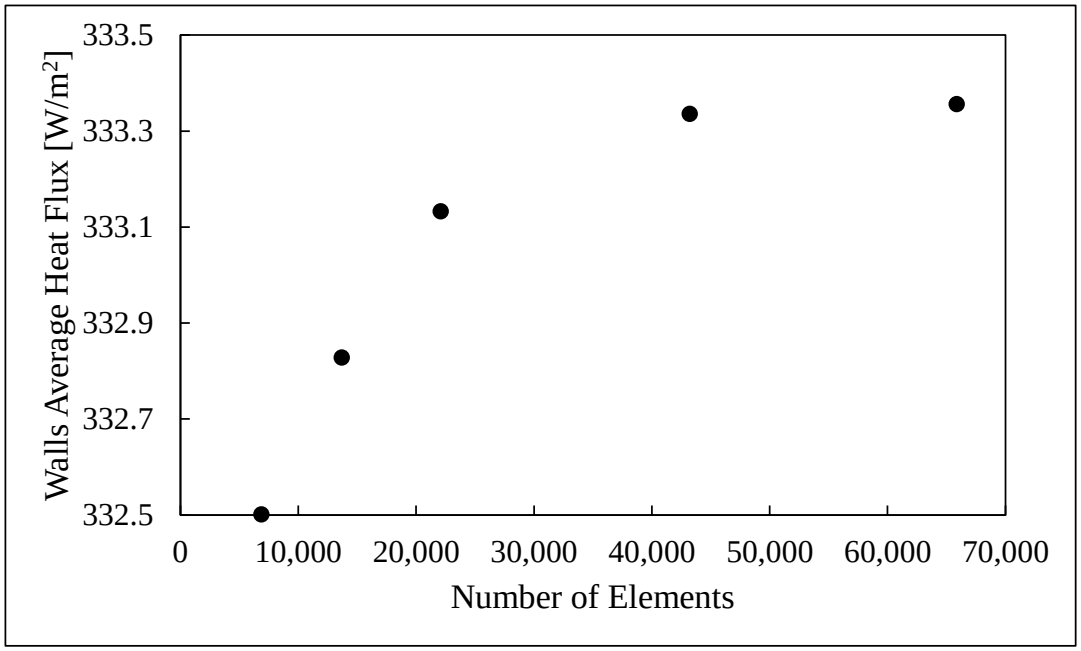

Figure 2.3. Grid independency study; walls average heat flux versus number of elements for the benchmark case (see Table 2.1)

The velocity and temperature domains are shown as results of the benchmark numerical studies in Figure 2.4. As shown in the figure, the diffusion of velocity and temperature in the gap region causes the air to reach the higher fin with higher velocity and lower temperature. This interruption in hydrodynamic and thermal boundary layers is the main cause for the improvement of heat transfer from the fins.

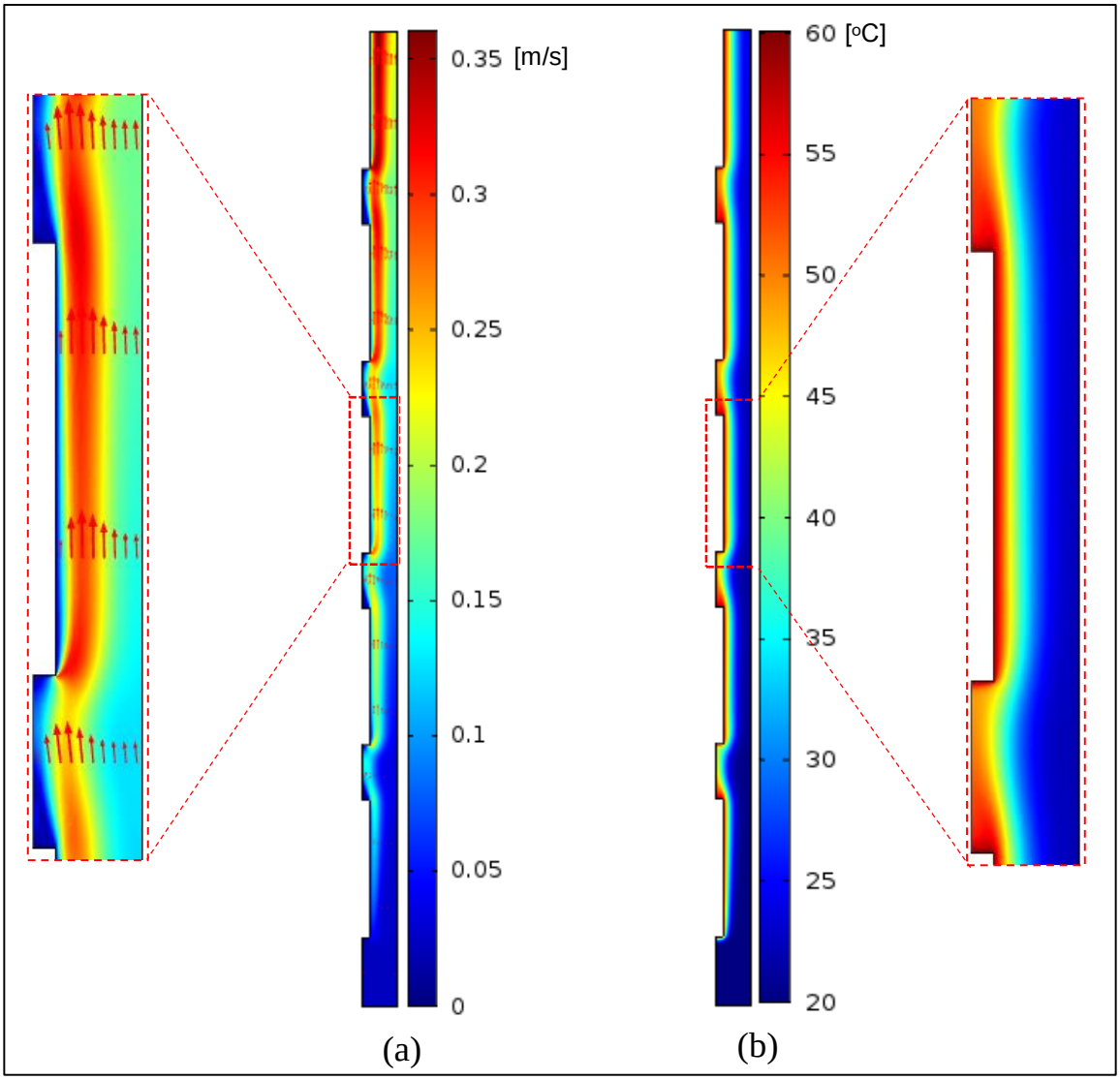

Figure 2.4. **a) velocity domain, and b) temperature domain for the benchmark case; the diffusion of velocity and temperature in the gap causes the air to reach the top wall with higher velocity and lower temperature**

2.2. Experimental Study

The objective of the experimental study is to investigate the effects of interruption length on the natural convection heat transfer from interrupted vertical walls, and also to validate the results from numerical simulations and mathematical modeling. To achieve this goal, a custom-made testbed is designed and built, and six interrupted wall samples with various geometrical parameters are machined from extruded aluminum profiles. A series of tests with different surface temperatures are conducted. The details about the testbed design, test procedure, and uncertainty analysis are given in the proceeding sections.

2.2.1. Testbed

The testbed is designed to measure natural convection heat transfer from interrupted vertical walls, as shown in Figure 2.5.a. The set-up included a metal framework from which the samples are hung, and an enclosure made of compressed insulation foam with a thickness of 20mm to insulate the backside of the samples. Inside the foam enclosure is filled with glass-wool to ensure the minimum heat loss from the backside of the baseplate. As such, any form of heat transfer from the backside of baseplate is neglected in our data analysis. The setup also includes a power supply, two electrical heaters, attached to the backside of the baseplate, T-type thermocouples, and three Data acquisition (DAQ) systems. Thermal paste (Omegatherm®201) is used to minimize the thermal contact resistance between the heater and the baseplate.

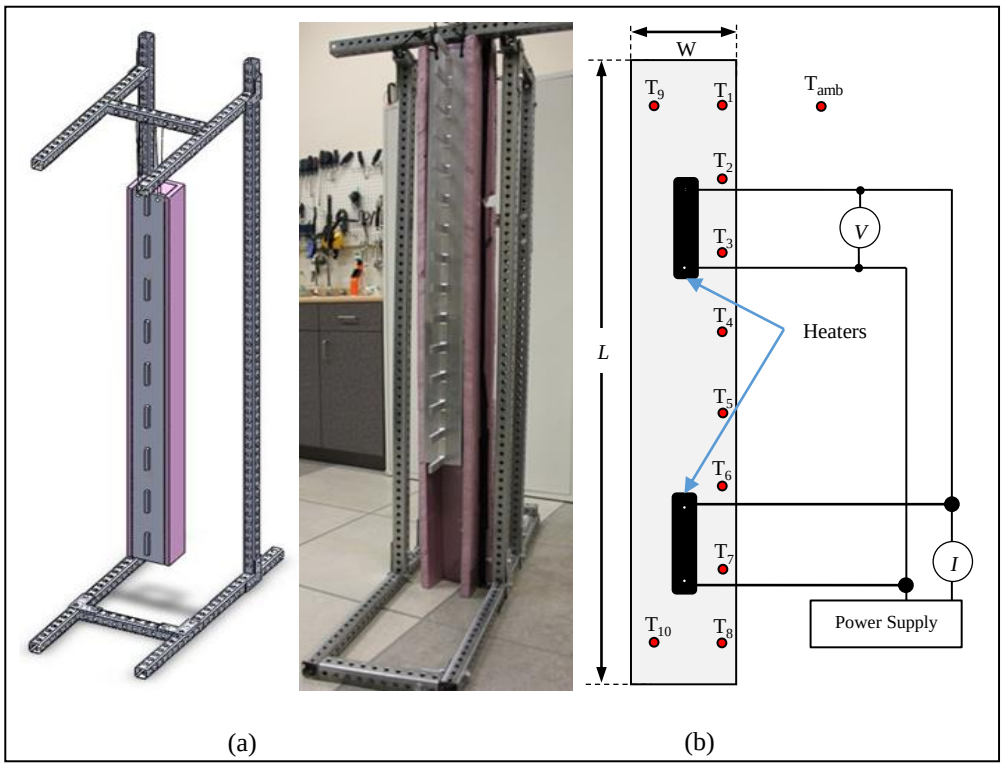

Figure 2.5. a) schematic and photo of the testbed; b) backside of the samples; positioning of the thermocouples and heater

Six heatsink samples with the same baseplate width but different fin and interruption lengths are prepared by machining extruded aluminium profiles. To fully investigate the effects of thermal boundary layer growth, different dimensions of the fins and interruptions are chosen, as listed in Table 2.2.

Table 2.2. Dimensions of the interrupted wall samples used in experimental study

Sample name #	*l* [mm]	m	*G* [mm]	*L* [m]	*G/l*	*l/t*
SW-1	50	14	50	1.35	1	5
SW-2	50	7	150	1.25	3	5
SW-3	50	10	100	1.40	2	5
SW-4	50	5	300	1.45	6	5
SW-5	50	10	150	1.85	3	5
SW-6	50	17	25	1.47	0.5	5

Note: The baseplate length is shown with *L*, and all the samples share baseplate width, *W* = 101 mm, fin height, *H* = 100 mm, and fin thickness, *t* = 10 mm.

2.2.2. Test Procedure

The experiments are performed in a windowless room with an environment free of air currents. The room dimensions are selected to be large enough to ensure constant ambient temperature during the test. The input power supplied to the heaters is monitored and surface temperatures are measured at various locations at the back of the baseplate. Electrical power is applied using a variable voltage transformer (Variac SC-20M), and using DAQ systems (National Instruments, NI9225 and NI9227), the voltage and the current are measured to determine the power input to the heater. Eight self-adhesive, copper-constantan thermocouples (Omega, T-type) are installed in various vertical locations on one side of the baseplate, as shown in Figure 2.5.b. Two extra thermocouples are installed on the same level with the highest and lowest thermocouples to make sure that the temperature is well distributed horizontally (T_9 and T_{10} in Figure 2.5.b). All thermocouples are taped down to the backside of the samples baseplate to prevent disturbing the buoyancy-driven air flow. One additional thermocouple is used to measure the ambient temperature during the experiments. Thermocouples are plugged into a DAQ system (National Instruments, NI9213). Temperature measurements are performed at ten points in order to monitor the temperature variation on the wall, and the average is taken as the baseplate temperature. Among all the experiments, the maximum standard deviation from the average temperature is 4˚C. Since the experiments are performed to mimic the uniform wall temperature boundary condition, the thickness of the baseplate and the fins are selected fairly high (10mm) to ensure the minimum thermal bulk resistance and uniform temperature distribution in the samples. An infrared camera (FLIR, SC655) is used to observe the temperature difference between the baseplate and the fins. The maximum measured difference between the fins and the baseplate is about 2˚C, so for the data reduction, the fins are assumed to be at the same temperature with the baseplate. For each of the six samples, the experimental procedure is repeated at various power inputs. The baseplate temperature, T_w, the ambient temperature, T_∞, and the heater power, p_{input}, are recorded at steady-state considering the power factor equals one. Table 2.3 lists the range of some important test parameters. The steady-state condition is considered to be achieved when the rate of all temperature variations is less than 0.1˚C/hr, which on average, takes 240 minutes from the start of the experiment.

Table 2.3. Range of important parameters in the experimental study

Parameter	Description	Range	Unit
m	Mass of the samples	1.2-2.1	[kg]
P	Heater power	30-150	[W]
T_∞	Ambient temperature	20-22	[°C]
T_w	Wall temperature	35-75	[°C]
Ra_l	Rayleigh number	105-108	-

For the data reduction, natural convection from the baseplate and fin tips are calculated using the available correlations in literature [19], and subtracted from total heat input to the system. Following Rao *et al*. [61], the effect of radiation heat transfer is also subtracted from the fins' total heat transfer (see Appendix B). Due to relatively low surface temperature and low emissivity of machined aluminum (between 0.09 and 0.1), the effect of radiation is not significant. The maximum calculated value for radiation heat transfer is 4.2% of total heat transfer from the sample.

2.2.3. Uncertainty Analysis

Voltage (V), and current (I), are the electrical parameters measured in our experiments, from which the input power (P), can be calculated (see Eq.2.6). The overall accuracy in the measurements is evaluated based on the accuracy of the measuring instruments, mentioned in Section 2.2.2. The accuracy of the voltage and current readings are 3% for both parameters, based on suppliers' information. The reported accuracy values are given with respect to the instruments readings, and not the maximum range of measurement. The maximum uncertainty for the measurements can be obtained using the uncertainty analysis method provided in [62]. To calculate the uncertainty with the experimental measurements the following relation is used [62]:

$$\omega_R = \left[\sum \left(\frac{\partial R}{\partial x_i} \omega_i \right)^2 \right]^{\frac{1}{2}} \qquad 2.6$$

where ω_R is the uncertainty in the general function of $R(x_1, x_2 ... x_n)$, and ω_i is the uncertainty of the independent variable x_i. The final form of the uncertainty for the input power becomes;

$$P = V\,I \tag{2.7}$$

$$\frac{\delta P}{P} = \left[\left(\frac{\delta V}{V} \right)^2 + \left(\frac{\delta I}{I} \right)^2 \right]^{\frac{1}{2}} \tag{2.8}$$

$$\frac{\delta \dot{Q}_{Rad.}}{\dot{Q}_{Rad.}} = \left[\left(4\frac{\delta T_w}{T_w} \right)^2 + \left(4\frac{\delta T_\infty}{T_\infty} \right)^2 + \left(\frac{\delta l}{l} \right)^2 + \left(\frac{\delta H}{H} \right)^2 + \left(\frac{\delta t}{t} \right)^2 \right]^{\frac{1}{2}} \tag{2.9}$$

$$\dot{Q}_{N.C.}[W] = P - \dot{Q}_{Rad.} \tag{2.10}$$

Substituting the values for $V, I, T_w, T_\infty, l, H$, and t into Eqs. 2.8 and 2.9, the maximum uncertainty value for $\dot{Q}_{NC}$ is calculated to be 8%. The measured temperature uncertainty ΔT is $\pm 1°C$. To calculate the heat transfer coefficient from measured $\dot{Q}_{N.C.}$ and ΔT, Eq. 2.11 can be used

$$h = \frac{\dot{Q}_{N.C.}}{A\Delta T} \tag{2.11}$$

so;

$$\frac{\delta h}{h} = \left[\left(\frac{\delta T_w}{T_w} \right)^2 + \left(\frac{\delta T_\infty}{T_\infty} \right)^2 + \left(\frac{\delta l}{l} \right)^2 + \left(\frac{\delta H}{H} \right)^2 + \left(\frac{\delta \dot{Q}_{N.C.}}{\dot{Q}_{N.C.}} \right)^2 \right]^{\frac{1}{2}} \tag{2.12}$$

For the calculation of Nusselt number, effective length, $L_{eff.}$, is used as the characteristic length, and since it is not measured, $L_{eff.}$ is not included in uncertainty analysis. Thermophysical properties such as thermal conductivity of air are also assumed to be constant. Table 2.4 shows a list of parameters used in the uncertainty analysis with their calculated value. The amount of uncertainty for Nusselt number, which is calculated to be 10%, is shown as error bars on experimental data.

Table 2.4. The uncertainty analysis parameters

Parameter	Maximum uncertainty
$\delta V/V$	0.3%
$\delta I/I$	0.3%
$\delta P/P$	0.4%
δT	±1[˚C]
δH	0.1 [mm]
δl	0.1 [mm]
δt	0.1 [mm]
$\delta \dot{Q}_{Rad.}/\dot{Q}_{Rad.}$	7.5%
$\delta \dot{Q}_{N.C.}/\dot{Q}_{N.C.}$	8%

2.3. Results and Discussion

In this section, a new concept called “effective fin length” is introduced to calculate the Nusselt number for the natural convection heat transfer along the interrupted vertical fins. The effective length is obtained through equating the heat transfer rate from the actual interrupted wall with an imaginary continuous vertical wall, with the length of $L_{eff.}$. Natural convection heat transfer from an isothermal vertical wall is a well-known subject in the literature and can be calculated from the following relationship [63]:

$$Nu_{L_{eff.}} = 0.59\left(Ra_{L_{eff.}}\right)^{\frac{1}{4}} \qquad 2.13$$

knowing that

$$Nu_{L_{eff.}} = \frac{h L_{eff.}}{k} \qquad 2.14$$

substituting $h = \frac{\dot{Q}_{N.C.}}{A\Delta T}$ into Eq. 2.14 and using Eq. 2.14, one can find;

$$L_{eff} = \left(\frac{\dot{Q}}{0.59\,k} \right)^2 \left(\frac{\alpha \nu}{g \beta} \right)^{\frac{1}{2}} \Delta T^{-\frac{5}{2}} \qquad 2.15$$

we also introduce ζ and γ, as follows;

$$\zeta = \frac{l}{t} \qquad 2.16$$

$$\kappa = \frac{G}{l} \qquad 2.17$$

In order to develop a general model for all ranges of κ, two asymptotes are recognized and a blending technique [64] is implemented to develop a compact relationship for the effective length and the corresponding Nusselt number. The first asymptote is developed for small values of κ, where $\kappa \to 0$, for which the flow behaviour resembles the flow over a vertical wall that has no interruptions with a total length of

$$L = m\,l \qquad 2.18$$

where m is the number of fin rows. For the first asymptote, $\kappa \to 0$, the effective length is correlated using the present numerical results.

$$\frac{L_{eff.,\kappa \to 0}}{m\,l} = 0.22\,\kappa + 1 \qquad 2.19$$

The second asymptote is when $\kappa \to \infty$, which is the limiting case where the fins are located far enough from each other and they act as an individual single wall. In other words, each fin's flow/heat transfer pattern will not get affected by the fins located at the bottom. For this asymptote, $\kappa \to \infty$, Eqs. 2.20 to 2.23, available in literature [16,65], are used to calculate the heat transfer from the wall. Natural convection heat transfer from the walls in this asymptote is the summation of heat transfer from all sides of the fin (bottom, two sides and the top surface). The relationships used for calculating the heat transfer from the top, bottom, and sides of the wall are given in [66].

$$\dot{Q}_{total} = \dot{Q}_{ends} + \dot{Q}_{sides} \qquad 2.20$$

$$Nu_{sides} = Nu_l = 0.59 Ra_l^{\frac{1}{4}} \qquad 2.21$$

$$Nu_{top} = 0.56 Ra_t^{\frac{1}{4}} \tag{2.22}$$

$$Nu_{bottom} = 0.27 Ra_t^{\frac{1}{4}} \tag{2.23}$$

Natural convection heat transfer, calculated from the above equations, should be substituted in Eq. 2.15 to give the $L_{eff.}$ for larger values of κ, i.e. $L_{eff.,\kappa\to\infty}$. As a result, for the top, bottom and sides of the wall, we can calculate the ratio of $L_{eff.}/ml$ as:

$$\frac{L_{eff.,\kappa\to\infty}}{ml} = m^{\frac{1}{3}}\left[0.83\left(\frac{1}{\zeta}\right)^{\frac{3}{4}}+1\right]^{\frac{4}{3}} \tag{2.24}$$

Having $L_{eff,\kappa\to\infty}$ and $L_{eff,\kappa\to 0}$ known, a compact relationship for L_{eff} can be developed using a blending technique, introduced by Churchill and Usagi [64];

$$L_{eff} = \left[\left(L_{eff,\gamma\to 0}\right)^c + \left(L_{eff,\gamma\to\infty}\right)^c\right]^{\frac{1}{c}} \tag{2.25}$$

where c is a fitting parameter, and its value is found by comparison with the present numerical data; the best fit is found for $c=-3$. This fitting parameter is found by minimizing the maximum difference between the model and the numerical data. $Nu_{L_{eff}}$ is calculated by substituting L_{eff} into Eq. 2.14. The final relationship is a function of, $\kappa, \zeta, m,$ and Ra, which in turn, is a function of temperature difference, as shown below:

$$Nu_{L_{eff.}} = \frac{hL_{eff.}}{k} = 0.59 Ra_l^{\frac{1}{4}} m^{\frac{3}{4}} \left\{ \left(0.22\kappa+1\right)^{-3} + \left[m\left(0.83\left(\frac{1}{\zeta}\right)^{\frac{3}{4}}+1\right)^4\right]^{-1}\right\}^{-\frac{1}{4}}, 5 \le \zeta \le 15 \tag{2.26}$$

where l is the fin length, ζ is the aspect ratio of the fin, m is the number of fin rows, and Ra_l is the Rayleigh number based on fin length.

Figure 2.6 shows the asymptotic behaviour of the natural convection from interrupted vertical walls for the two discussed limiting ranges of κ. Two different trends

can be seen in the present data, for the extreme values of κ. The first trend shows small values of κ, related to a long vertical wall, the region in which the data collapses into a straight line. The second trend corresponds to very large values of κ, related to a short fin with $L_{eff.} = l$, where the data approaches a horizontal asymptote.

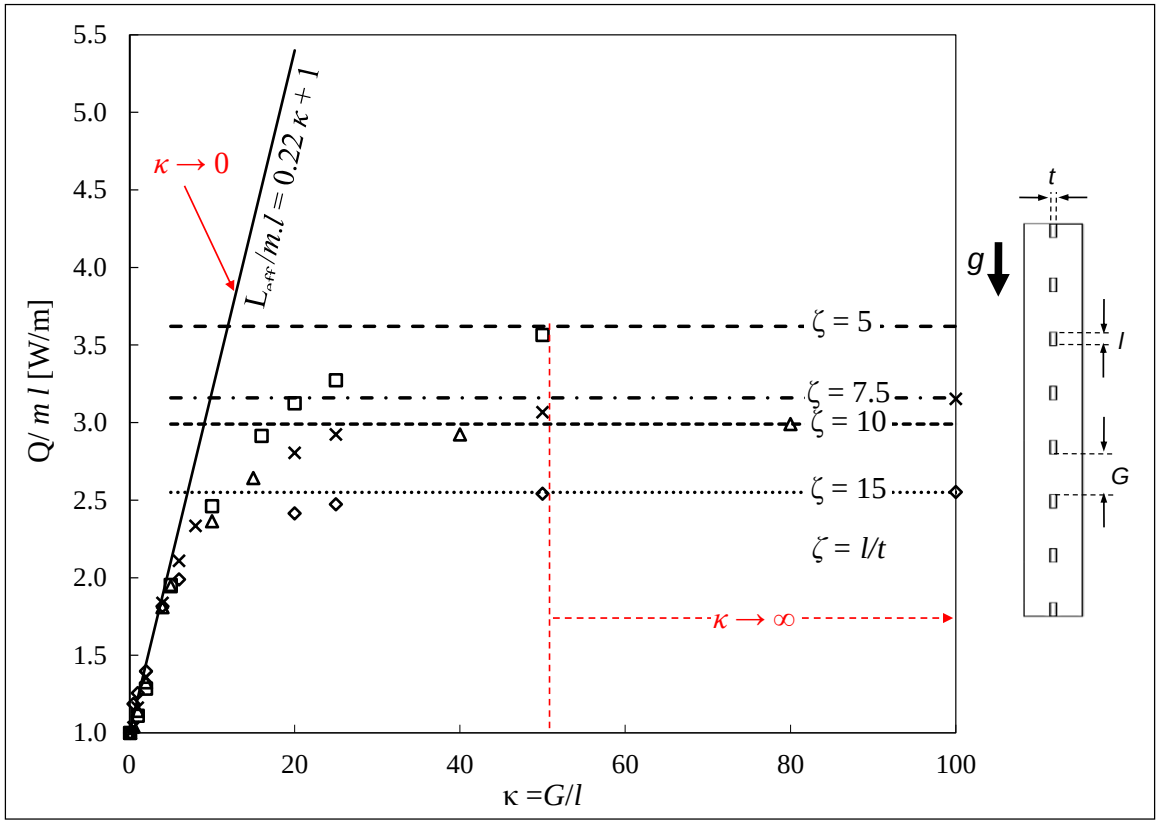

Figure 2.6. Heat transfer versus $\kappa(G/l)$ for different $\zeta(l/t)$ values. The figure also shows the comparison between the numerical data (symbols) and introduced asymptotes (Lines).

Figure 2.7 shows dimensionless form of the proposed effective length, calculated using numerical data, as a function of κ. Asymptotic behavior of the effective length can be observed in the numerical data. We developed a new compact correlation for the effective length using the blending technique [64] as follows;

$$\frac{L_{eff.}}{ml}=\left\{\left[0.22\kappa+1\right]^{-3}+\left[m^{\frac{1}{3}}\left(0.83\left(\frac{1}{\zeta}\right)^{\frac{3}{4}}+1\right)^{\frac{3}{4}}\right]^{-3}\right\}^{-\frac{1}{3}} \qquad 2.27$$

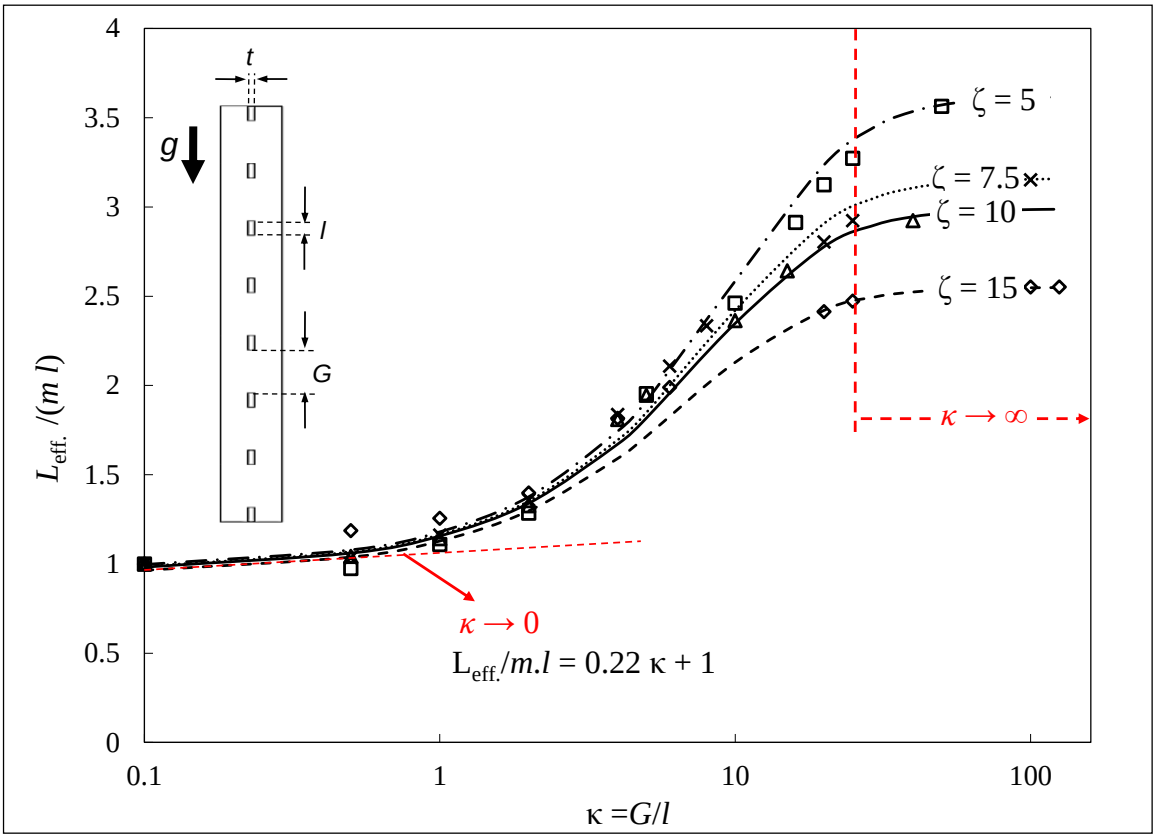

Figure 2.7. Effective length versus $\kappa(G/l)$ for different $\zeta(l/t)$ values. The figure also shows the comparison between the numerical data (symbols) and the proposed correlation (lines) for the effective length.

To calculate the Nusselt number from the numerical data, the average wall heat flux is obtained from the numerical simulations and having the wall and ambient temperature, the heat transfer coefficient is calculated. Using the heat transfer coefficient, the calculated effective length, and thermal conductivity of the air, the numerical Nusselt number is calculated. This allows developing a new compact correlation for Nusselt number based on the effective length, characterizing the natural convection heat transfer from interrupted vertical walls (Eq. 2.26). This Nusselt number can be used to calculate the heat transfer rate for any rectangular interrupted fin in the range of $5 \le \zeta \le 15$. The

parameter l/t represents the aspect ratio or slenderness of the fins. For $l/t<5$, the fin geometry will become closer to a cuboid/pin fin and the correlations used to calculate the heat transfer are no longer valid. Also for $l/t>15$, the fins will be too long and the effect of fin thickness will be negligible. The effect of fin thickness is considered in our calculations and appears in Eqs. 2.26 and 2.27.

In Figure 2.8, the experimental data obtained from the interrupted vertical wall samples, is compared against the proposed new relationship for the Nusselt number Eq. 2.26. Figure 2.8 also shows that the numerical simulation results are in very good agreement with experimental data. As can be seen, the proposed compact relationship is in very good agreement with both experimental and numerical results. The average relative difference between the proposed correlation and the experimental data is approximately 9% and the maximum relative difference is 15%.

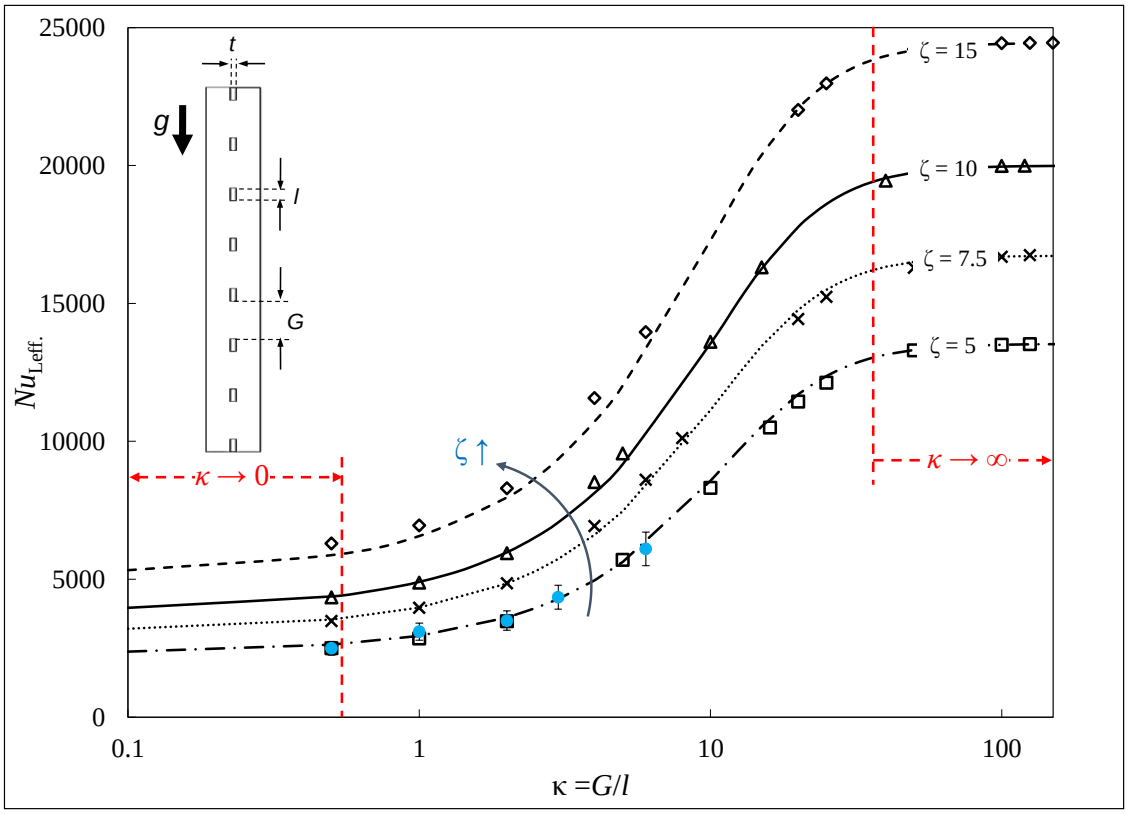

Figure 2.8. Nusselt number versus $\kappa(G/l)$ for different $\zeta(l/t)$ values. The figure also shows the comparison between the numerical data (hollow symbols), experimental data (solid blue symbols), and the proposed compact relationship (lines)

2.4. Conclusion

Experimental, numerical and analytical studies were performed to develop a compact correlation for natural convection heat transfer from vertical interrupted walls. The effects of interruption length in natural convection were thoroughly investigated. A comprehensive numerical modeling was performed using COMSOL Multiphysics. A custom-designed testbed was built and six aluminum interrupted wall samples were prepared and tested to verify the developed numerical and analytical models over the entire range of interrupted fin parameters. The collected data were successfully compared with the present numerical and analytical models. A new compact relationship was developed for the Nusselt number for natural convection heat transfer from interrupted fins using a blending technique, based on the non-dimensional geometrical parameters $\kappa(G/l)$ and $\zeta(l/t)$. This relationship can be used for calculating heat transfer rate for any rectangular interrupted fin in the range $\text{of } 5 \le \zeta \le 15$. The comparison of our experimental data to the available data in the literature [63], shows that with the similar baseplate dimensions, adding interruption to a single wall can improve the heat dissipation up to 16% compared to a continuous vertical wall.

Chapter 3.

Natural Convection from Vertical Parallel Plates

Steady-state external laminar natural convection heat transfer from isothermal vertical parallel fins is modeled analytically in this chapter. Integral technique is used to solve the governing equations. Compact relationships are developed for the velocity and temperature profiles for the buoyancy-driven channel flow for $100 \le Ra_l \le 4500$ range. Comprehensive numerical and experimental studies are performed, and the proposed analytical model is successfully validated against the numerical data with the maximum relative differences of 9.8% and 3.5% for velocity and temperature profiles, respectively. Also new closed-form correlation for local and average Nusselt numbers, as functions of Rayleigh number, temperature difference and fin aspect ratio are reported, and validated against the experimental data with 1.6% maximum relative difference.

3.1. Problem Statement

The main objective of this study is to develop a compact, analytical model that can predict the natural convection heat transfer from a squared array of vertically-mounted rectangular isothermal fins (see Figure 3.1). Figure 3.1.b schematically shows the front view of the considered geometry for two fins in the fin array. Due to symmetry, only one channel is needed to represent the entire fin array. The assumptions used in this study are listed below;

- Steady-state 2D heat transfer and fluid flow (fins are assumed long enough in the direction normal to the surface)
- Laminar flow
- Isothermal walls, at T_w
- Constant thermo-physical properties, except for the fluid density
- Boussinesq approximation for change of density as function of temperature [60].

It is assumed that the fin height in *z*-direction is large enough that the effects of baseplate can be neglected and the problem can be treated as a two dimensional flow.

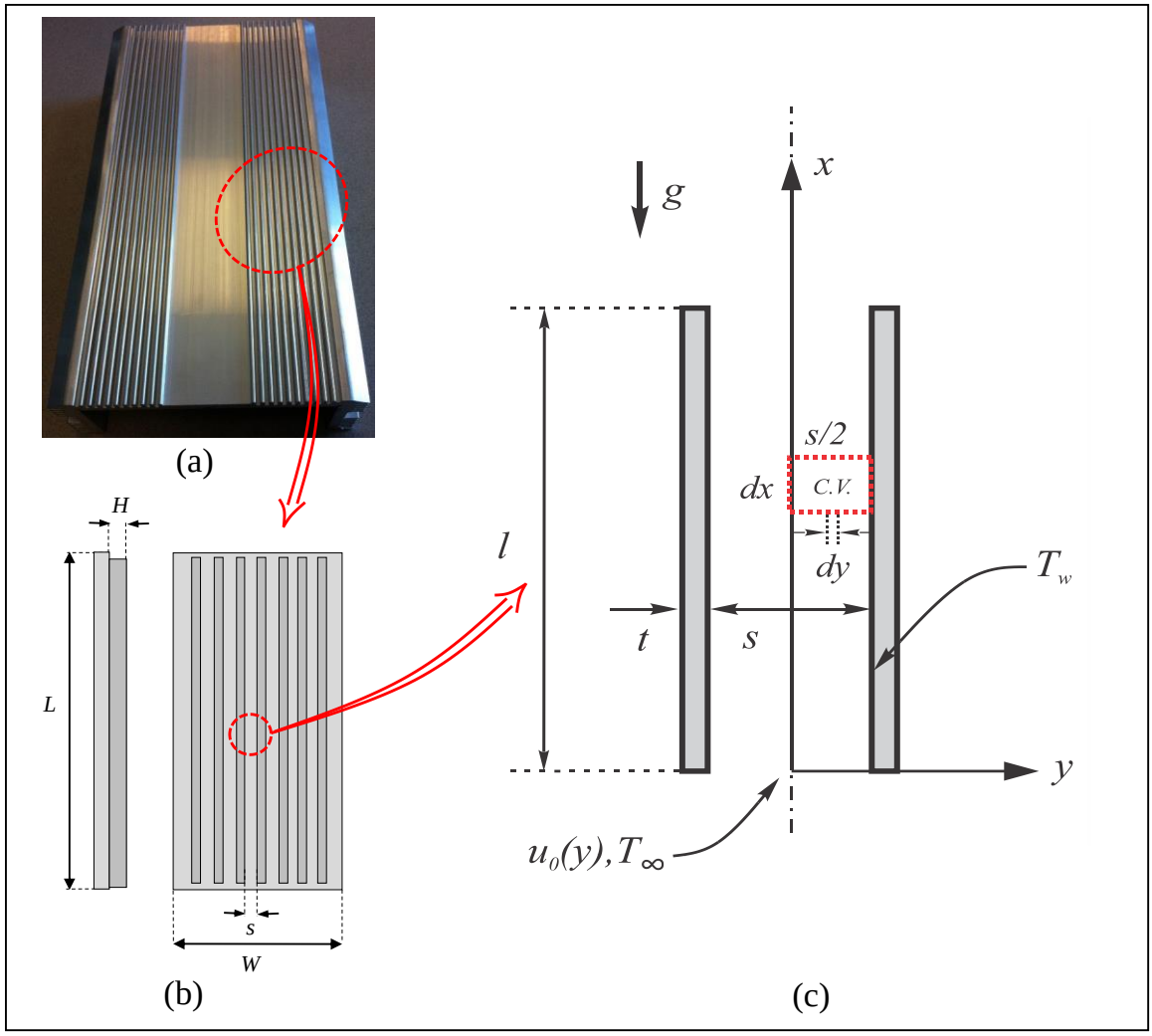

Figure 3.1. a) a naturally-cooled enclosure of a power converter; b) schematic of the heatsink, and c) solution domain, selected as the control volume

3.1.1. Governing Equations and Boundary Conditions

Integral technique is used to solve the governing equations subjected to constant wall temperature boundary conditions. Integral technique is a powerful analysis method developed by Pohlhausen and Von Karman in the first decade of twentieth century to obtain approximate solutions to complex problems [60]. It works based on the principle that the general behavior of the velocity and temperature profiles are known. Assuming a

profile for each, and satisfying conservation of mass, momentum, and energy in a lumped fashion across the region of interest, we can obtain velocity and temperature profiles within an acceptable accuracy by satisfying the boundary conditions. The conservation laws can be written for the control volume shown in Figure 3.1.c. Table 3.1 summarizes the integral form of momentum and energy balance equations for the considered integral control volume. To find more details about the methodology to obtain the governing equations from the control volumes shown in Table 3.1, readers are invited to see Appendix A. The conservation equations are subjected to the following boundary conditions;

at $y = 0$ $$\frac{\partial u(x,0)}{\partial y} = \frac{\partial T(x,0)}{\partial y} = 0 \quad (3.1)$$

at $y = s/2$ $$u(x, \frac{s}{2}) = 0 \quad and \quad T(x, \frac{s}{2}) = T_w \quad (3.2)$$

at $x = 0$ $$u(0, y) = u_{in}(y) \quad and \quad T(0, y) = T_\infty \quad (3.3)$$

as $x \to \infty$ $$u(x \to \infty, y) = u_{F.D.}(y) \quad and \quad T(x \to \infty, y) = T_w \quad (3.4)$$

Equation 3.1 is concluded from the symmetry at the centerline of the channel. The parameter $u_{in}(y)$ represents the velocity profile at the channel inlet and will be discussed later in Section 3.2.1. It should be noted that the velocity at the channel inlet cannot be zero, since the velocity has a non-zero profile at the channel outlet, and conservation of mass implies that the velocity should have a non-zero profile in the inlet.

Table 3.1. Integral form of conservation equations for the integral control volume

Equation	Schematic of C.V.	Terms description	Conservation equation
Momentum	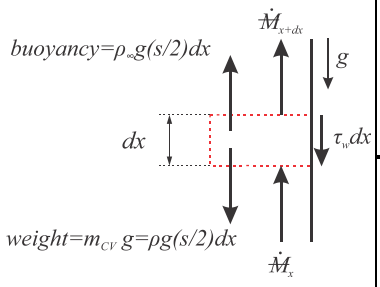	$\dot{M}_x = 2\rho\int_0^{s/2} u^2(x,y)dy$ $\dot{M}_{(x+dx)} = 2\rho\int_0^{s/2} u^2(x,y)dy$ $+\frac{\partial}{\partial x}(2\rho\int_0^{s/2} u^2(x,y)dy)$	$\frac{\partial}{\partial x}\int_0^{s/2} u^2(x,y)dy + \frac{\tau_w}{\rho}$ $=$ $g\beta\int_0^{s/2}\left(T(x,y)-T_\infty\right)dy$
Energy	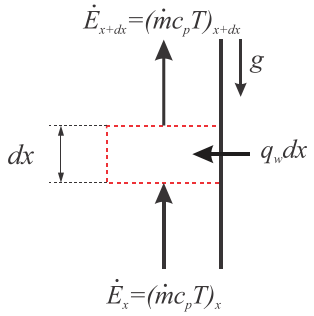	$\dot{E}_x = 2c_p\rho\int_0^{s/2} u(x,y)T(x,y)dy$ $\dot{E}_{(x+dx)} = 2c_p\rho\int_0^{s/2} u(x,y)T(x,y)dy$ $+\frac{\partial}{\partial x}(2c_p\rho\int_0^{s/2} u(x,y)T(x,y)dy)$	$\frac{\partial}{\partial x}\int_0^{s/2} u(x,y)T(x,y)dy$ $=$ $\frac{q_w}{c_p}$

Note: The buoyancy and weight forces are written for the unit depth.

3.2. Present Solution

The first step, before solving the governing equations, is to determine the velocity profile at the inlet of the channel, $x = 0$ (Eq. 3.3). The following section presents the details on how $u_{in}(y)$ can be obtained.

3.2.1. Entrance Velocity

To find the velocity profile at $x = 0$, conservation of mass can be written for a control volume enclosing the entire domain between the fins, as shown in Eq. 3.5. If the channel is long enough so that the velocity reaches fully-developed condition, the fluid temperature will be equal to the wall temperature [60]. Since the cross section area is

constant and fluid enters the channel with the ambient temperature, mass balance can be written as:

$$\rho\big|_{T=T_w} u_{F.D.}(y) = \rho_\infty u_{in}(y) \qquad 3.5$$

The fully-developed velocity profile at the outlet of parallel fins is known [60];

$$u_{F.D.}(y) = \frac{g\beta\Delta T s^2}{8\nu}\left(1-\frac{4y^2}{s^2}\right) \qquad 3.6$$

Equation 3.5 is the conservation of mass between the inlet and outlet of the channel. To find the density at the outlet which is assumed to be at the wall temperature, a linear approximation can be used similar to the assumption made in Boussinesq approximation;

$$\rho(T) = \rho_\infty\left[1-\beta\left(T-T_\infty\right)\right] \qquad 3.7$$

Substituting T_w for T in Eq. 3.7 and substituting the result in Eq. 3.5, $u_{in}(y)$ can be found as;

$$u_{in}(y) = \frac{\left(1-\beta\Delta T\right)\Delta T g\beta s^2}{8\nu}\left(1-\frac{4y^2}{s^2}\right) \qquad 3.8$$

Now, all the boundary conditions are known, and integral technique can be implemented to find the velocity and temperature profiles in the channel, as discussed in the following section.

3.2.2. Integral Technique

A second order polynomial in the *y*-direction is assumed for both temperature and velocity profiles;

$$u(x,y) = a_1(x)y^2 + b_1(x)y + c_1(x) \qquad 3.9$$

$$\mathrm{T}(x,y) = a_2(x)y^2 + b_2(x)y + c_2(x) \qquad 3.10$$

Applying the boundary conditions in the *y*-direction (Eqs. 3.1 and 3.2), into Eqs. 3.9 and 3.10, we will have;

$$u(x,y) = f(x)\left(y^2 - \frac{s^2}{4}\right) \tag{3.11}$$

$$T(x,y) = g(x)\left(y^2 - \frac{s^2}{4}\right) + T_w \tag{3.12}$$

Both $f(x)$ and $g(x)$ are unknown functions to be found, and can be interpreted as the velocity and temperature at the centerline of the channel along the *x*-direction. Physics of the flow and heat transfer suggest that both velocity and temperature at centerline would increase rapidly at the beginning of the channel (entry region), and approach an asymptotic value as the fluid moves along the *x* axis (fully developed flow). Using similarity solution technique for buoyancy-driven flow, Sparrow and Gregg [67,68] showed the temperature variation that gives rise to a similarity in the laminar boundary layer governing equations is either a power law or exponential distributions. Similar assumptions have been made by Gebhart *et al.* [69,70] for solving natural convection heat transfer equations in buoyancy induced flow over an adiabatic vertical surface and laminar natural convection plume above a horizontal line heat source. Therefore, a general exponential behavior can be assumed for $f(x)$ and $g(x)$, as follows:

$$f(x) = -\frac{s^2}{4}\left(\chi - \psi e^{-\lambda x}\right) \tag{3.13}$$

$$\mathrm{g}(x) = -\frac{s^2}{4}\left(\eta - \delta e^{-\gamma x} - T_w\right) \tag{3.14}$$

where $\chi, \psi, \lambda, \eta, \delta,$ and γ are constants that should be determined. The coefficient $-s^2/4$ in Eqs. 3.13 and 3.14 and T_w in Eq. 3.14, are added for convenience and have no effect on the generality of the solution. Having Eq. 3.8, substituting Eqs. 3.13 and 3.14 into Eqs. 3.11 and 3.12, and applying the boundary conditions in the *x*-direction, the parameters $\chi, \psi, \eta,$ and δ will be determined as bellow;

$$\chi = \frac{1}{8}\frac{g\beta\Delta T s^2}{\nu} \tag{3.15}$$

$$\psi = \frac{1}{8}\frac{g\beta^2\Delta T^2 s^2}{\nu} \tag{3.16}$$

$$\eta = T_w \tag{3.17}$$

$$\delta = \Delta T \tag{3.18}$$

Substituting the above calculated constants in Eqs. 3.11 and 3.12 and solving the integrated energy and momentum equations (Table 3.1), the two remaining constants, λ and γ can be obtained. After some mathematical manipulations, the velocity and temperature domain can be determined in the form of Eqs. 3.19 and 3.20.

$$u(x,y)=\frac{g\beta\Delta T}{4\nu}\left(\beta\Delta T\mathrm{e}^{-\frac{40\nu^2\left(3\beta\Delta T^2-4\Delta T\right)x}{g\beta^2 s^4\Delta T^3\left(1-\beta\Delta T\right)}}-1\right)\left(y^2-\frac{s^2}{4}\right) \qquad 3.19$$

$$T(x,y)=\frac{4\Delta T}{s^2}\mathrm{e}^{-\frac{120\alpha\nu x}{g\beta\Delta T s^4\left(1-\beta\Delta T\right)}}\left(y^2-\frac{s^2}{4}\right)+T_w \qquad 3.20$$

Eqs. 3.19 and 3.20 can be presented in a more compact form, after non-dimensionalizing by introducing the dimensionless parameters shown in Table 3.2.

Table 3.2. Dimensionless parameters

Parameter	Description
X	x/l
Y	y/s
U	us/α
θ	$\left(T_w-T\right)/\left(T_w-T_\infty\right)$
ε	l/s
Pr	ν/α
Gr_s	$g\beta\Delta T s^3/\nu^2$
Ra_s	$Gr_s\,\mathrm{Pr}$

Using dimensionless parameters, the velocity and temperature distribution inside the channel can be presented as;

$$U(X,Y)=-\frac{1}{4}Ra_s\left(1-\beta\Delta T\mathrm{e}^{-\frac{160\left(1-\frac{3}{4}\beta\Delta T\right)}{\beta\Delta T\left(1-\beta\Delta T\right)}\frac{\varepsilon X}{Gr_s}}\right)\left(Y^2-\frac{1}{4}\right) \qquad 3.21$$

$$\theta(X,Y) = 4\exp\left(-120\frac{\varepsilon X}{Ra_s(1-\beta\Delta T)}\right)\left(Y^2 - \frac{1}{4}\right) \qquad 3.22$$

3.3. Numerical Simulation

In order to validate the present analytical model, an independent 2-dimensional numerical model of the problem is developed in the commercially available software package, ANSYS FLUENT 14.0. In order to couple the momentum and energy equations and add the buoyancy effects to the simulation, Boussinesq approximation is imposed to the air density behavior as a function of temperature, and gravity effect is added to the domain as body force in negative *y*-direction. Figure 3.2.a shows a schematic of the domain considered for the numerical simulation, along with the boundary conditions assumed for the channel. Inlet atmospheric pressure and constant temperature, $T = T_\infty$, is applied at the bottom of the domain as the boundary condition. For the top of the domain, outlet pressure boundary condition is applied which imposes the pressure to be atmospheric pressure. No-slip, isothermal solid surface ($u = 0 \, and \, T = T_w$) is considered for the walls, and symmetry boundary condition is assumed for the centerline, which imposes no momentum and heat transfer, in the direction normal to the boundary. The parameters used for the benchmark case are shown in Table 3.3.

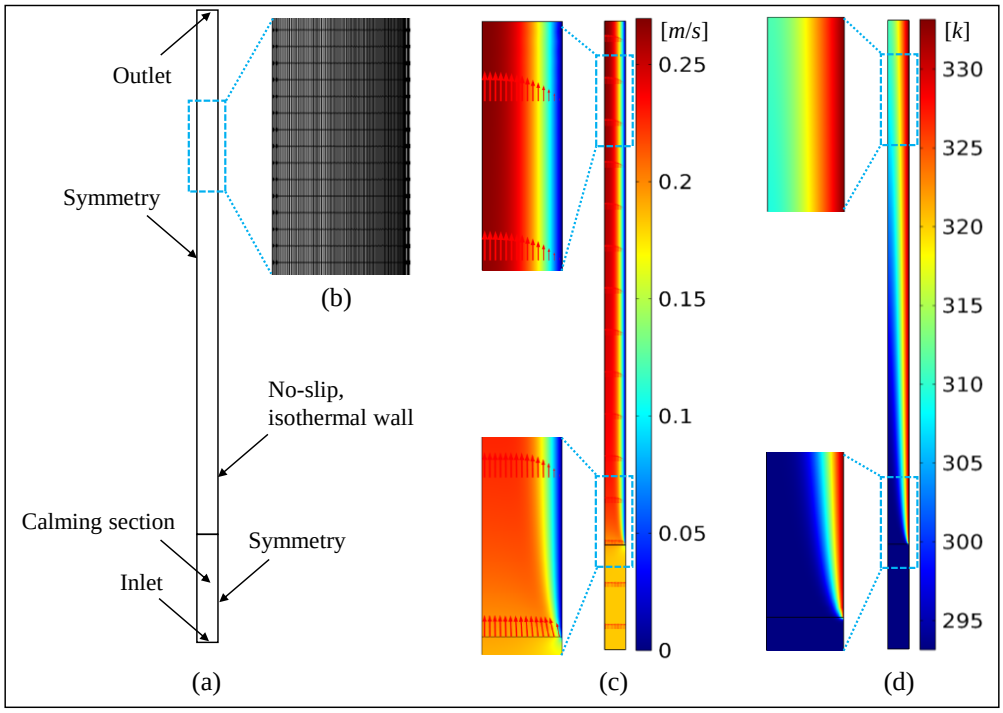

Figure 3.2. **a) schematic of the numerical domain and boundary conditions, b) the grid used in the model, c) velocity domain, and d) temperature domain for the benchmark case**

Table 3.3. **Parameters used for the numerical simulation benchmark**

Parameter	Description	Value	Unit
l	Wall length	10	[cm]
s	Wall spacing	8	[mm]
T_∞	Ambient temperature	20	[°C]
T_w	Wall temperature	60	[°C]
Ra_s	Rayleigh number	1700	-

To ensure a mesh independent solution, different grid sizes were tested and total heat transfer rate from the fins was chosen as monitoring parameter. Figure 3.3 shows the mesh independency analysis for the benchmark case. For the mesh number of approximately 900, we found that the simulation gives approximately 0.85% deviation in average heat transfer rate from walls compared to the simulation with mesh number of 3000, while for the number of elements less than 900 the model does not converge to a reasonable solution. The relative deviation for average wall heat flux, is 0.20%, 0.05%,

0.02%, 0.01%, and 0.00% for 10,000, 20,000, 30,000, 40,000, and 50,000 number of elements, respectively. Consequently, 40,000 elements is chosen for numerical simulations. As shown in Figure 3.2.b, finer grid size is used at the vicinity of the solid wall to resolve the boundary layer effects with higher accuracy. The maximum skewness, calculated based on the equilateral volume method, was 0.21 which assures high quality of the grid. A sample of velocity and temperature domains are shown as results of the numerical studies in Figure 3.2.c and Figure 3.2.d.

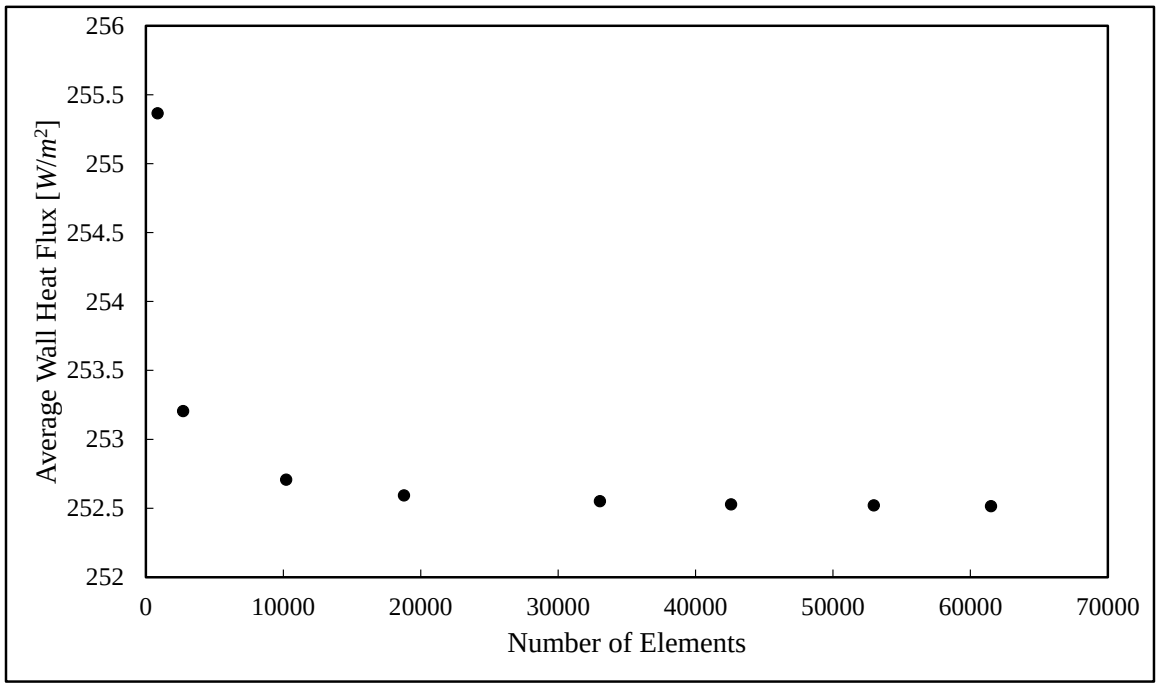

Figure 3.3. Grid independency study; walls average heat flux versus number of elements for the benchmark case (see Table 3.3)

3.4. Experimental Study

A custom-made testbed is designed and built, in order to validate the results from integral solution and numerical simulations. Five samples, with various fin spacing are prepared, and a series of tests with different surface temperatures are conducted.

3.4.1. Testbed

A custom-made testbed is designed for measuring natural convection heat transfer from the finned heatsinks, as shown in Figure 3.4. The set-up includes an enclosure made of Plexiglas (PMMA) which is insulated by a layer of foam with a thickness of 20 mm. The testbed also includes 20 cm long 150 W Chromalox strip heaters which are attached to the backside of the fins baseplate, and a data acquisition system, supplied by National Instruments (NI DAQ Chassis). High conductive thermal paste provided by Omega is used to decrease the thermal contact resistance between the heater and the samples baseplate. The voltage and the current of the supplied power are measured with an Agilent 34405A digital multimeter.

Five samples with the same baseplate size, and different fin spacing (s) and fin height (H), are prepared. Dimensions of the finned plate samples are given in Table 3.4.

Table 3.4. Dimensions of the finned plate samples

Sample #	*s* [mm]	*n*	*H* [mm]	*l* [mm]
1	9.5	8	17	300
2	6.0	12	17	300
3	14.0	6	17	300
4	9.5	8	10	300
5	9.5	8	25	300

Note: Baseplate width is similar in all samples, W= 101 mm.

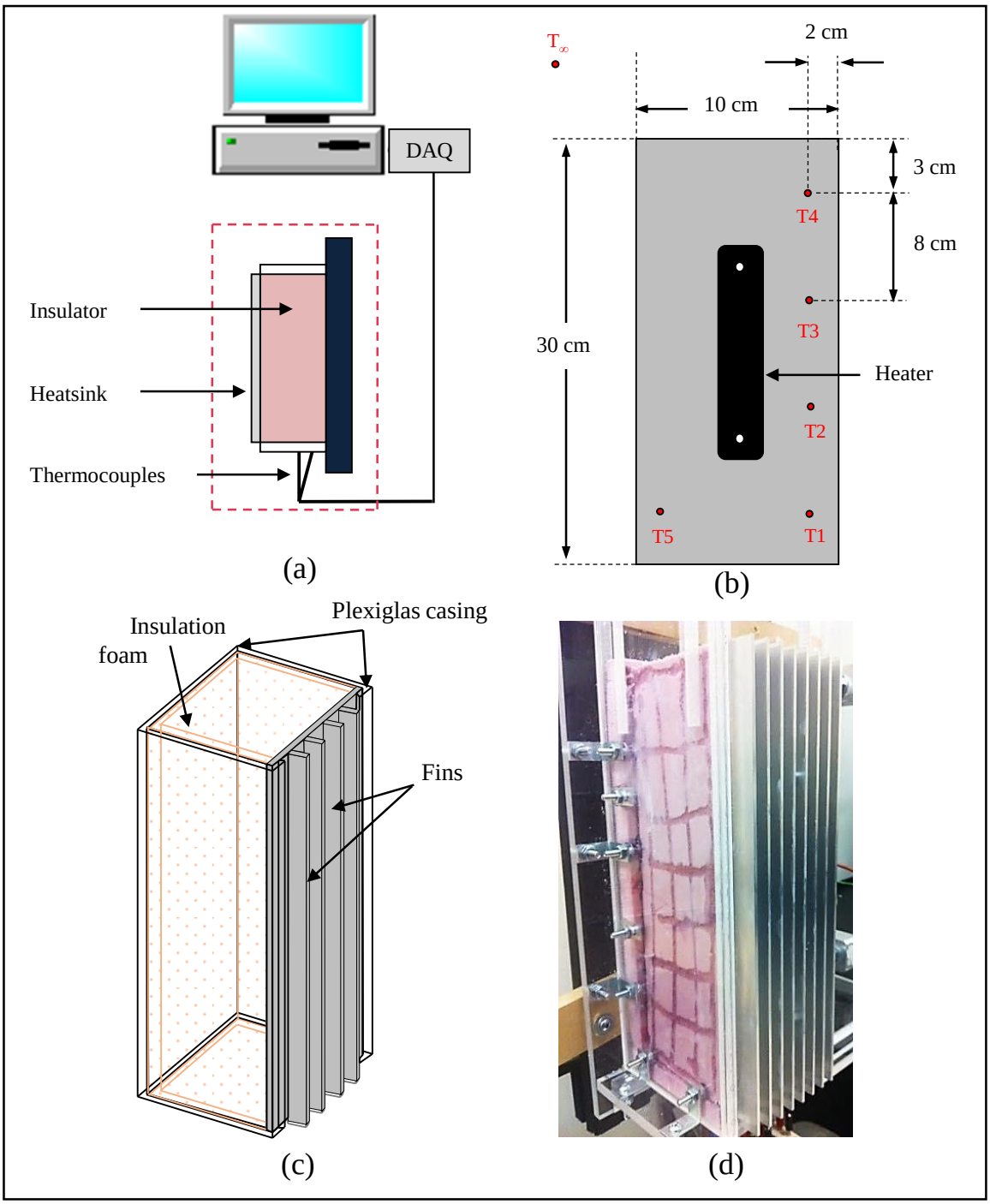

Figure 3.4. **a) schematic of the test-bed; b) samples dimensions, heater and thermocouples positioning; c) testbed casing and insulation; and d) a photo of the testbed**

3.4.2. Uncertainty Analysis

Uncertainty analysis for the experimental study on continuous fin heatsinks is very similar to what performed in Section 2.2.3. Equations 2.6 to 2.10 are directly used for the uncertainty analysis of the experimental study. Table 2.4 is also valid to be used for the current experiments. Performing the uncertainty analysis for the Nusselt number, the maximum uncertainty value for Nu_s is calculated to be 4%. The measured temperatures uncertainty ΔT is $\pm 2°C$, which is twice as the accuracy of the thermocouples. The calculated uncertainties for Nu_s is reported as error bars in the experimental results.

3.5. Results and Discussion

Figure 3.5 shows the comparison between the numerical results and the analytical solution. Equations 3.21 and 3.22, are used for the velocity and temperature distributions at different cross sections along the *x*-direction. As shown, at the entrance of the channel, because of a sudden jump in temperature and velocity in the *y*-direction due to the effects of wall, the integral technique cannot precisely predict the temperature and velocity profiles. This is an expected shortcoming of the integral technique, and it happens because a smooth continuous functions is used for both temperature and velocity distributions over the entire domain and these profiles cannot completely conform to the sudden changes in the flow characteristics at the entrance region. However, the agreement between the numerical data and analytical model improves at regions farther from the entrance region. Neglecting the entrance of the channel, $x \geq 0.01\left(Ra_s / \varepsilon\right)$ [71], the maximum relative difference for the velocity and temperature distribution between the analytical solution and the numerical simulation are 9.8% and 3.5%, respectively.

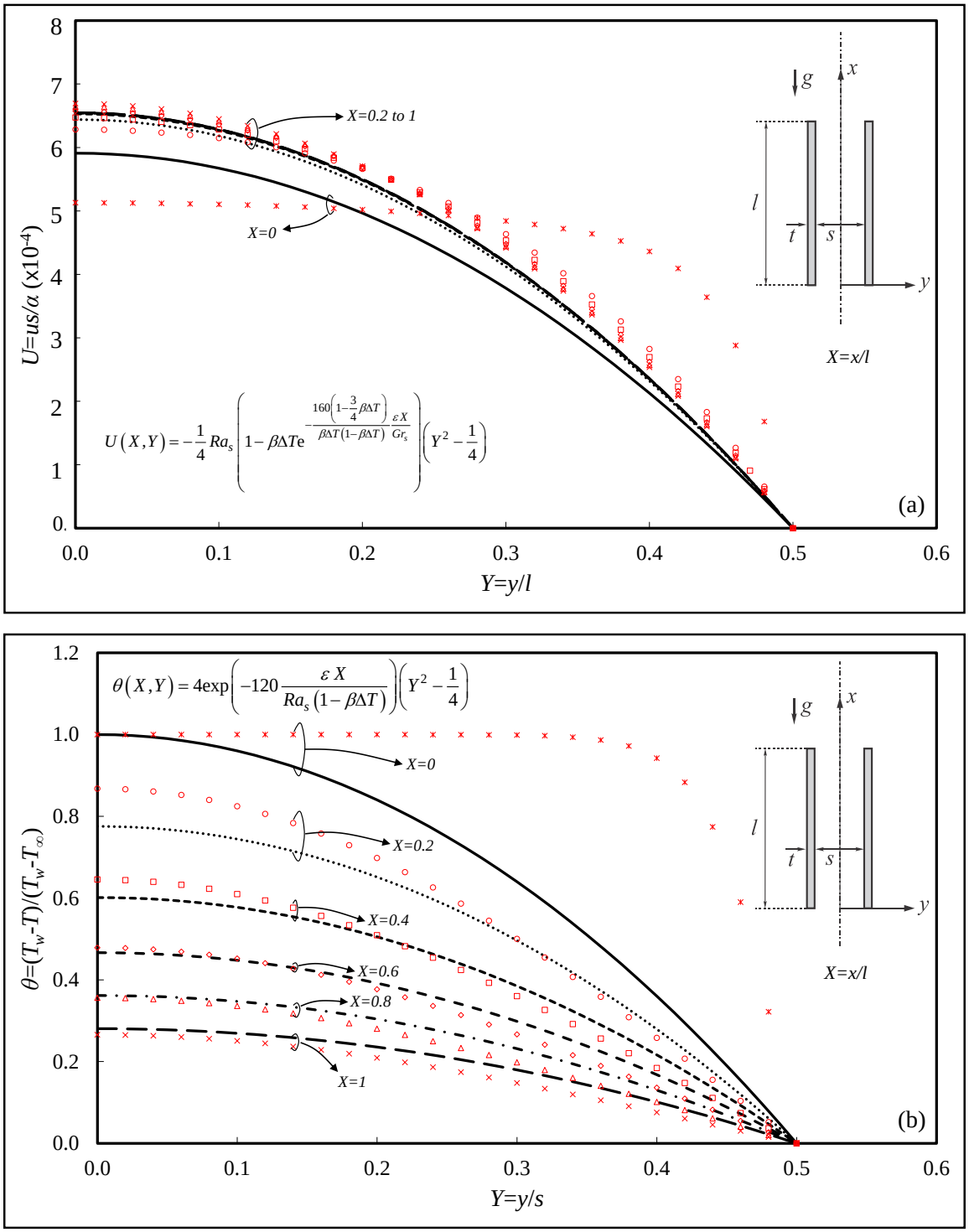

Figure 3.5. **Comparison between the analytical solution (lines), a) velocity b) temperature distribution and numerical results (symbols) at various cross sections along the channel**

Local and average Nusselt numbers can also be calculated based on the temperature distribution obtained from the proposed analytical solution, Eq. 3.22. Equations 3.23 and 3.24 show the local and average Nusselt numbers for laminar natural convection heat transfer between two parallel plates as a function of Rayleigh number, temperature difference, and the channel aspect ratio, $\varepsilon = l / s$.

$$Nu_s(X) = \frac{h(X)s}{k} = 4\exp\left(-180\frac{\varepsilon X}{Ra_s\left(1-\beta\Delta T\right)}\right) \qquad 3.23$$

$$Nu_s = \frac{hs}{k} = \frac{4}{14}\frac{Ra_s\left(1-\beta\Delta T\right)}{\varepsilon}\left[1-\exp\left(-180\frac{\varepsilon}{Ra_s\left(1-\beta\Delta T\right)}\right)\right] \qquad 3.24$$

Figure 3.6 shows a comparison between the proposed average Nusselt number, Eq. 3.24, and the semi-empirical results from Elenbaas [24] and Bar-Cohen [26] for $1000 \le Ra_s \le 4500$. As can be seen in Figure 3.6, for the mentioned range of Rayleigh numbers, there is a reasonable agreement between the present solution and the existing correlations in the literature with a maximum relative difference of 6%. The maximum relative difference between the present relationship for Nusselt number and our experimental data is 1.6%. For higher Rayleigh numbers $\left(Ra_s \ge 4500\right)$, as shown by Nat [71], the flow regime is similar to forced convection. In spite of being initiated by different mechanisms, the physics of the flow in the fully-developed region is independent of how the flow is driven. Although in natural convection heat transfer the flow is buoyancy-driven, its behavior becomes similar to laminar forced convection [71].

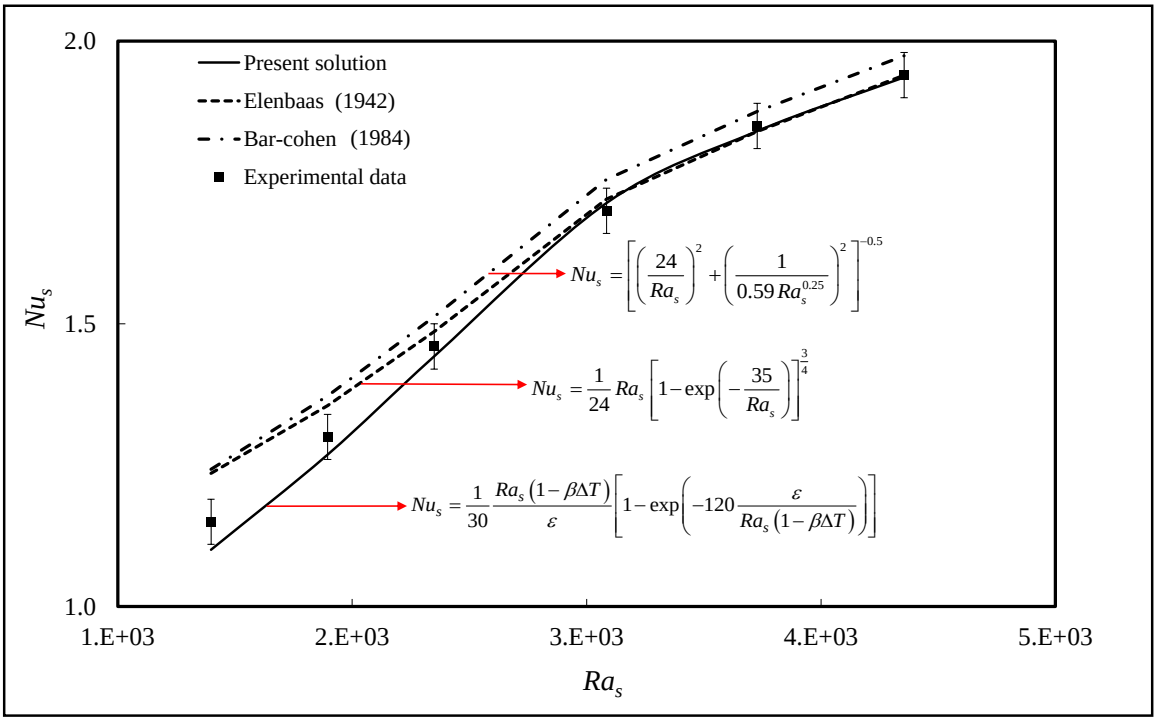

Figure 3.6. Comparison between the present average Nusselt number, existing semi-empirical relations in the literature [24] **and** [26]**, and our experimental data**

3.6. Conclusion

A new analytical solution for steady-state natural convection from isothermal parallel plates is presented. New compact analytical relationships are developed for velocity and temperature distributions for the buoyancy-driven channel flow. Integral technique is used in combination with power law assumption in the presented analytical solution. An independent numerical simulation is performed using commercial software package, ANSYS FLUENT, for validation purposes. A custom-made testbed is built and five different aluminum heatsinks are prepared and tested to validate the numerical and analytical results. The proposed temperature and velocity profiles are compared to the numerical simulations results and good agreement is observed. For the first time, an analytical compact model is proposed for calculating the local Nusselt numbers in natural convection heat transfer from parallel plates, which is successfully validated by experimental data.

Chapter 4.

Natural Convection from Interrupted Fins

The focus of this chapter is on the design of high performance naturally-cooled heatsinks with vertical rectangular interrupted fins. A systematic analytical approach is taken, to solve the governing equations of the air flow and heat transfer from the heatsink. Closed-form correlations are presented for temperature and velocity distribution, and an easy-to-use method is introduced to design such heatsinks. Numerical simulations are used to provide better understanding of the physics of flow and heat transfer mechanism. An extensive experimental study is also conducted to verify the results from analytical solution and numerical simulation. Results show that the new-designed heatsinks are capable of dissipating heat around five times more than currently available naturally-cooled heatsinks, with weight up to 30% lighter. The new heatsinks can increase the capacity of passive thermal management systems significantly.

4.1. Problem Statement

The objective of this chapter is to develop an analytical model that can predict the natural convection heat transfer from a square array of vertical rectangular isothermal fins. Figure 4.1 schematically shows the fins arrangement, parameters used to define the geometry, and control volumes used to model the heat transfer. To solve the problem, the domain is divided into multiple sub-domains, containing the channels made by two adjacent columns of fins, and the gaps region between two fin rows. The effects of neighboring channels on each other are neglected, so the problem is only solved between two fin columns and then the solution is extended to the whole domain. The problem is divided into two parts; i) channel flow which contains the region between two neighboring fins, and ii) gap flow which is related to the void region between two rows of fins. Each part is solved separately, and the solution of each part is superposed to solve the whole domain.

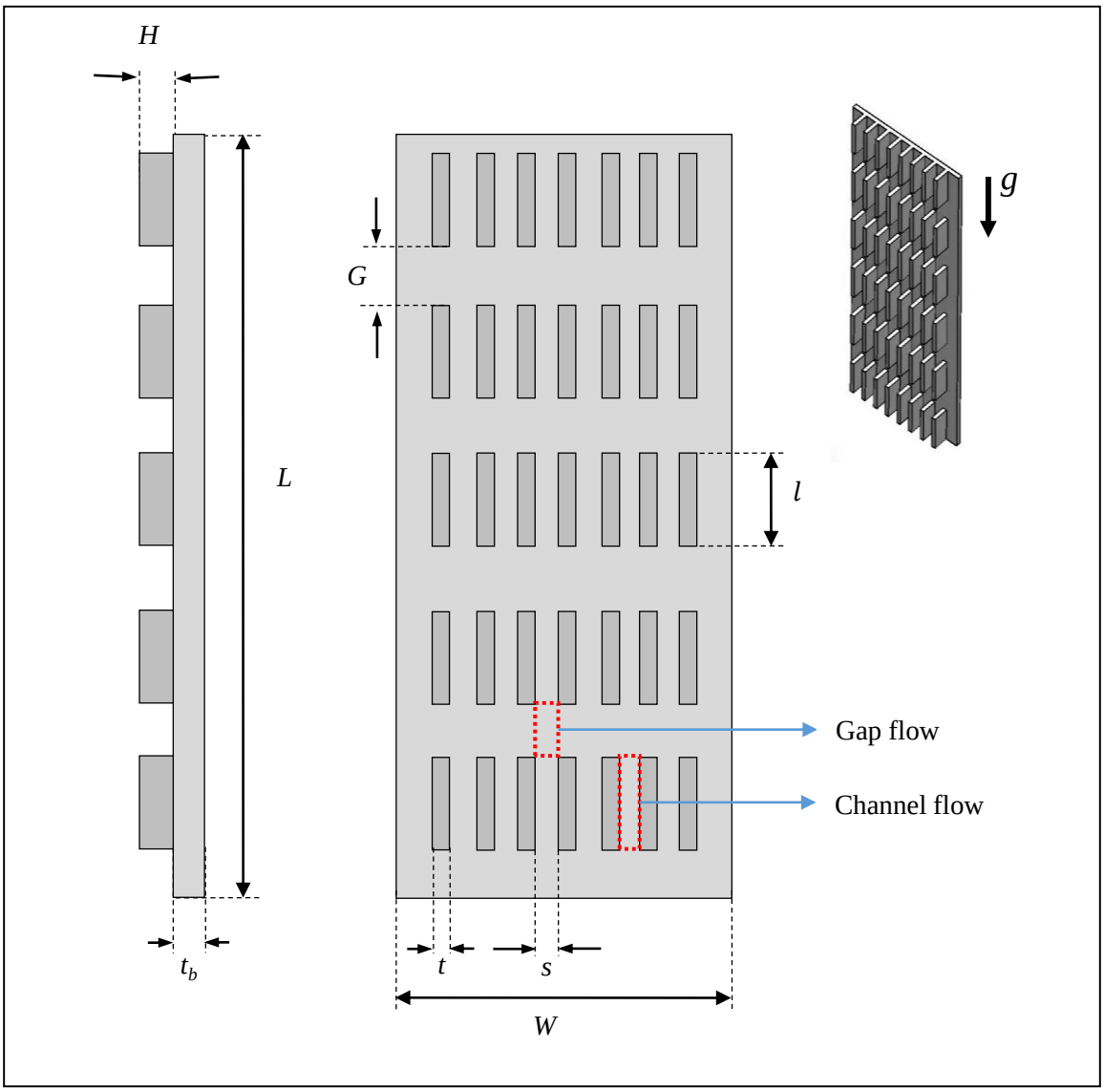

Figure 4.1. A schematic of heatsink with interrupted fins, geometrical parameters used to address fin parameters, and the regions related to channel flow and gap flow

4.2. Solution Methodology

As shown in [55] and [57], adding interruption to a fin array will force the boundary layer to reset and increase the heat flux from the fins; however, cutting fins to add interruptions will result in losing surface area, which leads to a decrease in total heat transfer from the heatsink. In order to consider these two competing trends in our heatsink

design, it is intended to find the optimum geometrical parameters, i.e. fin spacing, S, fin length, l, and gap length, G, to maximize the total heat transfer from an available area of baseplate by length of L and width of W. As explained briefly in Section 4.1, the problem is broken into a number of channels and gaps, stacked on top of each other. To solve for the whole domain, using the known boundary conditions at *x*-direction, the velocity and temperature profiles are obtained separately for the channels and the gaps, with outlet condition from the first channel considered as inlet condition to the first gap, and outlet condition from the first gap used as inlet condition to the second channel, and so on. After obtaining all the velocity and temperature profiles for the whole domain, the heat transfer from each channel is calculated and summed up to find the overall heat transfer from the heatsink.

4.2.1. Channel Flow

The control volume considered for the channel flow is shown in Figure 4.2. In Section 3.2.2, we used integral technique to find the velocity and temperature distribution in the channel made by two parallel isothermal walls, Eqs. 3.19 and 3.20. These equations can be rewritten in terms of channel average inlet velocity, as;

$$u_C(x,y) = -\frac{1}{4\nu}\left(g\beta\Delta T s^2 - \left(\beta g s^2 \Delta T - 8\nu u_{C,in}\right) \mathrm{e}^{-\frac{5\nu\left(\beta g\, s^2\Delta T + 24\,\nu\, u_{C,in}\right)x}{s^2 u_{C,in}\left(\beta g s^2 \Delta T - 8\nu\, u_{C,in}\right)}} \right)\left(\left(\frac{y}{s}\right)^2 - \frac{1}{4} \right) \qquad 4.1$$

$$T_C(x,y) = 4\Delta T \mathrm{e}^{-\frac{15\alpha x}{s^2 u_{C,in}}} \left(\left(\frac{y}{s}\right)^2 - \frac{1}{4} \right) + T_w \qquad 4.2$$

The index C is used for the equations related to channel flow to separate them from gap flow parameters, which are indexed by G, wherever necessary. The average inlet velocity to each channel, $u_{C,in}$, is used in Eqs. 4.1 and 4.2, for sake of simplicity of calculations. This term is required for calculation of the velocity and temperature profiles in each channel. For the first channel located at the bottom row of the fin array, this term can be calculated using Eq. 3.8, to give;

$$u_{C,in} = \frac{(1-\beta\Delta T)\, g \beta \Delta T\, s^2}{12\nu} \tag{4.3}$$

The term ΔT in Eq. 4.3 is the difference between wall temperature and average air temperature entering the channel. For the higher rows of channels, the inlet velocity can be calculated using the equations developed for gap region in Section 4.2.2. Equations 3.19 and 3.20 will be used to find the velocity and temperature profiles in the channels. To calculate the heat transfer from the fins for each channel, using correlations we developed in Section 3.2.2, heat transfer coefficient can be found as;

$$h = \frac{4}{15}\frac{s u_{C,in} k}{l\alpha}\left(1 - e^{-\frac{15\alpha l}{s^2 u_{C,in}}}\right) \tag{4.4}$$

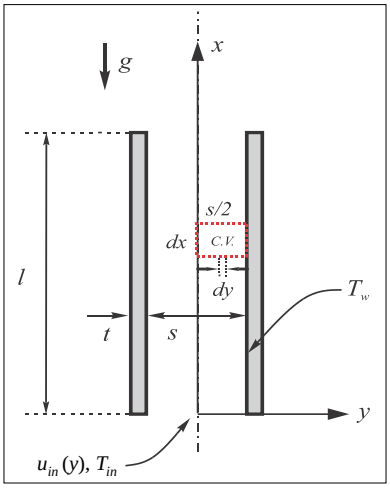

Figure 4.2. Schematic of the control volume selected for the channel flow

4.2.2. Gap Flow

Figure 4.3 shows the control volume selected for the gap flow. At steady-state condition, when air leaves a channel with a specific velocity/temperature profile, and since it is not introduced to any external mass, momentum, or heat source, its mass flow, total momentum, and total energy will remain constant. Consequently the flow will go through a one-directional diffusion of mass, momentum, and energy in the direction normal to the velocity of the flow. In other words, as air moves along the *x*-axis in the gap region, the velocity profile which used to be maximum at the center and minimum on the sides when entering the gap, will start to get flattened, keeping the total momentum of the flow

constant. The same phenomenon will happen to the temperature profile, meaning that the temperature profile which had its minimum value at the center and maximum value on the sides when entering the gap, will get more and more flat, maintaining the total energy of the flow.

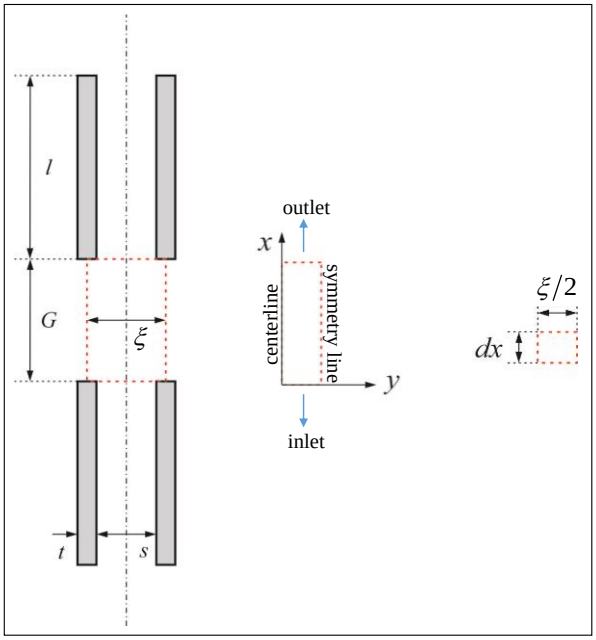

Figure 4.3. Schematic of the control volume selected for the gap flow

Governing equations and boundary conditions

Based on the general behavior of the flow, explained above, the assumptions used in this study are listed below;

- Laminar, steady-state flow
- 1-directional flow parallel to the fin walls (velocity component normal to the fin wall is zero)
- 2-dimensional heat and momentum diffusion in *x*-direction and *y*-direction
- Constant thermo-physical properties
- No body-force in the gap region

It is also assumed that the fin height, the depth of domain normal to the paper in Figure 4.3, is large enough that the effects of baseplate can be neglected. Applying the assumptions, the momentum and energy conservation equations will be reduced to;

$$u\frac{\partial u}{\partial x}=\nu\nabla^2 u \tag{4.5}$$

$$u\frac{\partial T}{\partial x}=\alpha\nabla^2 T \tag{4.6}$$

The conservation equations are subjected to the following boundary conditions;

$$at\ y=0; \qquad \frac{\partial u(x,0)}{\partial y}=\frac{\partial T(x,0)}{\partial y}=0 \tag{4.7}$$

$$at\ y=\frac{\xi}{2}; \qquad \frac{\partial u(x,\frac{\xi}{2})}{\partial y}=\frac{\partial T(x,\frac{\xi}{2})}{\partial y}=0 \tag{4.8}$$

$$at\ x=0; \qquad u(0,y)=u_{in}(y), \quad T(0,y)=T_{in}(y) \tag{4.9}$$

$$as\ x\to\infty; \qquad u_{x\to\infty}=\frac{2}{\xi}\int_0^{\frac{\xi}{2}}u_{in}(y)\,\mathrm{dy}, \quad T_{x\to\infty}=\frac{2}{\xi u_{x\to\infty}}\int_0^{\frac{\xi}{2}}u_{in}(y)T_{in}(y)\,\mathrm{dy} \tag{4.10}$$

Equations 4.7 and 4.8 result from geometric symmetry at the gap centerline and at the boundary between two adjacent gaps. The terms u_{in} and T_{in} in Eq.4.9 are the gap inlet velocity and temperature profiles respectively. These gap inlet profiles are required to be calculated to be used as inlet boundary condition for each gap. The method to calculate these profiles explained in detail in the Integral technique section. Equation 4.10 implies that, given enough space to the flow, both the velocity and temperature profiles will reach a uniform state, equal to the bulk momentum and energy entering the gap. Due to the symmetrical boundary condition at *x*-direction, the uniform velocity and temperature will remain unchanged after reaching this state.

Following Ref. [60] and integrating the conservation equations across the gap in *y*-direction, from $y=0$ to $y=\xi/2$, the integral form of governing equations will be obtained as;

$$\frac{\partial}{\partial x}\int_0^{\frac{\xi}{2}}u^2dy=\nu\left[\left(\frac{\partial u}{\partial y}\right)_{y=\frac{\xi}{2}}-\left(\frac{\partial u}{\partial y}\right)_{y=0}\right]=0 \tag{4.11}$$

$$\frac{\partial}{\partial x}\int_0^{\frac{\xi}{2}} uTdy = \alpha\left[\left(\frac{\partial T}{\partial y}\right)_{y=\frac{\xi}{2}} - \left(\frac{\partial T}{\partial y}\right)_{y=0}\right] = 0 \qquad 4.12$$

The interpretation of Eqs. 4.11 and 4.12 is that the integral form of momentum and energy does not change along the *x*-direction, so the governing equations can be re-written as;

$$\int_0^{\frac{\xi}{2}} u^2(x,y)dy = \int_0^{\frac{\xi}{2}} u_{in}^2(\mathrm{y})dy \qquad 4.13$$

$$\int_0^{\frac{\xi}{2}} u(x,y)T(x,y)dy = \int_0^{\frac{\xi}{2}} u_{in}(y)T_{in}(y)dy \qquad 4.14$$

Inlet velocity and temperature profiles, $u_{in,G}$ and $T_{in,G}$, are still required to solve Eqs. 4.13 and 4.14. They will be found in the Integral technique section. To apply the integral technique, knowing the general behavior of the velocity and temperature profiles, we assume a known profile for each. Satisfying conservation laws in a lumped fashion across the region of interest, we can obtain velocity and temperature profiles within acceptable accuracy after applying the boundary conditions.

Integral technique

Considering the symmetrical boundary conditions in *y*-direction, third order polynomials are assumed for both temperature and velocity profiles;

$$u(x,y) = a_1(x)y^3 + b_1(x)y^2 + c_1(x)\,\mathrm{y} + d_1(x) \qquad 4.15$$

$$T(x,y) = a_2(x)y^3 + b_2(x)y^2 + c_2(x)\,\mathrm{y} + d_2(x) \qquad 4.16$$

Applying the boundary conditions in the *y*-direction (Eqs. 4.7 and 4.8), into Eqs. 4.15 and 4.16, we will have;

$$u(x,y) = f_1(x)(y^3 - \frac{3\xi}{4}y^2) + g_1(x) \qquad 4.17$$

$$T(x,y) = f_2(x)(y^3 - \frac{3\xi}{4}y^2) + g_2(x) \qquad 4.18$$

The terms $f_1(x)$, $f_2(x)$, $g_1(x)$, and $g_2(x)$ are all unknown functions that need to be determined, but before applying the governing equations, the terms related to inlet velocity and temperature must be determined. Since Eqs. 4.17 and 4.18 are chosen to describe the flow behavior inside the gap region, they should be valid everywhere in the domain, including the entrance. The only difference at the entrance is that the terms $f_1(x)$, $f_2(x)$, $g_1(x)$, and $g_2(x)$ will not be functions of *x* anymore, and they will be constants. These constants can be found by setting the flow conditions at the channel outlet and gap inlet to be equal.

$$u_{G,in}(0) = u_G(0,0) = u_C(l,0),\ T_{G,in}(0) = T_G(0,0) = T_C(l,0) \tag{4.19}$$

$$u_{G,in}(\frac{\xi}{2}) = u_G(0,\frac{\xi}{2}) = u_C(l,\frac{s}{2}) = 0,\ T_{G,in}(\frac{\xi}{2}) = T_G(0,\frac{\xi}{2}) = T_C(l,\frac{s}{2}) = T_w \tag{4.20}$$

Applying Eqs. 4.19 and 4.20 to Eqs. 3.19, 3.20, 4.17, and 4.18, the gap inlet velocity and temperature profiles will be obtained as;

$$u_{G,in}(y) = -\frac{1}{\nu\xi^3}\left(y^3 - \frac{3\xi}{4}y^2 + \frac{\xi^3}{16}\right)\left[\left(\beta g s^2\Delta T - 8\nu u_{C,in}\right)e^{-\frac{5\nu l\left(\beta g s^2\Delta T - 24\nu u_{C,in}\right)}{s^2 u_{in}(\beta g s^{2\Delta T} - 8\nu u_{C,in})}} - \beta g s^2\Delta T\right] \tag{4.21}$$

$$T_{G,in}(y) = T_w - \frac{16\Delta T}{\xi^3}\left(y^3 - \frac{3\xi}{4}y^2 + \frac{\xi^3}{16}\right)e^{-\frac{15\alpha l}{s^2 u_{C,in}}} \tag{4.22}$$

Having the gap inlet velocity and temperature profiles, Eqs. 4.21 and 4.22 can be substituted into Eqs. 4.13 and 4.14, and then Eqs. 4.17 and 4.18 can be substituted into the new governing equations to give;

$$u(x,y) = f_1(x)(y^3 - \frac{3\xi}{4}y^2 + \frac{\xi^3}{32}) - \frac{1}{32\nu}\left[\left(\beta g s^2\Delta T - 8\nu u_{C,in}\right)e^{-\frac{5\nu l\left(\beta g s^2\Delta T - 24\nu u_{C,in}\right)}{s^2 u_{C,in}(\beta g s^2\Delta T - 8\nu u_{C,in})}} - \beta g s^2\Delta T\right] \tag{4.23}$$

$$T(x,y) = f_2(x)\left(y^3 - \frac{3\xi}{4}y^2 + \frac{\xi^3}{32} - \frac{17\xi^3}{1120}f_1(x)\right) + T_W - \frac{26\Delta T}{35}e^{-\frac{15\alpha l}{s^2 u_{C,in}}} \tag{4.24}$$

The conventional way to use the integral method is to apply the two remaining boundary conditions, Eqs. 4.9 and 4.10, to Eqs. 4.23 and 4.24 to find $f_1(x)$ and $f_2(x)$, but doing so will not help to find the desired parameters. To address this issue, a simplified integral technique is used, and based on the physics of the flow, we assume an exponential behavior for $f_1(x)$ and $f_2(x)$. Physics of the flow and heat transfer suggest that both velocity and temperature at the centerline, will change more rapidly at the beginning of the gap, and approach an asymptotic value as the fluid moves along the *x*-axis, so;

$$f_1(x) = \phi - \varphi e^{-\varsigma x} \tag{4.25}$$

$$f_2(x) = \vartheta - \iota e^{-\sigma x} \tag{4.26}$$

where $\phi, \varphi, \varsigma, \vartheta, \iota,$ and σ are constants to be determined. Substituting Eqs. 4.25 and 4.26 into Eqs. 4.23 and 4.24, and satisfying boundary conditions defined by Eqs. 4.9 and 4.10, the temperature and velocity profiles in the gap region will be determined as;

$$u(x,y) = -\frac{1}{32\nu\xi^3}(32y^3e^{-\varsigma x} - 24\xi y^2 e^{-\varsigma x} + \xi^3 e^{-\varsigma x} + \xi^3)\left[\left(\beta g s^2 \Delta T - 8\nu u_{in}\right)e^{-\frac{5\nu l\left(\beta g s^2 \Delta T - 24\nu u_{in}\right)}{s^2 u_{in}(\beta g s^2 \Delta T - 8\nu u_{in})}} - \beta g s^2 \Delta T\right] \tag{4.27}$$

$$T(x,y) = T_w - \left(y^3 - \frac{3\xi}{4}y^2 + \frac{\xi^3}{32} - \frac{17\xi^3}{1120}e^{-\varsigma x}\right)\frac{16\Delta T}{\xi^3}e^{-\frac{15\alpha l}{s^2 u_{in}} - \sigma x} - \frac{26\Delta T}{35}e^{-\frac{15\alpha l}{s^2 u_{in}}} \tag{4.28}$$

As can be seen in Eqs. 4.27 and 4.28, ς and σ are still unknown, and need to be determined. In order to find the two constants, numerical simulation is used. More details on the numerical simulations and the method to find ς and σ is explained in Section 4.3.

4.3. Numerical Simulation

In order to find the unknown constants, ς and σ, from the integral solution, a two dimensional numerical model of the gap flow is developed, using the commercially available software package, COMSOL Multiphysics 4.3. Known velocity and temperature profiles are applied to the bottom of domain as inlet condition, and symmetry boundary condition is considered for the sides of the domain. At the top of the domain, outlet

pressure is considered to be atmospheric pressure. The numerical domain and the boundary conditions are shown in Figure 4.4.a.

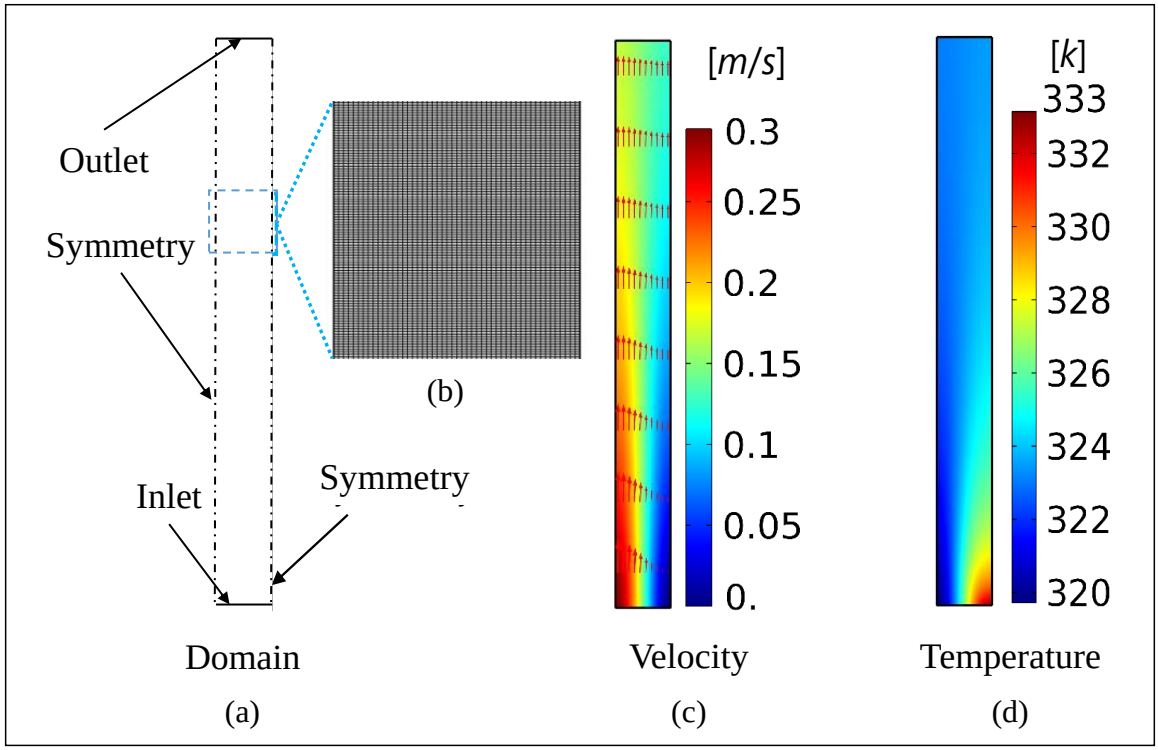

Figure 4.4. Numerical simulation-benchmark case; a) the domain and boundary condition, b) a sample of mesh, c) velocity distribution, and d) temperature distribution

Table 4.1. Parameters used for numerical simulation benchmark case

Parameter	Description	Value	Unit
G	Gap length	5	[cm]
ξ	Gap width	11	[mm]
$u_{in,\max}$	Maximum velocity at the inlet temperature (centerline)	0.3	[m/s]
$u_{in,\min}$	Minimum velocity at the inlet (side boundaries)	0	[m/s]
$T_{in,\max}$	Maximum temperature at the inlet (side boundaries)	60	[°C]
$T_{in,\min}$	Minimum temperature at the inlet temperature (centerline)	47	[°C]

Different number of mesh elements have been tested and the results were compared for the temperature in the outlet at the centerline, to ensure a mesh independent

solution. Accordingly, choosing a mesh number of 1000, we found a 0.05% deviation in the results, compared to the simulation of the gap with mesh number of 100. Similarly, the results for simulation with 2000 mesh elements deviated up to 0.01%, compared to those from the case with 1000 elements. Therefore, we chose element number of 1000 for numerical investigation purposes. Figure 4.5 shows the grid independency analysis for the benchmark case. As can be observed in the figure, the number of elements does not have significant effect on the results, and the simulation is not very sensitive to the grid size. Table 4.1 lists the parameters used for the benchmark case. Figure 4.5.b shows a sample of the grid used in numerical studies. Velocity distribution, and temperature distribution obtained from numerical simulation on the benchmark case are shown in Figure 4.4.c and Figure 4.4.d, respectively.

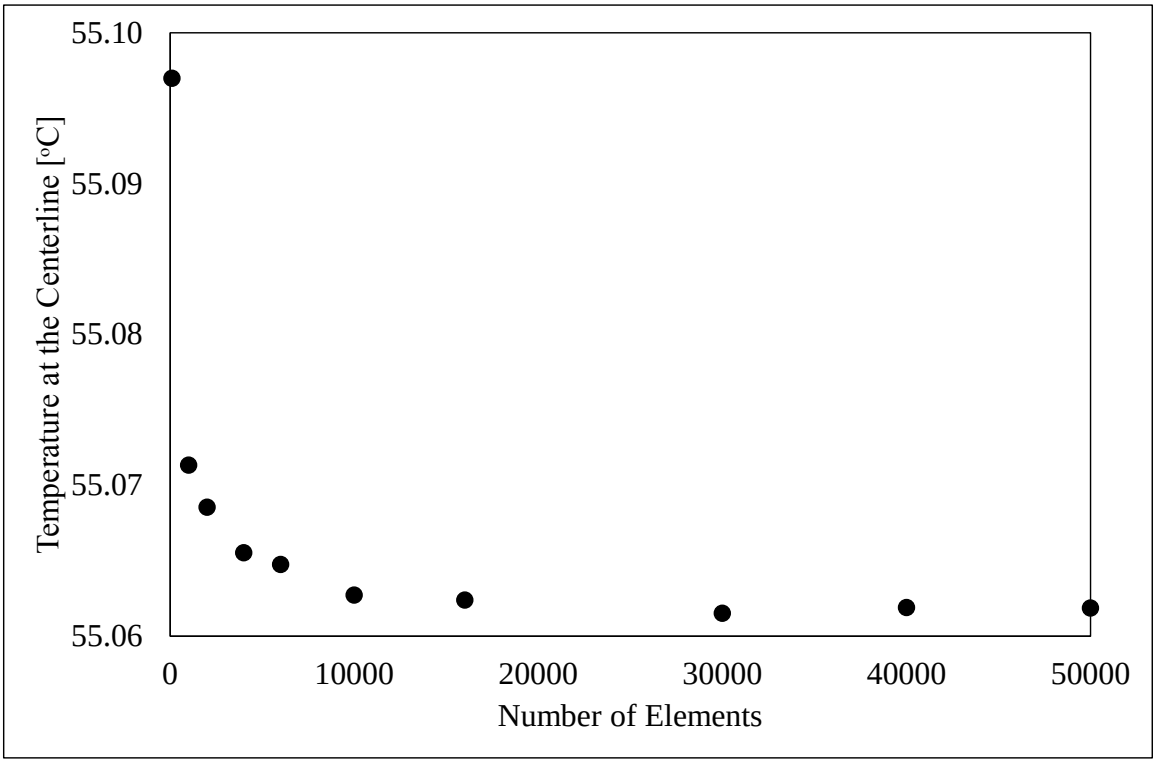

Figure 4.5. Mesh independency study for the benchmark case

Comparing the results from integral technique and the numerical simulation results and trying to fit the temperature and velocity profiles, the unknown constants, ς and σ for air, will be found as follow;

$$\varsigma = 40 \qquad 4.29$$

$$\sigma = 95 \tag{4.30}$$

Substituting the obtained constants in the gap velocity and temperature profiles, Eqs. 4.27 and 4.28, closed-form solution are obtained for temperature and velocity inside the gap. Figure 4.6 shows the worst case we observed, comparing the results from integral solution and numerical simulation with the constants introduced in Eqs. 4.29 and 4.30. The maximum relative difference between the integral solution and numerical simulation, is 5.4% and 8.6%, respectively for velocity and temperature distribution.

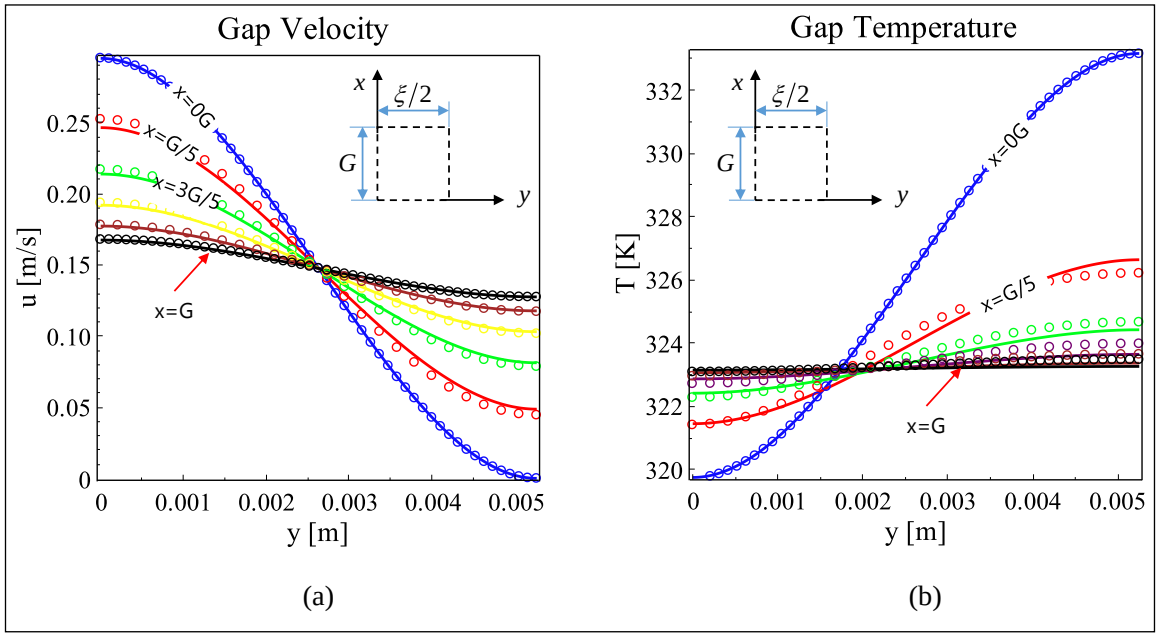

Figure 4.6. Comparison between the result from integral technique with $\varsigma = 40$ and $\sigma = 95$, and numerical simulations at the benchmark case , a) velocity domain, b) temperature domain

4.4. Experimental Study

The objective of the experimental study is to verify the results of the proposed method to calculate total heat transfer from the interrupted fins, explained in Section 4.2. To accomplish this, a custom-made testbed was designed and built, and 13 finned plate samples, with different fin spacing, gap length, and fin length were prepared. A series of tests with different average surface temperatures were conducted to validate the results from integral solution.

4.4.1. Testbed

A custom-made testbed is designed for measuring natural convection heat transfer from the finned heatsinks, as shown in Figure 4.7. The set-up includes a wooden frame which is insulated at the backside by two layers of compressed polyester foam with a thickness of 25mm each. The input heat is provided by a 30cm long 150W Chromalox strip heater, attached to the backside of the sample. High conductive thermal paste provided by Omega is used to minimize the thermal contact resistance between the heater and the samples. A variable voltage regulator, Variac model SC-20M, is used to provide the power to the heater. To measure the temperature, T-type thermocouples provided by Omega, are attached to backside of the samples. Data logging is performed through a data acquisition system (DAQ), supplied by National Instrument. The supplied AC voltage and current to the heater are measured by National Instruments DAQ modules, NI 9225 and NI 9227, respectively. Temperature data are logged by National Instruments DAQ module, NI 9213.

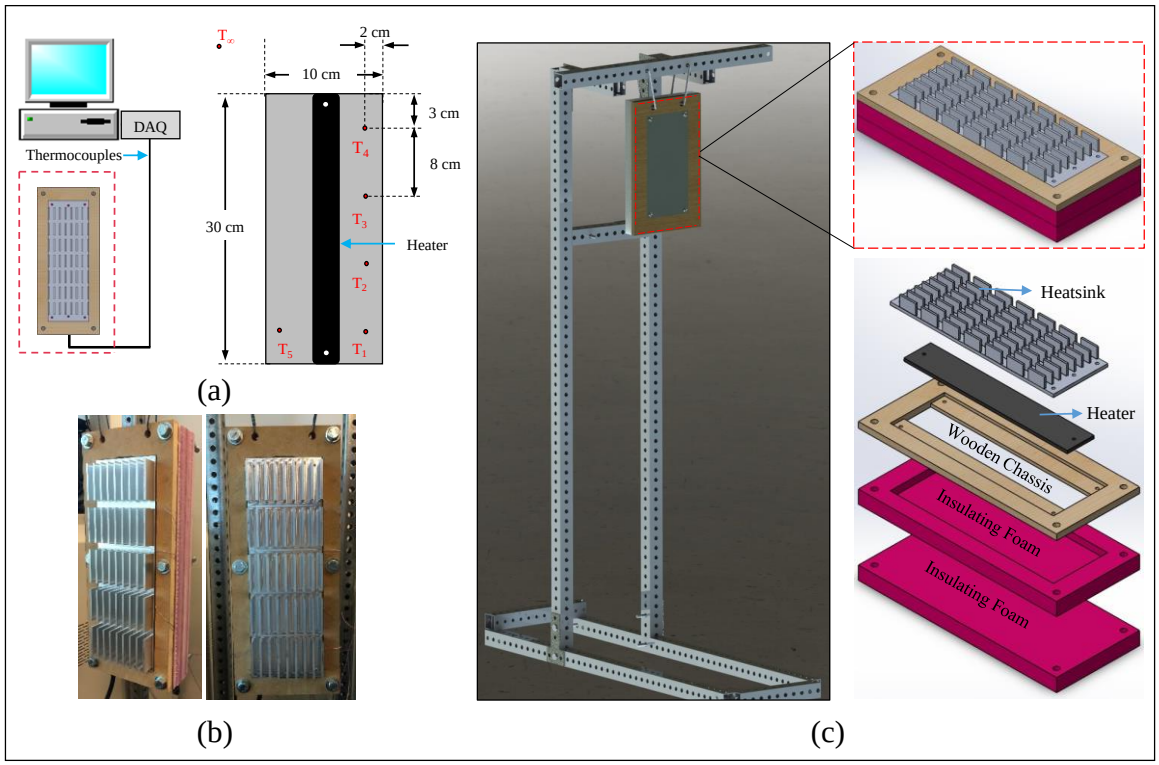

Figure 4.7. Experimental setup, a) the position of thermocouples and the heater, b) photos of sample under test, c) schematic of the test bed and insulations

Thirteen samples with the same fin height and baseplate dimensions are prepared. To ensure similar surface finishing for all the samples, CNC machining was used to prepare the samples. Geometrical dimensions of the samples are designed in a way to enable parametric study on fin spacing, fin length, and gap length. Based on the developed model, fin parameters are selected to cover the optimum range. Dimensions of the test samples are given in Table 4.2.

Table 4.2. Dimensions of the interrupted fin samples used in the experiments

Schematic and Sample Photos	Sample Name	*s* [mm]	*l* [mm]	*G* [mm]	*m*	*n*
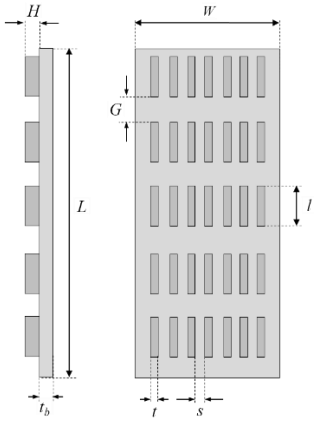	Int. 9-30-10	9	30	10	7	9
	Int. 9-10-10	9	10	10	15	9
	Int. 9-20-10	9	20	10	10	9
	Int. 9-40-10	9	40	10	6	9
	Int. 9-50-10	9	50	10	5	9
	Int. 9-140-10	9	140	10	2	9
	Int. 5-30-10	5	30	10	7	13
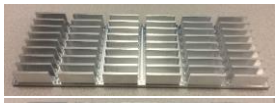	Int. 7-30-10	7	30	10	7	10
	Int. 11-30-10	11	30	10	7	8
	Int. 13-30-10	13	30	10	7	7
	Int. 9-30-6	9	30	6	1	9
	Int. 9-30-8	9	30	8	8	9
	Int. 9-300-0	9	300	0	8	9

4.4.2. Test Procedure

The experiments are performed in a windowless room with an environment free of air currents. The room dimensions are selected to be large enough to ensure constant ambient temperature during the test. The input power supplied to the heaters is monitored and surface temperatures were measured at five locations at the back of the baseplate.

Four self-adhesive, copper-constantan thermocouples (Omega, T-type) are attached in vertical locations on one side of the samples backplate, as shown in Figure 4.7.a. An extra thermocouple is installed on the same level with the lowest thermocouples, at the other side of backplate, to make sure that the temperature is well distributed horizontally (T_5 in Figure 4.7.a). All thermocouples are taped down to the backside of the samples to prevent disturbing the air flow on the finned side of the samples. An additional thermocouple is used to measure the ambient temperature during the experiments. Temperature measurements are performed at five points and the average value is taken as the baseplate temperature. Among all the experiments, the maximum standard deviation from the average temperature is measured to be less than 2.5˚C. Since the experiments are performed to mimic the uniform wall temperature boundary condition, the thickness of the baseplate and the fins are selected fairly high, 5mm and 3mm, respectively, to ensure the minimum thermal bulk resistance and uniform temperature distribution in the samples. An infrared camera, model SC655 from FLIR, is used to observe the temperature variation along the fins. The maximum temperature difference between the fins and the baseplate is measured to be about 2.1˚C, so the fins are assumed to be at the same temperature with the baseplate. For each of the 13 samples, the experimental procedure is repeated for different power inputs. Table 4.3 lists the range of some important test parameters. The steady-state condition is considered to be achieved when the rate of all temperature variations are less than 0.1˚C/hr which in average, takes 120 minutes for the test samples used in the experiments.

Table 4.3. Range of some important parameters in test procedure

Parameter	Description	Range	Unit
P	Heater power	5-50	[W]
T_∞	Ambient temperature	24-27	[°C]
T_w	Wall temperature	30-70	[°C]

For the data analysis, heat transfer due to natural convection from the baseplate and fin tips are calculated using the available correlations in literature [19], and subtracted from total heat input to the system. Following Rao *et al*. [61], the effect of radiation heat transfer is also subtracted from the fins total heat transfer (see Appendix B). Due to relatively low surface temperature and low emissivity of machined aluminum (between

0.09 and 0.1), the effect of radiation is not significant. The maximum calculated value for radiation heat transfer is 3.2% of total heat transfer.

4.4.3. Uncertainty Analysis

Uncertainty analysis for the experimental study of the interrupted fin heatsinks is very similar to that performed in Section 2.2.3. Equations 2.6 to 2.10 are directly used for the uncertainty analysis of the experimental study. Table 2.4 is also valid to be used for the current experiments. Performing the uncertainty analysis for total heat transfer, the maximum uncertainty value for $\dot{Q}_{N.C.}$ is calculated to be 8%. The measured temperatures uncertainty ΔT is $\pm 2°C$, which is twice the accuracy of the thermocouples. The calculated uncertainties for $\dot{Q}_{N.C.}$ are reported as error bars in the experimental results.

4.4.4. Test Results

The comparison between the experimental data and the values obtained from the combination of the channel solution and gap solution are shown in Figure 4.8 for different values of ΔT, which is the difference between average surface temperature and ambient temperature. The details on how to calculate the total heat transfer to develop the analytical results of Figure 4.8 are explained in Section 4.5.1. As can be seen in the figure, there is a fairly good agreement between the experimental data and the analytical solution. For the fin spacing, s, the maximum, minimum, and average relative difference between the experimental data and closed-form solution is 32%, 2% and 10%, respectively (Figure 4.8.a). These values for the fin length, l, are 26%, 1% and 11%, respectively (Figure 4.8.b). Comparing the result from analytical solution to the experimental data, gives maximum, minimum, and average relative difference of 23%, 1% and 7%, respectively for the gap length, G (Figure 4.8.c). Maximum errors always occur at low temperature differences between the surface and ambient, $\Delta T \approx 7°C$, which is not normally a value for naturally-cooled heatsinks in real applications.

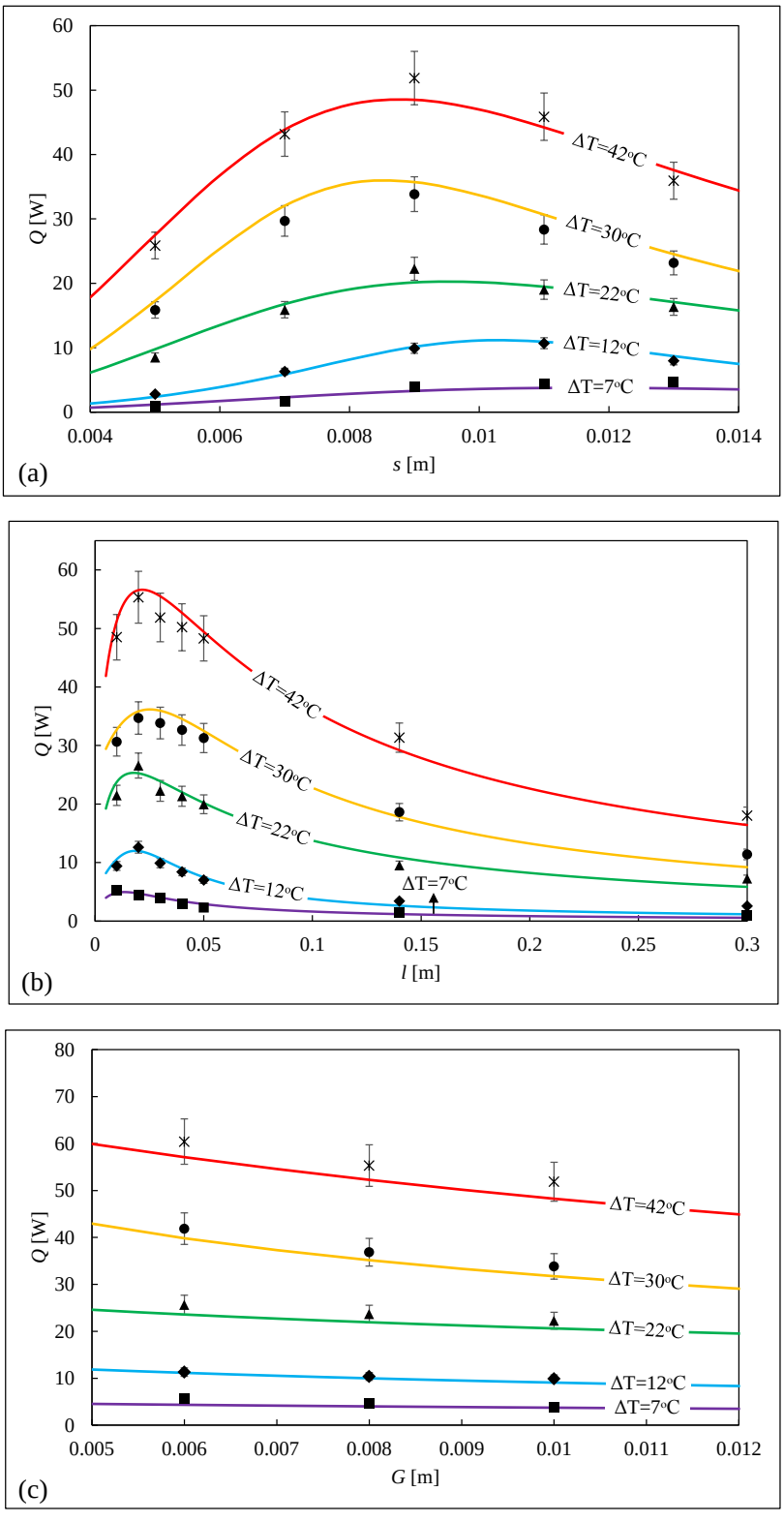

Figure 4.8. Comparison between the experimental data and analytical solution, a) fin spacing, b) fin length, c) gap length

4.4.5. Validity of Uniform Wall Temperature Assumption

One of the major assumptions to develop our analytical model in section 4.2 is uniform wall temperature as thermal boundary condition. In this section is we try to examine the validity of this assumption by taking two different approaches: i) lumped system analysis, ii) IR thermography.

A simple, yet reliable method to test the validity of uniform wall temperature assumption is using Biot number as a measure for validity of "lumped system assumption" [72]. Biot number, $Bi = hL/k$, is ratio of convection to conduction heat transfer. The length scale selected for this analysis is the baseplate length, L, and h and k are convection heat transfer coefficient and thermal conductivity of the aluminum heatsinks respectively. For Biot numbers less than unity, thermal conductivity of the solid is larger than the convective heat transfer coefficient at the solid-fluid interface. This implies that due to high resistance against heat transfer at the solid boundaries, the heat generated at the source, can spread through the solid and create more uniform temperature distribution. For the experimental studies conducted in this section, the convective heat transfer coefficient is around 20 W/m^2K, the baseplate length is 0.3 *m*, and the thermal conductivity of aluminum is around 200 *W/mK*. The Biot number for this conditions will be 0.03, which is much less than 0.1 and makes the lumped capacitance assumption valid.

To back up this analysis, infrared thermography is used to map the temperature of the heatsinks under test condition. Figure 4.9 shows a sample of IR images. Two series of IR images are taken, one from front and the other from side of the heatsinks. Figure 4.9.a shows the temperature distribution in the heatsink sample, to verify the uniform heatsink temperature assumption. As shown in this Figure 4.9, the maximum, minimum and average temperature of the heatsink is 51˚C, 48˚C, and 49˚C respectively. The IR image in Figure 4.9.b shows the temperature distribution along the fins, to verify the uniform wall temperature assumption. As shown, the maximum, minimum and average temperature of a single fin is measured 50˚C, 48˚C, and 49˚C respectively, which makes the uniform wall temperature, a fair assumption.

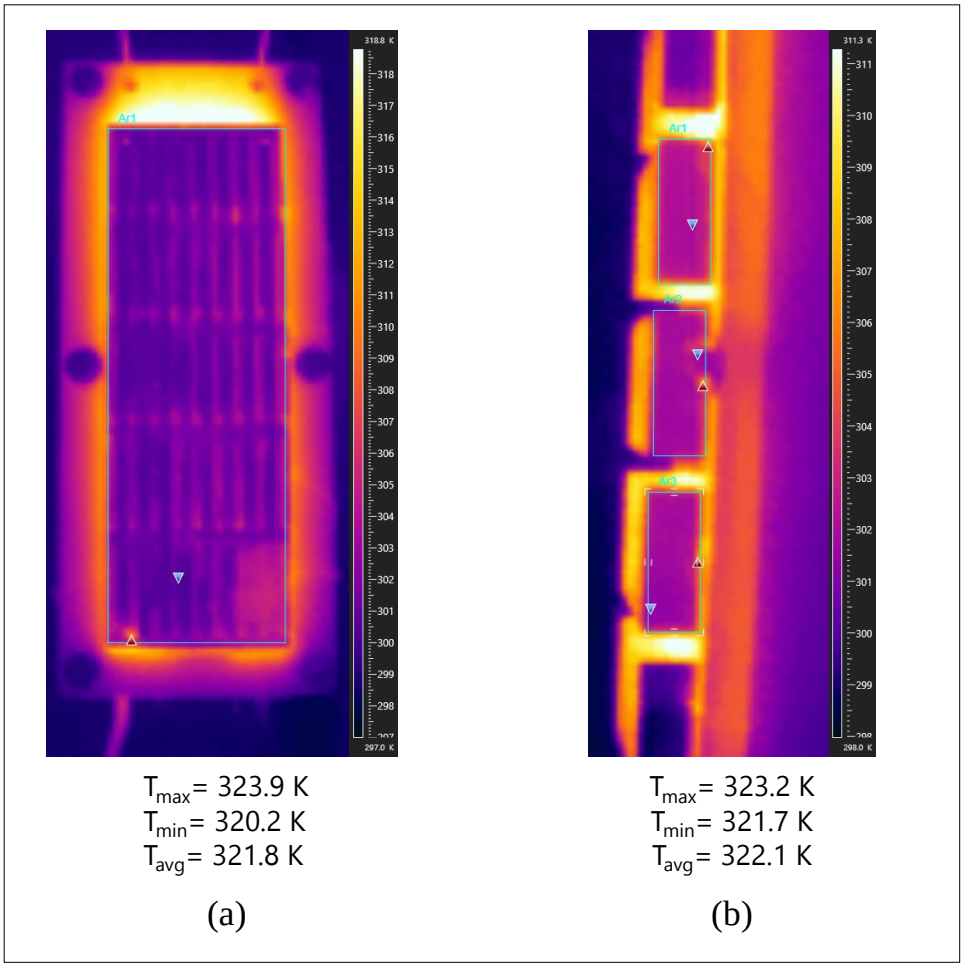

Figure 4.9. IR image from a) front view, b) side view of the heatsink sample under test

4.5. Results and Discussion

4.5.1. Total Heat Transfer Calculation

Having all the geometrical parameters, fin height, H, fin thickness, t, fin spacing, s, fin length, l, and gap length, G, known, on a baseplate with dimensions L and W, number of fin rows, m, and number of fin columns, n, can be calculated as follows;

$$m = \frac{L}{l + G} \tag{4.31}$$

$$n = \frac{W}{s+t} \tag{4.32}$$

The total heat transfer area can be calculated as follows;

$$A = 2\,m\,n\,l\,H \tag{4.33}$$

To calculate the heat flux from the first row of fins, Eq. 4.3 for the inlet velocity to the first row, $u_{C,in,1}$, can be substituted into Eq. 4.4 to find the heat transfer coefficient associated with first row of fins, h_1. The calculated heat transfer coefficient can be substituted in Eq. 4.34 to find the heat flux, knowing that the inlet temperature to the first row, $T_{\mathrm{C,in,1}}$, is equal to ambient temperature, T_∞.

$$\dot{q}_1 = h_1 (T_w - T_{C,in,1}) \tag{4.34}$$

Now Eqs. 4.21 and 4.22 can be used to find the inlet condition to the first gap $u_{G,in,1}$ and $T_{G,in,1}$. Having the first gap inlet conditions, Eqs. 4.23 and 4.24 can be used to calculate the average inlet velocity $\left(u_{C,in,2}\right)$ and temperature $\left(T_{C,in,2}\right)$ to the second row of fins. The same procedure can be followed to find the heat flux for the i^{th} row of fins, until the march through all the rows is finished. The total heat flux and total heat transfer can be found as follows;

$$\dot{q} = \sum_{i=1}^{m} \dot{q}_i \tag{4.35}$$

$$\dot{Q} = A\dot{q} \tag{4.36}$$

All fluid properties can be evaluated at the average temperature, $T_{avg} = \left(T_w + T_\infty\right)/2$. A simple computer code, in any language, can be developed to find the heat flux and total heat transfer from any arbitrary fin arrangement.

4.5.2. Parametric Study

Effect of Fin Spacing

Figure 4.10 shows the effect of fin spacing on total heat transfer from the heatsink. As expected, an optimum fin spacing exists that maximizes the heat transfer and interestingly enough, our various parametric studies show that the optimum fin spacing will remain unchanged compared to continuous fins case. Therefore, the correlation from [26] for optimum fin spacing is valid for case of interrupted fins as well.

$$s_{opt.} = 2.714\left[\frac{\nu\alpha L}{g\beta\left(T_w - T_\infty\right)}\right]^{\frac{1}{4}} \qquad 4.37$$

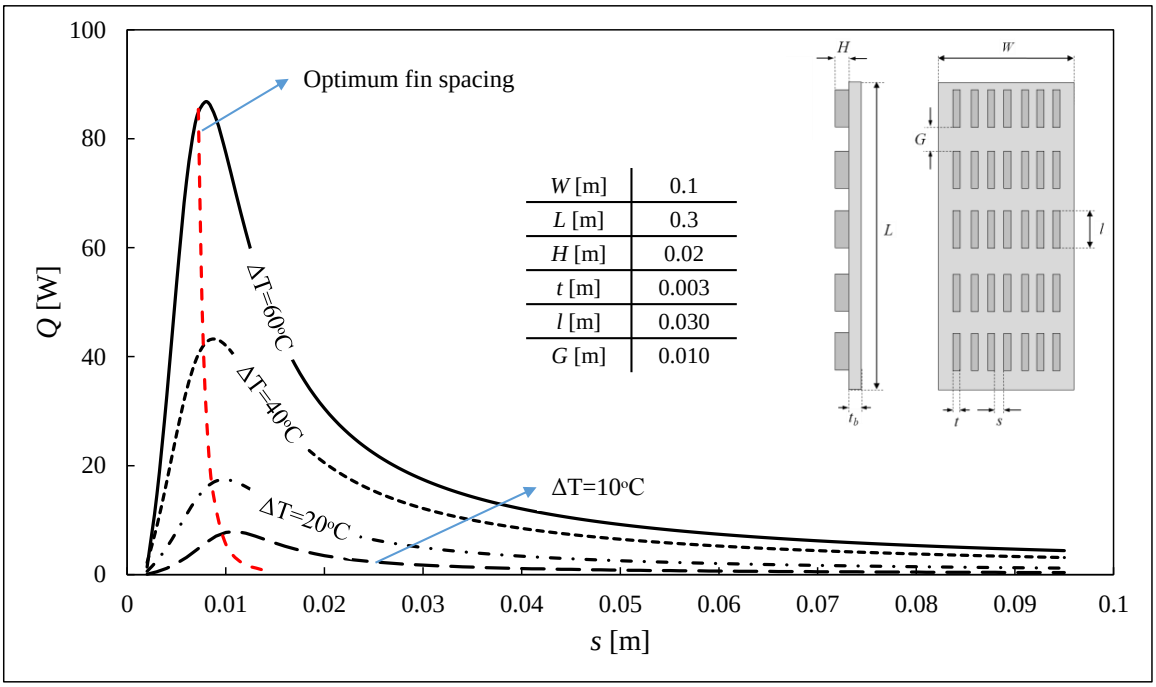

Figure 4.10. Effect of fin spacing on heat transfer from the heatsink

Effect of Gap Length

The effect of gap length on total heat transfer at different temperatures is shown in Figure 4.11.a. At first look, one may conclude that the best gap length is $G = 0$; however, it should be noted that gap length has an asymptotic effect on the heat transfer. As $G \to 0$, total heat transfer will increase dramatically but at $G = 0$, which is related to continuous fins, there will be a sudden drop in total heat transfer value. To shed more light on the

effect of gap length, Figure 4.11.b shows the ratio of heat transfer from interrupted fins to the heat transfer from continuous fins with the same fin spacing, $Q / Q_{cont.}$, versus G / L. This figure shows how at small values of gap length the heat transfer from interrupted fins dominate the heat transfer from continuous fins, due to the effect of gap on thermal boundary layer. As the gap length increases, due to loss of heat transfer area, total heat transfer keeps decreasing until the interrupted fin arrangement loses its privilege over continuous fins. It is also worth mentioning that as gap length increases, the weight of heatsink decreases, which can play a key role for the applications in which weight is an important matter.

Effect of Fin Length

Figure 4.12.a shows the total heat transfer from the fins for different fin lengths at various surface temperatures. As shown in the figure, fin length plays an important role in the heatsink performance. Depending on the baseplate dimensions, an optimum fin length can be found to maximize the total heat transfer rate. Figure 4.12.b shows the ratio of heat transfer from interrupted fins to continuous fins, which as shown, can be over 12 times more for the specific case shown in Figure 4.12.b.

A noteworthy trend that can be observed in Figure 4.12.b is that the enhancement effect of adding interruptions to the fins decreases at higher temperatures. The reason for this phenomena is that the buoyancy force is stronger at higher temperatures, causing more air flow to pass from the channel. More air flow leads to higher velocity and heat transfer rate. Adding interruption to fins at high surface temperatures, decreases this effect by removing high temperature solid surface, which is the main cause for buoyancy force. However at practical ranges of heatsink temperature, $40 - 60°C$, interrupted fin arrangement can dissipate heat about 3 times more than continuous fins, which is still a considerable contribution to the heatsink performance.

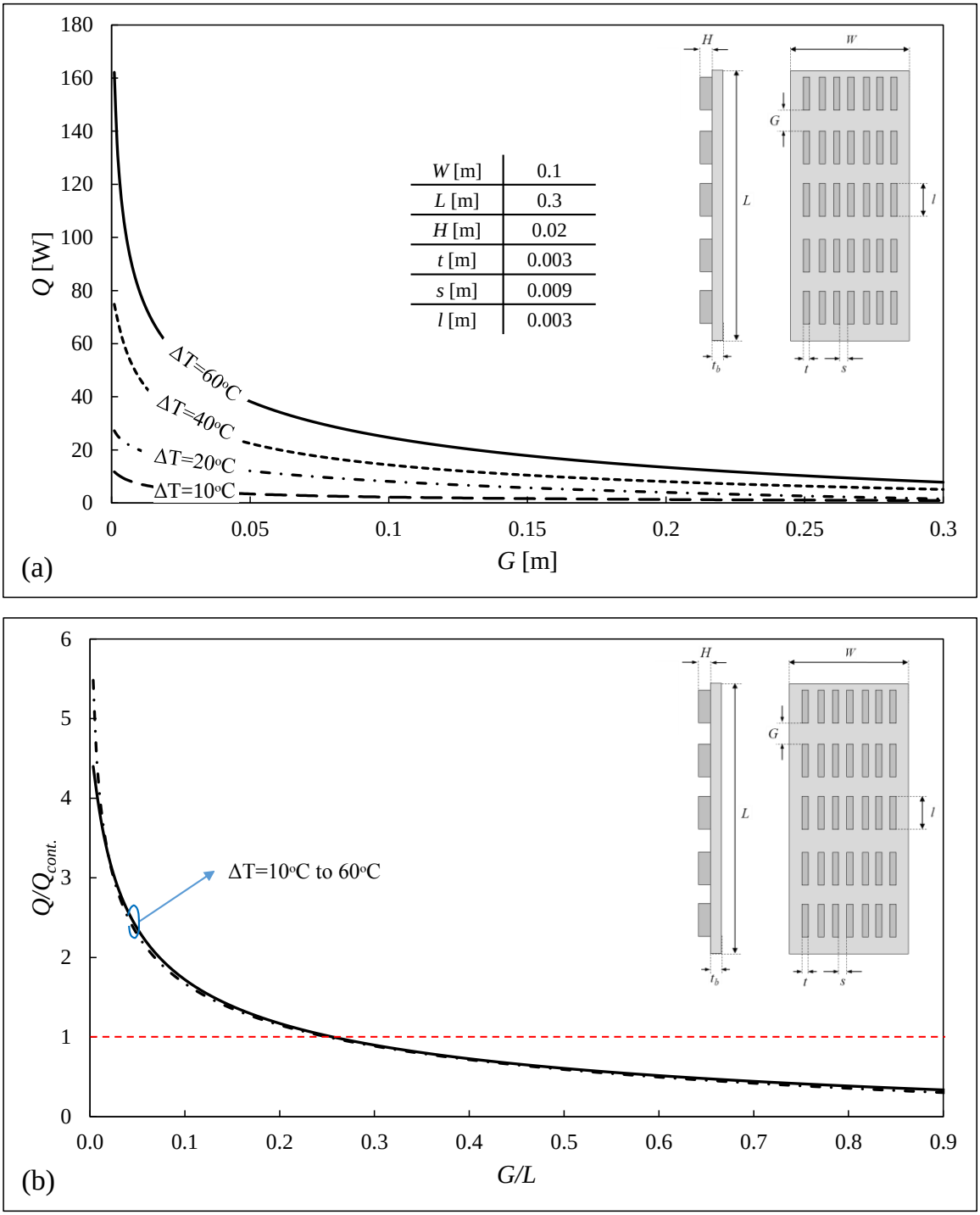

Figure 4.11. Effect of gap length on heat transfer from the heatsink, a) total heat transfer, b) dimensionless heat transfer with respect to continuous fins

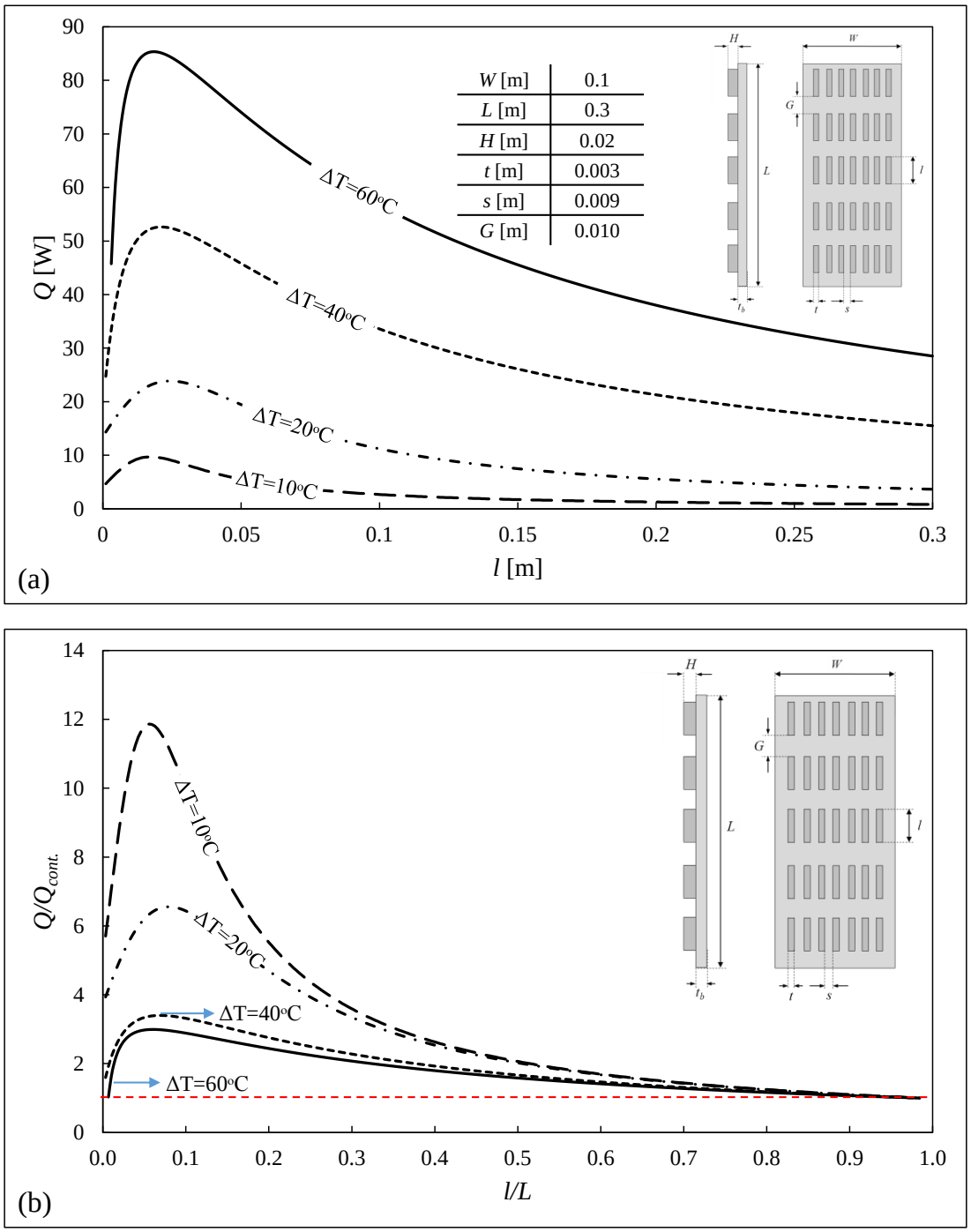

Figure 4.12. Effect of fin length on heat transfer from the heatsink, a) total heat transfer, b) dimensionless heat transfer with respect to continuous fins

4.5.3. Heatsink Design Procedure

In this section, it is intended to find the best fin arrangement, by determining the geometrical parameters, to maximize the total heat transfer rate from an available surface area, with a known operating temperature. The design procedure for the fin arrangement is explained in this section as following;

Step 1: Selecting the fin thickness, t. Fin thickness selection is mostly a matter of mechanical strength, so depending on the application and required robustness of the heatsink, the fin thickness can be selected. However, when selecting the thickness of the fins, we should keep in mind that thicker fins present lower thermal bulk resistance, which leads to more uniform temperature distribution along the fin and higher heat transfer. It also worth noting that thicker fin means heavier heatsink.

Step 2: Calculating the optimum fin spacing, $s_{opt.}$, using Eq. 4.37. The number of fin columns can be evaluated using Eq. 4.32, when the optimum fin spacing is determined.

Step 3: Determining the gap length, G. Selecting the gap length is highly dependent on manufacturing limitations, cost, and weight considerations. As shown in Section 4.5.2, the smaller gap length leads to higher total heat transfer rate; however sometimes due to manufacturing limitations, small gap length is not practical. Very small gaps can also get blocked due to contamination and corrosion and lose their effects. On the other hand, the higher the gap, the lighter the heatsink. Therefore, in applications where weight is a limiting factor, higher gap lengths are better choices. Based on the above-mentioned considerations, one or more gap length option(s) can be selected for the analysis in next step.

Step 4: Finding the optimum fin length. Having all the fin parameters determined, and assuming an average operation temperature for the heatsink, a simple computer code can be used to perform a parametric study on the fin length to maximize the total heat transfer from the heatsink.

4.6. Conclusion

A new analytical solution for steady-state laminar natural convection from isothermal vertical rectangular interrupted fins is presented and close-form compact correlations are introduced for velocity and temperature distribution for the first time. Integral technique was used in combination with numerical simulations to solve the governing equation. A custom-made testbed is built and 13 different aluminum heatsinks are tested to validate the numerical and analytical results. An easy-to-apply method is introduced, using the obtained correlations, to calculate total heat transfer from any arbitrary arrangement of interrupted fins, and a step-by-step method is presented to design naturally-cooled heatsinks with interrupted fins. Results show that naturally-cooled heatsinks with interrupted fins are capable of dissipating heat up to 12 time higher than currently available heatsinks with similar baseplate dimensions. This is while the weight of such heatsinks can get up to 30% lighter than the heatsinks with continuous fins, but similar baseplate dimensions.

Chapter 5.

Summary and Future Work

5.1. Summary of Thesis

Advantages such as; being noise-free, reliable with no parasitic power demand, and less maintenance requirements, make passive cooling a preferred thermal management solution for electronics. The focus of this thesis is to design high performance naturally-cooled heatsinks, to increase the cooling capacity of available passive thermal management systems. Heatsinks with interrupted rectangular vertical fins are the target of this study.

Due to the complexities associated with interrupted fins, interrupted rectangular single wall is chosen as the starting point of the project. Asymptotic solution and blending technique is used to present a compact correlation for average Nusselt number of such wall, for the first time. The proposed correlation is verified by the results obtained from numerical simulations, and experimental data obtained from a custom-designed testbed.

In the next step natural convection heat transfer from parallel plates is considered. Integral technique is used to solve the governing equations, and closed-form correlations for velocity, temperature, and local Nusselt number are developed for the first time. The results are successfully verified with the result of an independent numerical simulation and experimental data obtained from tests conducted on aluminum heatsink sample.

In the last step, to model heat transfer from interrupted finned heatsinks, analytical approach is used, to obtain compact correlations for velocity and temperature inside the domain. Numerical simulations are performed to provide some information, required by our analytical approach. An extensive experimental study is also conducted to verify the results from analytical solution and numerical simulation. Results show that the new-designed heatsinks are capable of dissipating heat up to 12 times more than currently available naturally-cooled heatsinks, with weight up to 30% lighter. The new heatsinks can

increase the capacity of passive cooling systems significantly. The list of contributions resulted from the present study is listed below;

- Developing a closed-form correlation for average Nusselt number from interrupted single walls [73]
- Introducing an effective length to describe heat transfer from interrupted single walls analogous to heat transfer from a continuous vertical wall [73]
- Developing closed-form solutions for local Nusselt number, velocity, and temperature distribution in laminar natural convection heat transfer between parallel plates [74]
- Developing compact correlation for velocity and temperature in two dimensional momentum and energy diffusion in a one directional laminar flow, submitted to international journal of heat and mass transfer
- Design of interrupted fin naturally-cooled heatsinks with average heat dissipation of 5 time higher than similar commercially available heatsinks [55]
- Developing an easy to use tool to design high performance naturally-cooled heatsinks with interrupted fins, submitted to international journal of heat and mass transfer
- Design and prototyping of a fully passive thermal management system for outside plant telecom enclosures [15]

5.2. Future Work

The following research directions can be considered as the continuation of this dissertation:

- Extend the analysis to other fin orientations, such as inclined fins or louvered fins (see Figure 5.1.a). Inclined fins have the potential to accommodate higher fin density on an available surface area, and also to create separate paths for fresh air and hot air.
- Extend the analysis to fin arrangement with variable fin/gap length along the flow (see Figure 5.1.b). Considering the significant effect of geometrical parameters on heat transfer, variation of these parameters in a way that they can adopt to the flow characteristic could be a potential improvement to this work.
- Extend the analysis to conductive heat transfer inside the heatsink and fins, to include the effect of bulk and spreading resistance in the problem. Numerical methods can be the best option to solve this problem.
- Investigate the effects of thermal load variations, i.e. transient natural convection heat transfer from interrupted fins, however; due to high thermal

inertia in naturally-cooled systems quasi-steady models may be sufficient to predict the system behavior.

- To investigate the effect of surface roughness on natural convection heat transfer from the heatsinks.

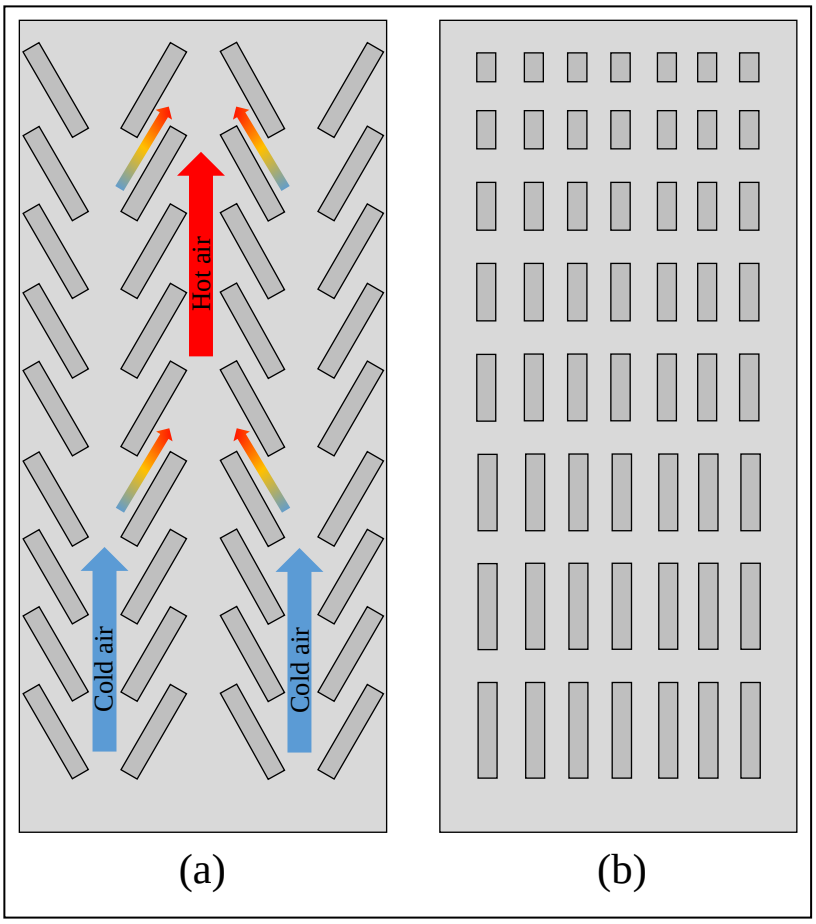

Figure 5.1. Proposed geometries for the future work, a) inclined interrupted fins, b) variable fin parameters along the flow

References

[1] Anandan S., and Ramalingam V., 2008, “Thermal management of electronics: A review of literature,” Int. J. Therm. Sci., **12**(2), pp. 5–26.

[2] Gurrum S. P. S., Suman S., Shivesh K., Joshi Y. K., and Fedorov A. G., 2004, “Thermal Issues in Next-Generation Integrated Circuits,” IEEE Trans. DEVICE Mater. Reliab., **4**(4), pp. 709–714.

[3] Wankhede M., Khaire V., and Goswami A., 2007, “evaluation of cooling solutions for outdoor electronics,” 13th International Conference on Thermal Investigation of ICs and Systems, ©EDA Publishing, Budapest, Hungary, pp. 1–6.

[4] Jahkonen J., Puolakka M., and Halonen L., 2013, “Thermal Management of Outdoor LED Lighting Systems and Streetlights Variation of Ambient Cooling Conditions,” LEUKOS, **9**(3), pp. 155–176.

[5] Christensen A., Ha M., and Graham S., 2007, “Thermal Management Methods for Compact High Power LED Arrays,” 7th International Conference on Solid State Lighting, I.T. Ferguson, N. Narendran, T. Taguchi, and I.E. Ashdown, eds., SPIE UK, San Diego, California, USA, p. 66690Z–66690Z–19.

[6] BCCResearch, 2014, The Market for Thermal Management Technologies, Wellesley, MA, USA.

[7] 2012, Information and Communication Technology Portfolio: Improving Energy Efficiency and Productivity in America’s Telecommunication Systems and Data Centers.

[8] Roy S. N., 2008, “Energy logic: A road map to reducing energy consumption in telecommunications networks,” INTELEC 2008 - 2008 IEEE 30th Int. Telecommun. Energy Conf., pp. 1–9.

[9] Lange C., Kosiankowski D., Weidmann R., and Gladisch A., 2011, “Energy Consumption of Telecommunication Networks and Related Improvement Options,” IEEE J. Sel. Top. Quantum Electron., **17**(2), pp. 285–295.

[10] Lange C., Kosiankowski D., Gerlach C., Westphal F., and Gladisch A., 2009, “Energy Consumption of Telecommunication Networks,” 35th European Conference on Optical Communication, ECOC 09, IEEE, Vienna, pp. 1–2.

[11] Kilper D. C., Member S., Atkinson G., Korotky S. K., Goyal S., Vetter P., Suvakovic D., and Blume O., 2011, “Power Trends in Communication Networks,” Sel. Top. Quantum Electron., **17**(2), pp. 275–284.

[12] Lubritto C., and Petraglia A., 2008, “Telecommunication power systems: energy saving, renewable sources and environmental monitoring,” IEEE Electrical Power & Energy Conference (EPEC), Vancouver Canada, pp. 1–4.

[13] Hernon D., Silvestre-Castillo P., and Hayden P., 2011, “Significantly extending the operational range of free cooling in radio Base Station indoor shelters,” IEEE 33rd International Telecommunications Energy Conference (INTELEC), Ieee, Amsterdam, Netherlands, pp. 1–7.

[14] Gholami A., 2014, “A New Integrated Approach for Modeling Green Passive Cooling Systems,” M.A.Sc. Thesis, Simon Fraser University.

[15] Ahmadi M., Gholami A., Lau K., and Bahrami M., 2014, “Passive Cooling of Outside Plant Power Systems , a Green Solution to Reduce Energy Consumption,” IEEE 36th International Communications Energy Conference (INTELEC), IEEE, Vancouver Canada, pp. 1–9.

[16] Ostrach S., 1952, "An analysis of laminar free-convection flow and heat transfer about a flat plate parallel to the direction of the generating body force," Thecnical Report, NACA.

[17] Sparrow E., and Gregg J., 1956, “Laminar free convection from a vertical plate with uniform surface heat flux,” ASME J. Heat Transf., **78**(1), pp. 435–440.

[18] Merkin J., 1985, “A note on the similarity solutions for free convection on a vertical plate,” J. Eng. Math., **19**(1), pp. 189–201.

[19] Churchill S. W., and Chu H., 1975, “Correlating equations for laminar and turbulent free convection from a vertical plate,” Int. J. Heat Mass Transf., **18**(11), pp. 1323–1329.

[20] Yovanovich M., and Jafarpur K., 1993, “Bounds on Laminar Natural Convection From Isothermal Disks and Finite Plates of Arbitrary Shape for All Orientations and Prandtl Numbers,” ASME Winter Annual Meeting, New Orleans, Louisiana, pp. 93–111.

[21] Cai R., and Zhang N., 2003, “Explicit analytical solutions of 2-D laminar natural convection,” Int. J. Heat Mass Transf., **46**(5), pp. 931–934.

[22] Yousefi T., and Ashjaee M., 2007, “Experimental study of natural convection heat transfer from vertical array of isothermal horizontal elliptic cylinders,” Exp. Therm. Fluid Sci., **32**(1), pp. 240–248.

[23] Suryawanshi S., and Sane N., 2009, “Natural Convection Heat Transfer From Horizontal Rectangular Inverted Notched Fin Arrays,” J. Heat Transfer, **131**(8), pp. 797–805.

[24] Elenbaas W., 1942, “Heat dissipation of parallel plates by free convection,” Physica, **9**(1), pp. 1–28.

[25] Stuart W. Churchill, 1977, “A Comprehensive Correlation Equation for Buoyancy Induced Flow in Channels,” Lett. Heat Mass Transf., **4**(3), pp. 193–199.

[26] Bar-Cohen A., and Rohsenow W. M., 1984, “Thermally Optimum Spacing of Vertical, Natural Convection Cooled, Parallel Plates,” J. Heat Transfer, **106**(1), pp. 116–123.

[27] Bodoia J. R., and Osterle J. F., 1962, “The Development of Free Convection Between Heated Vertical Plates,” J. Heat Transfer, **84**(1), pp. 40–44.

[28] Ofi O., and Hetherington H. J., 1977, “Application of the finite element method to natural convection heat transfer from the open vertical channel,” Int. J. Heat Mass Transf., **20**(11), pp. 1195–1204.

[29] Culham J. R., Yovanovich M. M., and Lee S., 1995, “Thermal modeling of isothermal cuboids and rectangular heat sinks cooled by natural convection,” IEEE Trans. Components, Packag. Manuf. Technol. Part A, **18**(3), pp. 559–566.

[30] Sparrow E. M., and Acharya S., 1981, “A natural convection fin with a solution-determined nonmonotonically varying heat transfer coefficient,” J. Heat Transfer, **103**(2), pp. 218–226.

[31] Starner K. E., and McManus H. N., 1963, “An Experimental Investigation of Free-Convection Heat Transfer From Rectangular-Fin Arrays,” J. Heat Transfer, **85**(3), pp. 273–275.

[32] Welling J. R., and Wooldridge C. B., 1965, “Free Convection Heat Transfer Coefficients From Rectangular Vertical Fins,” J. Heat Transfer, **87**(4), p. 439.

[33] Edwards J., and Chaddock J., 1963, “An experimental investigation of the radiation and free convection heat transfer from a cylindrical disk extended surface,” ASHRAE Trans., **69**(1), pp. 313–322.

[34] Chaddock J., 1970, “Natural Convection Heat Transfer from Vertical Rectangular Fin Array,” ASHRAE J, **12**(August), pp. 53–60.

[35] Aihara T., 1970, “Natural Convection Heat Transfer from Vertical Rectangular Fin Arrays: (Part 3, Heat Transfer from Fin Flats),” Trans. Japan Soc. Mech. Eng., **13**(64), pp. 1192–1200.

[36] Aihara T., 1970, “Natural Convection Heat Transfer from Vertical Rectangular Fin Arrays: (Part 2, Heat Transfer from Fin Edges),” Trans. Japan Soc. Mech. Eng., **36**(282), pp. 239–247.

[37] Aihara T., 1970, “Natural Convection Heat Transfer from Vertical Rectangular Fin Arrays : (Part 1,Heat Transfer from Base Plates),” Trans. Japan Soc. Mech. Eng., **36**(261), pp. 915–926.

[38] Aihara T., 1970, “Natural Convection Heat Transfer from Vertical Rectangular-Fin Arrays : Part 4, Heat-Transfer Characteristics of Nonisothermal-Fin Arrays,” Trans. Japan Soc. Mech. Eng., **36**(292), pp. 2077–2086.

[39] Leung C. W., and Probert S. D., 1985, “Heat Exchanger: Optimal Separation for Vertical Ractangular Fins Proturding from Vertical Rectangular Base,” Appl. Energy, **19**(1), pp. 77–85.

[40] Leung C. W., Probert S. D., and Shilston M. J., 1985, “Heat exchanger design: Optimal uniform separation between rectangular fins protruding from a vertical rectangular base,” Appl. Energy, **19**(4), pp. 287–299.

[41] Leung C., Probert S., and Shilston M., 1985, “Heat exchanger design: thermal performances of rectangular fins protruding from vertical or horizontal rectangular bases,” Appl. Energy, **20**(2), pp. 123–140.

[42] Leung C., Probert S., and Shilston M., 1986, “Heat transfer performances of vertical rectangular fins protruding from rectangular bases: effect of fin length,” Appl. Energy, **22**(4), pp. 313–318.

[43] Leung C. W., and Probert S. D., 1987, “Natural-Convective Heat Exchanger with Vertical Rectangular Fins and Base: Design Criteria,” Proc. Inst. Mech. Eng. Part C J. Mech. Eng. Sci., **201**(5), pp. 365–372.

[44] Leung C. W., and Probert S. D., 1989, “Heat-exchanger performance: Effect of orientation,” Appl. Energy, **33**(4), pp. 235–252.

[45] Leung C. W., and Probert S. D., 1989, “Thermal effectiveness of short-protrusion rectangular heat exchanger fins,” J. Appl. energy, **34**(1), pp. 1–8.

[46] Pol D. Van de, and Tierney J., 1974, “Free convection heat transfer from vertical fin-arrays,” IEEE Parts, Hybrids, Packag., **10**(4), pp. 267–271.

[47] Dejong N. C., and Jacobi A. M., 1995, "An Experimental Study of Flow and Heat Transfer in Offset Strip and Louvered-Fin Heat Exchangers," Technical Report, ACRC, University of Illinois, Urbana.

[48] Brutz J. M., Dutton J. C., and Jacobi A. M., 2005, "Use of Unsteady Forcing in Interrupted-Fin Heat Exchangers: An Assessment of Potential," Technical Report, ACRC, University of Illinois, Urbana.

[49] Ndao S., Peles Y., and Jensen M. K., 2009, “Multi-objective thermal design optimization and comparative analysis of electronics cooling technologies,” Int. J. Heat Mass Transf., **52**(19-20), pp. 4317–4326.

[50] Da Silva a. K. K., Lorente S., and Bejan a., 2004, “Optimal distribution of discrete heat sources on a wall with natural convection,” Int. J. Heat Mass Transf., **47**(2), pp. 203–214.

[51] Sobel N., Landis F., and Mueller W., 1966, “NATURAL CONVECTION HEAT TRANSFER IN SHORT VERTICAL CHANNELS INCLUDING EFFECTS OF STAGGER,” Proc. 3rd Int. Heat Transf. Conf., **2**(1), pp. 121–125.

[52] Sparrow E. M., and Prakash C., 1980, “Enhancement of Natural Convection Heat Transfer by a Staggered Array of Discrete Vertical Plates,” J. Heat Transfer, **102**(2), pp. 215–220.

[53] Daloglu a., and Ayhan T., 1999, “Natural convection in a periodically finned vertical channel,” Int. Commun. Heat Mass Transf., **26**(8), pp. 1175–1182.

[54] Gorobets V., 2002, “Heat transfer for vertical surfaces with discrete fins in the case of free convection,” J. Eng. Phys. Thermophys., **75**(5), pp. 100–107.

[55] Ahmadi M., Mostafavi G., and Bahrami M., 2014, “Natural convection from rectangular interrupted fins,” Int. J. Therm. Sci., **82**(1), pp. 62–71.

[56] Mostafavi G., 2012, “NATURAL CONVECTIVE HEAT TRANSFER FROM INTERRUPTED RECTANGULAR FINS,” M.A.Sc. Thesis, Simon Fraser University.

[57] Fujii M., 2007, “Enhancement of natural convection heat transfer from a vertical heated plate using inclined fins,” Heat Transf. Res., **36**(6), pp. 334–344.

[58] Nada S. A., 2007, “Natural convection heat transfer in horizontal and vertical closed narrow enclosures with heated rectangular finned base plate,” Int. J. Heat Mass Transf., **50**(3-4), pp. 667–679.

[59] Ben-Nakhi A., and Chamkha A. J., 2007, “Conjugate natural convection in a square enclosure with inclined thin fin of arbitrary length,” Int. J. Therm. Sci., **46**(5), pp. 467–478.

[60] Bejan A., 2004, Convection heat transfer, John Wiley and Sons, Inc., New York.

[61] Rao V. D., Naidu S. V., Rao B. G., and Sharma K. V., 2006, “Heat transfer from a horizontal fin array by natural convection and radiation—A conjugate analysis,” Int. J. Heat Mass Transf., **49**(19-20), pp. 3379–3391.

[62] Holman J. P., 2001, Experimental Methods for Engineers, McGrawHill, New York.

[63] McAdams W. H., 1954, Heat Transmission, McGrawHill, New York.

[64] Churchill S. W., and Usagi R., 1972, “A general expression for the correlation of rates of transfer and other phenomena,” AIChE J., **18**(6), pp. 1121–1128.

[65] Güvenç A., and Yüncü H., 2001, “An experimental investigation on performance of fins on a horizontal base in free convection heat transfer,” J. Heat mass Transf., **37**(1), pp. 409–416.

[66] Goldstein R. J., Sparrow E. M., and Jones D. C., 1973, “Natural convection mass transfer adjacent to horizontal plates,” Int. J. Heat Mass Transf., **16**(5), pp. 1025–1035.

[67] Sparrow E. M. E., and Gregg J. L., 1958, “similar solutions for natural convection from a non isothermal vertical plate,” J. Heat Transfer, **80**(1), pp. 379–386.

[68] Sparrow E. M., and Gregg J. L., 1956, “Laminar Free Convection Heat Transfer from the Outer Surface of a Vertical Circular Cylinder,” Trans. ASME, **78**(1), pp. 1823–1829.

[69] Gebhart B., Pera L., and Schorr A. ., 1970, “Steady laminar natural convection plumes above a horizontal line heat source,” Int. J. Heat Mass Transf., **13**(1), pp. 161–171.

[70] Jaluria Y., and Gebhart B., 1977, “Buoyancy-induced flow arising from a line thermal source on an adiabatic vertical surface,” Int. J. Heat Mass Transf., **20**(2), pp. 153–157.

[71] Nat Vorayos, 2000, “Laminar natural convection within long vertical uniformly heated parallel-plate channels and circular tubes,” Oregon State University.

[72] Incropera F., DeWitt D., and Bergrnan T., 2007, Fundamentals of Heat and Mass Transfer (The 6th Edition).

[73] Ahmadi M., Mostafavi G., and Bahrami M., 2014, “Natural Convection From Interrupted Vertical Walls,” J. Heat Transfer, **136**(11), pp. 112501/1–8.

[74] Ahmadi M., Fakoor-Pakdaman M., and Bahrami M., 2014, “Natural Convection from Vertical Parallel Plates: An Integral Method Solution,” J. Thermophys. Heat Transf., pp. 1–10.

[75] Saikhedkar N. H., and Sukhatme S. P., 1981, “Heat transfer from rectangular cross-sectioned vertical fin arrays,” Proceedings of the Sixth National Heat and Mass Transfer Conference, HMT, pp. 9–81.

[76] SPARROW E. M., and VEMURI S. B., “Natural convection/radiation heat transfer from highly populated pin fin arrays,” J. Heat Transfer, **107**(1), pp. 190–197.

[77] Sparrow E. M., and Vemuri S. B., 1986, “Orientation effects on natural convection/radiation heat transfer from pin-fin arrays,” Int. J. Heat Mass Transf., **29**(3), pp. 359–368.

[78] Azarkish H., Sarvari S. M. H., and Behzadmehr a., 2010, “Optimum geometry design of a longitudinal fin with volumetric heat generation under the influences of natural convection and radiation,” Energy Convers. Manag., **51**(10), pp. 1938–1946.

[79] Holman J. P., 2010, Heat Transfer, McGrawHill, Boston.

Appendix A.

Integral Method for Natural Convection

In this section, the integral method for natural convection heat transfer is explained. The goal of this section is to clarify the methodology to obtain the governing equations from the control volumes shown in Table 3.1. The problem here is explained for a general case, however extending the introduced equation here, to the governing equations of Table 3.1 is straight forward.

Consider a boundary layer flow driven by buoyancy forces originating from density variations in a fluid (Figure A1).

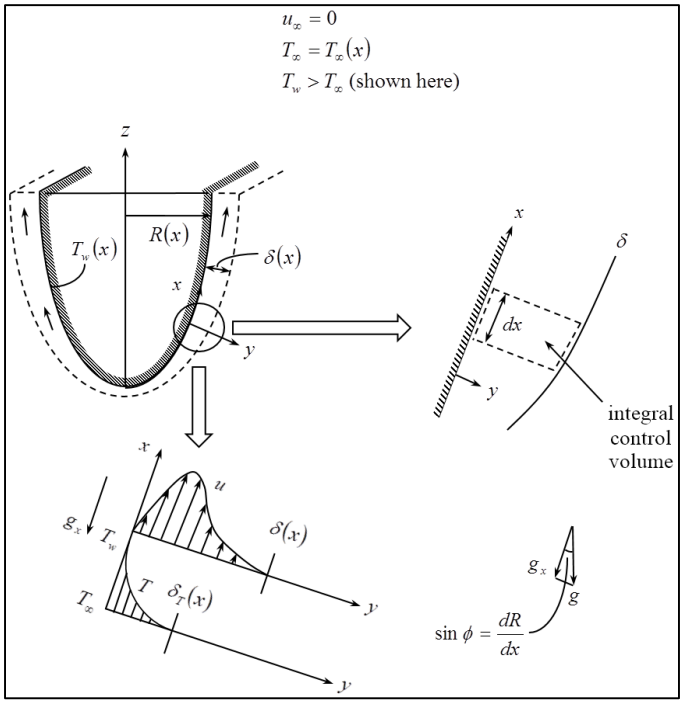

Figure A1. General control volume used in integral method for free convection

The integral conservation equations can be obtained by directly integrating the governing equations term-by-term across the control volume. Here, we start from first principles and perform mass, momentum, and energy balances on the integral control volume shown in the preceding figure.

Conservation of mass

Figure A2 shows the control volume considered for the mass conservation analysis.

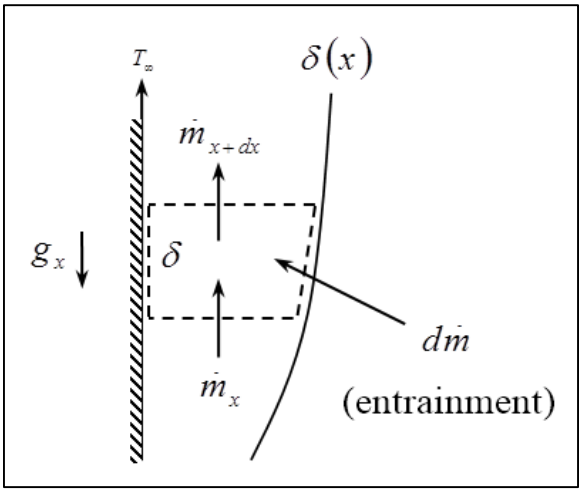

Figure A2. Conservation of mass in a control volume

$$\dot{m}_{in} - \dot{m}_{out} = \underbrace{\frac{d}{dt}\left(m_{CV}\right)}_{=0}$$

$$\dot{m}_x = \int_0^\delta \rho u dy$$

$$\dot{m}_{x+dx} = \dot{m}_x + \frac{\partial}{\partial x}\left(\dot{m}_x\right)dx$$

$$\therefore d\dot{m} = \frac{d}{dx}\left[\int_0^\delta \rho u dy\right]dx$$

Conservation of momentum

Figure A3 shows the control volume considered for the momentum conservation analysis.

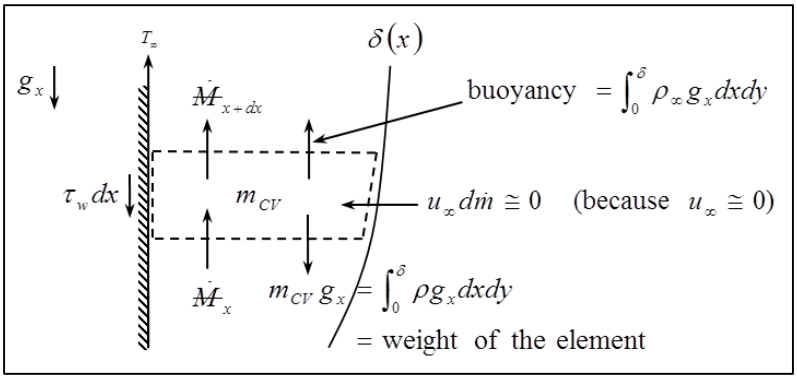

Figure A3. Conservation of momentum in a control volume. Note that τ_w is per unit depth in z-direction.

$$\sum F_x + \dot{M}_{x,in} - \dot{M}_{x,out} = \underbrace{\frac{d}{dt}\left(M_{x,CV}\right)}_{=0}$$

$$\therefore \int_0^\delta p_x dy - \int_0^\delta p_{x+dx} dy = \int_0^\delta \rho_\infty g_x dxdy = \text{buoyancy force}$$

Thus, the *x*-momentum balance becomes:

$$\left(-\tau_w dx\right) + \int_0^\delta \rho_\infty g_x dxdy - \int_0^\delta \rho g_x dxdy + \dot{M}_x - \dot{M}_x - \frac{\partial}{\partial x} \underbrace{\left(\dot{M}_x\right)}_{=\int_0^\delta \rho u^2 dy} dx = 0$$

Using $\rho_\infty - \rho = \rho\beta(T - T_\infty)$, we obtain:

$$\frac{d}{dx}\left[\int_0^\delta u^2 dy\right] = \beta g_x \int_0^{\delta_T} \left(T - T_\infty\right) dy - \frac{\tau_w}{\rho}$$

where the integration limits have been set, keeping in mind that outside the hydrodynamic boundary layer the velocity is zero, and the temperature outside the thermal boundary layer is ambient temperature. The shear stress at the wall can be defined as;

$$\tau_w = -\mu \left.\frac{\partial u}{\partial y}\right|_{y=0}$$

Conservation of energy

The dominant terms relevant to the energy balance are shown in Figure A4. Consistent with the usual boundary layer approximations, heat conduction in the *x*-direction is neglected.

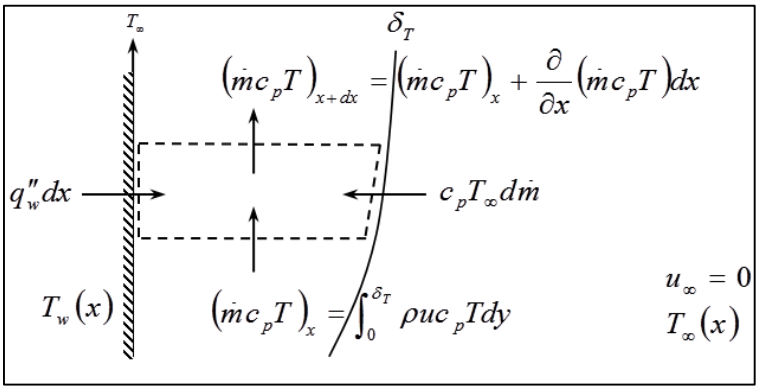

Figure A4. Conservation of energy in a control volume. Note that q''_w is per unit depth in z-direction.

$$\dot{E}_{in} - \dot{E}_{out} = \underbrace{\frac{d}{dt}(E_{CV})}_{=0}$$

$$q''_w dx + c_p T_\infty \frac{d}{dx}\left[\int_0^\delta \rho u dy\right]dx - \frac{d}{dx}\left[\int_0^{\delta_T} \rho u c_p T dy\right]dx = 0$$

which can be rearranged to:

$$\frac{d}{dx}\int_0^{\min(\delta,\delta_T)} u(T - T_\infty)dy + \left(\frac{dT_\infty}{dx}\right)\int_0^\delta u dy = \frac{q''_w}{\rho c_p}$$

where the heat flux at the wall can be defined as;

$$q''_w = -k\left.\frac{\partial T}{\partial y}\right|_{y=0}$$

Appendix B.

Calculation of Radiation Heat Transfer from Test Samples

Depending on the application and range of temperature, radiation heat transfer can play an important role in the heat transfer from fin arrays. This has been shown by Edwards and Chaddock [33], Chaddock [34], Sparrow and Acharya [30], Saikhedkar and Sukhatme [75], Sparrow and Vemuri [76,77], Azarkish *et al*. [78], and Rao *et al*. [61]. The common conclusion of the aforementioned studies is that the radiation heat transfer contributes 25% to 40% to the total heat transfer from fin arrays in the naturally-cooled heatsinks. However; in case of our experimental studies we measured the contribution of the radiation heat transfer to be around 5% of total measured heat transfer. This difference is mainly caused by the difference between the surface emissivity of the test samples. In most of the above mentioned studies anodized sample are used in the testing procedure. Adonization can increase the emissivity of aluminum to approximately 0.9, [79] which has a significant effect on radiation heat transfer from aluminum heatsinks. Reported emissivity for machined aluminum is in the range of 0.1 [79]. In this section, the methodology to approximate radiation heat transfer from the heatsink samples is explained. Figure B1 shows the domain considered for radiation analysis of the heatsink samples.

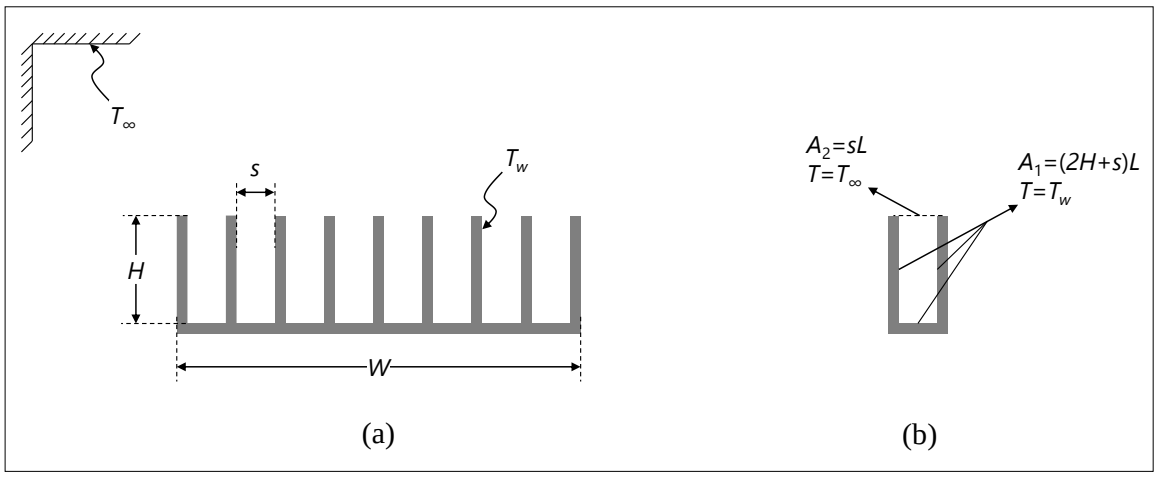

Figure B1. a) top view of the geometry considered for radiation heat transfer analysis, b) surfaces and temperatures used in view factor analysis

To perform the analysis we assume the length of the heatsink normal to the page, L, is larger than fin height, H and fin spacing, s. The surrounding might be represented by hypothetical surface A_2. The net rate of radiation heat transfer to this surface is therefore equivalent to the rate of heat rejection by a unit section of the array.

$$Q_{Rad.,2} = A_1 \sigma \varepsilon F_{12} \left(T_w^4 - T_\infty^4 \right)$$

with;

$$A_1F_{12} = A_2F_{21} \quad and \quad F_{21} = 1$$

then;

$$Q_{Rad.,2} = sL\varepsilon\sigma\left(T_w^4 - T_\infty^4\right)$$

Including all the section in the analysis, and adding the radiation heat transfer from the fin tips, the total radiation heat transfer from the heatsinks samples can be found as below;

$$Q_{Rad.} = WL\varepsilon\sigma\left(T_w^4 - T_\infty^4\right)$$

Emissivity measurement

To measure the emissivity of the heatsink samples, we used an infrared thermography method. The heatsinks are placed inside an environmental chamber made by ESPEC (see Figure B2), with ambient temperature set on a specific value. Enough time is given to the samples to reach the equilibrium temperature with surrounding temperature. At this point, IR images are taken from the samples and knowing the surface temperature, the value of emissivity is changed inside an image analysis software (FLIR R&D) until the results much between the value shown by software and known temperature set by environmental chamber. IR images are taken by FLIR SC655 camera. Range of emissivity obtained for the machined aluminum samples is from 0.078 to 1.12, and the average value of 0.09 is used for the analysis. This value matches the reported value for the emissivity of machined aluminum in the literature [72,79].

Figure B2. ESPEC environmental chamber used for emissivity measurement tests